Quantitative Interpretation of Magnetic Measurements in Archaeological Prospecting

Dissertation
zur Erlangung des Doktorgrades

der Mathematisch-Naturwissenschaftlichen Fakultät
der Christian-Albrechts-Universität zu Kiel

vorgelegt von

Natalie Marie Pickartz

Kiel, 2020

Erster Gutachter:	Prof. Dr. Wolfgang Rabbel
Zweiter Gutachter:	Prof. Dr. Jörg Ebbing
Tag der mündlichen Prüfung:	27. April 2020

Zusammenfassung

Die zerstörungsfreie Erkundung archäologischer Fundorte mit magnetischen Gradiometermessungen ist von großer Bedeutung für die Archäologie, da diese ermöglichen einen Gesamtplan des Fundorts zu erstellen. Bislang beschränkt sich in vielen Fallbeispielen die Auswertung auf die Bildinterpretation der kartierten Messwerte. Dies schöpft nicht das volle Potential der Magnetik aus. Es fehlt die Bestimmung eines quantitativen Modells der magnetischen Störkörper, d.h. der archäologischen Befunde. Die hier erarbeiteten Inversionskonzepte, angepasst an den jeweiligen Fundort, zur quantitativen Auswertung der Messungen nutzen dieses vernachlässigte Potential. Die Inversionsrechnungen müssen die Charakteristika der jeweiligen archäologischen Überreste beachten, um die Mehrdeutigkeit magnetischer Messungen einzuschränken.
Diese Arbeit untersucht zwei archäologische Fundorte mit unterschiedlichen Befunden.

Der Fundort Maidanetske (Ukraine; ~ 3950 - 3650 BCE) gehört zur kupferzeitlichen Cucuteni-Tripolye Kultur. Er umfasst die Überreste von etwa 3000, meist verbrannten, Häusern. Mittels Vorwärtsrechnungen der dokumentierten Funde wurde der Brandlehm als Quelle der magnetischen Anomalien bestimmt. Der Brandlehm befindet sich in einem diskreten Tiefenbereich und die Charakteristika dieser Schicht werden als *a priori* Informationen für die Inversion verwendet. Auf Grund der Annahme, dass die Magnetisierung des umgebenden Materials wesentlich geringer ist als diejenige der Brandlehmschicht, wird erstere vernachlässigt. Der Tiefenbereich der magnetisierten Schicht wird auf denjenigen der Brandlehmschicht begrenzt. Über Inversion wird die Magnetisierungsverteilung dieser Schicht bestimmt. Der Vergleich der Magnetisierungsverteilung dreier ausgegrabener Häuser mit der Massenverteilung des Brandlehms liefert eine empirische Beziehung zwischen diesen Größen. Zur quantitativen Interpretation nicht ausgegrabener Häuser wird zunächst deren Magnetisierungsverteilung berechnet und dann über die Magnetisierungs-Massen-Beziehung die Gesamtmasse bestimmt. Die Auswertung der Gesamtmassen von 45 nicht ausgegrabenen Häusern lässt auf zwei unterschiedliche Gruppen schließen, die möglicherweise auf zwei unterschiedliche Bauweisen hindeuten.

Die Überreste der Häuser der linearbandkeramischen Siedlung Vráble (Slowakische Republik; ~ 5250 - 4950 cal BCE), bestehen aus Ansammlungen von Gruben, die sich zu Längsgruben entlang beider Seiten der ehemaligen Gebäude zusammensetzen. Die Gruben wurden in den Löss gegraben und sind nun mit Material verfüllt, das in Bezug zum jeweiligen Haus steht. Als Teil der Grabungsdokumentation wurden Multimethodenmessungen in der Ausgrabung durchgeführt. Die gemeinsame Interpretation

von Bodenradar- und elektromagnetischen Induktionsmessungen ermöglicht die Abbildung der Unterkante der Gruben inklusive deren Mikrotopographie, die die schrittweise Entstehung der Längsgruben belegt. Die geophysikalischen Messungen bestimmen die Unterkante der Gruben in einer größeren Tiefe als in der Ausgrabung erwartet.

Außerdem zeigt sich, dass die gemessenen Magnetikanomalien nicht durch ausschließlich induzierte Magnetisierung erklärt werden können. Diese Schlussfolgerung resultiert aus Vorwärtsrechnungen basierend auf zweidimensionalen Suszeptibilitätsverteilungen, die in Bohrlöchern entlang von Profilen aus dicht platzierten Bohrpunkten durch die Gruben gemessen wurden. Die remanente Magnetisierung wird daraufhin über eine Inversion basierend auf der Suszeptibilitätsverteilung bestimmt und durch das Königsberger Verhältnis beschrieben. Für die sechs untersuchten Bohrprofile ergeben sich Werte des mittleren Königsbergerverhältnis zwischen 1.8 und 7.0, wobei die meisten Werte kleiner als 4.0 sind. Mittels geoarchäologischer Daten werden magnetotaktische Bakterien in der Grubenfüllung als Ursache der Remanenz bestimmt, da sie den Anteil von ferrimagnetischen Eisenverbindung erhöhen.

Abstract

The non-destructive investigation of archaeological sites with magnetic gradiometry is of great importance for archaeological research since the layout of the complete site can be mapped. However, in most case studies the interpretation solely consists of an image interpretation. This does not exploit the full potential of the method since no quantitative model of the magnetic source bodies, i.e. the archaeological features, is derived. Therefore, we have developed site-specific inversion approaches for a quantitative interpretation of magnetic measurements. The inversion approaches need to be customized to the characteristics of the features to reduce ambiguity and consequently be able to yield suitable results. This thesis targets two archaeological sites with each a specific inversion approach.

The site Maidanetske (Ukraine; ~ 3950 - 3650 BCE) belongs to the Chalcolithic Cucuteni-Tripolye culture. The site comprises remains of approx. 3000 houses, that are mostly burned. Forward calculations of documented finds identify the burned clay (daub) as source of the magnetic anomalies. The daub is concentrated in a distinct depth range and the characteristics of this layer are used as *a priori* information in the inversion computations. We neglect the magnetization of the surrounding material under the assumption of a much smaller magnetization than in the burned layer. Moreover, we restrict the depth range of the magnetized layer to the depth range of the daub layer. Via inversion computations the magnetization of this layer is calculated. The magnetization distribution of three excavated buildings is compared to the mass distribution of daub to infer a magnetization-mass-relation. The quantitative interpretation of not excavated buildings then comprises two steps: the calculation of the magnetization distribution; and the application of magnetization-mass-relation to infer the total mass. The evaluation of total masses of 45 not excavated buildings indicated two different sets of buildings, possibly related to different construction types.

At the Linearbandkeramik site Vráble (Slovakia; ~ 5250 - 4950 cal BCE), the remains of the houses are accumulations of pits forming a longpit at each side of the former building. The pits were dug into the Loess and are filled with material related to the use of the house. Multi-method geophysical measurements were conducted during an excavation as part of the documentation. The joint interpretation of ground penetrating radar and electromagnetic induction measurements enabled us to image the bottom of the pits with their distinct microtopography related to their evolution. The geophysical measurements show that the bottom of the pits is in greater depth than expected due to the archaeological excavation.

Moreover, we show that the observed magnetic anomalies can not be explained solely by induced magnetization. This conclusion is derived from forward calculations of two-dimensional susceptibility distributions that were measured downhole along

profiles of densely spaced drillings crossing the pits. We derive the remanent magnetization with an inversion approach based on the susceptibility distribution. The remanent magnetization is described by the Koenigsberger ratio. For the six coring profiles, the mean Koenigsberger ratio varies between 1.8 and 7.0 with most values smaller than 4.0. Considering geoarchaeological data, the source of the remanent magnetization is determined as magnetotactic bacteria that increase the amount of ferrimagnetic iron compounds in the pit filling.

Contents

Chapter 1

Introduction

1.1 Motivation and objective

Archaeological sites are each a unique cultural heritage. Therefore, they require investigation and protection at the same time. This is also stated by the Council of Europe in the 'European Convention on the Protection of the Archaeological Heritage', the so-called *Valetta Convention*. Herein, Article 3,i,b demands that 'non-destructive methods of investigation are applied wherever possible' (cf. Trinks et al., 2018). Geophysical methods are non-destructive methods that investigate the variability of physical subsurface properties. Each method is sensitive to specific physical properties of the subsurface. In this sense, an archaeological feature can be defined as the subsurface volume that differs in one or several properties from those of the surrounding subsurface and is related to an anthropogenic origin. The purpose of geophysical measurements is to derive location, geometry and physical properties of archaeological features.

Magnetic measurements are one of the most commonly applied geophysical methods for the prospection of archaeological sites and landscapes (e.g. Gaffney, 2008; Linford, 2006). Magnetic surveys derive maps of the variation of the earth's magnetic field indicating the location and rough shape of subsurface features in form of anomalies, i.e. areas of increased or decreased measurements compared to a background level. The method is commonly applied as it has a high data acquisition speed and is suitable for a variety of different archaeological features in different geological settings (e.g. Gaffney, 2008; Linford, 2006).

In most cases, the interpretation of the generated maps stops with the identification, classification, size estimation and evaluation of the relative location of features. This kind of image interpretation does not consider the physical properties and the true subsurface geometry of the magnetic source body, i.e. the archaeological feature. Therefore, the full potential of the interpretation of magnetic survey data is not accessed by image interpretation alone. This leads to the main objective of this thesis: the development of

two interpretation schemes for a quantitative evaluation of magnetic data. With these interpretation schemes the magnetic properties or the geometry of archaeological features are derived and can be related to their archaeological properties. The result is an enlarged database with new, additional information on the features for archaeological interpretation.

In general, magnetic surveys aim at mapping entire sites whereas archaeological excavations aim at opening a small window into the site at distinct key targets. A comprehensive documentation of excavations is essential since the excavated feature is destroyed in the process of excavation (e.g. Trinks et al., 2018). Apart from standard archaeological documentation techniques, also geophysical measurements can be conducted during ongoing excavations in archaeological trenches. Even though the documentation of archaeological excavations with geophysical methods have supplementary advantages, only few examples are published (e.g Bevan, 2005; Hulin et al., 2014; Kainz, 2016). Advantages can be i.a.

(a) detection of features that are invisible to the human eye,

(b) imaging of gradual changes with high spatial resolution,

(c) detection of deeper structures and

(d) objective documentation independent from lighting conditions.

Therefore, the second objective of this thesis is to present a case study that shows how a multimethod approach is used to objectively document archaeological structures in ongoing excavations. We demonstrate how different methods image the same archaeological features, how a three-dimensional image of the features is derived and how the measurements can be incorporated in the excavation process to make it more efficient. The latter has the potential to reduce excavation time and cost since areas of special interest can be detected with geophysical documentation.

Briefly, this thesis examines three different research questions in the context of quantitative interpretation of magnetic measurements and quantitative documentation of archaeological excavations. Besides a methodical geophysical aspect each question has also the aim to derive new knowledge for the respective archaeological case study:

- How can we quantitatively interpret the magnetic map of the site Maidanetske (Ukraine), that means to derive the spatial distribution of magnetized remains of buildings and determine their masses? Can we distinguish different types of buildings based on the mass of their remains derived with this method?

- How strong is the influence of remanent magnetization as this influence is not obvious in the magnetic maps? And what does this tell us about site formation processes?

- Which geophysical methods can be applied during ongoing excavations to document the remaining part of the archaeological structure in three dimensions and how can these guide archaeological excavations?

1.2 Magnetics and inherent ambiguity

The magnetic measurements used in these studies are magnetic gradiometry measurements. Magnetic gradiometry measures the vertical component of the earth's magnetic field (B_z) in two different heights above the ground. Their difference $\Delta B_z = B_z^{h_1} - B_z^{h_2}$ is formed, where $B_z^{h_1}$ is the measurement at height h_1 above the ground and $B_z^{h_2}$ respectively at h_2 with $h_1 < h_2$. The advantage of gradiometry data compared to total field measurements is that variations in the magnetic field which affect both sensors in the same extent do not need to be considered in the data interpretation. These are on the one hand temporal variations and on the other hand regional variations of distant sources (e.g. Breiner, 1973).

Magnetic source bodies differ in their magnetization from the magnetization of the surrounding subsurface. The difference in magnetization leads to anomalies in the magnetic gradiometry measurements. These anomalies can be mapped and detected if their amplitudes are larger than the sensitivity of the sensors.

The magnetization is the sum of an induced and a remanent magnetization. The Koenigsberger ratio is the ratio between remanent and induced magnetization. The induced magnetization is dependent on the magnetic susceptibility distribution and the ambient earth's magnetic field. So the induced magnetization is parallel to the direction of the ambient earth's magnetic field whereas direction and intensity of the remanent magnetization are dependent on the process that leads to the remanent magnetization. Examples for different kinds of remanent magnetization in terms of the process are thermoremanent magnetization (TRM), detrital or depositional remanent magnetization (DRM) or chemical remanent magnetization (CRM) (e.g. Evans and Heller, 2003; Fassbinder, 2015; Moskowitz et al., 2015). Brief descriptions of these processes, that are of great importance in archaeological contexts, are:

TRM occurs when a material is exposed to temperatures above its Curie temperature and cools down again. The magnetic grains align in direction of the ambient magnetic field and this direction is fixed after cooling. Additionally, supplementary magnetic grains can form during the heating process. TRM is of great importance in archaeological contexts with kilns, bricks, pottery, burned soils and so forth.

DRM develops when particles with a magnetic moment become aligned parallel to ambient magnetic field direction and a net magnetization direction apart from random orientation settles. This effect can be important in ground depressions that can fill with water, like pits or ditches.

CRM occurs when the chemical composition of the iron-bearing minerals change or new minerals form and from this a remanent magnetization results.

The aim of a quantitative interpretation of magnetic prospection data should thus be to quantify the magnetic source bodies beyond image interpretation. Inversion calculations (cf. following section) infer the distribution of the magnetic properties in the subsurface from the measured anomalies. To quantify archaeological features by their volume, thresholds in the subsurface properties (magnetization or susceptibility) between magnetic source bodies and surrounding materials need to be defined to infer location and geometry of the source. However, because of the inherent ambiguity of potential field methods (e.g. Li and Oldenburg, 1996), different subsurface models can be derived that explain the measured data with the same accuracy. Therefore, it is necessary to incorporate *a priori* information in interpretation approaches. On the one hand, these can comprise spatial information like location, depth range or geometry (e.g. Herwanger et al., 2000; Schneider et al., 2014). On the other hand, these can comprise information about the magnetic properties, e.g. susceptibility distribution, susceptibility contrast or magnetization direction (e.g. Eder-Hinterleitner et al., 1996; Neubauer and Eder-Hinterleitner, 1997) or, thirdly, a combination of both (e.g. Cheyney et al., 2015). Spatial information can be derived from other geophysical measurements like ground penetrating radar (GPR), electromagnetic induction measurements (EMI) or electric resistivity tomography (ERT). The susceptibility can be measured directly on the features and their surroundings in excavations and downhole as well as in the laboratory on samples.

1.3 Inversion

Inversion is the concept of deriving a spatial distribution of physical subsurface parameters that would result in a set of synthetic measurements $\mathbf{d}^{syn}$ that fit the actually measured data $\mathbf{d}^{obs}$. The spatial distribution of physical subsurface parameters is called model $\mathbf{m}$ and is an approximation of the true subsurface. The calculation of synthetic measurements based on this model is called forward problem and necessitates a set of mathematical relations between the model parameters and the synthetic measurements $\mathbf{d}^{syn} = \mathbf{F}[\mathbf{m}]$ with the forward operator $\mathbf{F}$. In inversion calculations the synthetic data is compared with the observed data aiming to minimize the misfit $\Delta = \sqrt{\frac{1}{N}\sum_{i=1}^{N}(d_i^{syn} - d_i^{obs})^2}$ between the two data sets by adjusting the model parameters. There are several optimization methods described for the adjustment of the model parameters (e.g. Tarantola, 2005; Everett, 2013). The discretization of the model space and definition of the model parameters are part of the set up of inversion calculations. *A priori* information can be included by a) the discretization and parametrization and b) the setting of constraints on the model parameters.

In this thesis, inversion is applied in all three papers. In the first paper, the subsurface is discretized in regular right rectangular prisms with restricted depth range and unknown magnetization to be determined by the inversion based on the magnetic gradiometry data. In the second paper, a constant Koenigsberger ratio that is only acting on model cells with a susceptibility above a threshold is derived. The susceptibility distribution is generated with downhole measurements and tapered towards the model boundaries over a variable length. Koenigsberger ratio, threshold and taper length are the unknown model parameters that are adjusted with the inversion calculations. In the third paper, measured apparent conductivity values with the electromagnetic induction method are inverted to derive at each sample point a one-dimensional conductivity depth function. The inversions are performed by defining ten layers with fixed thicknesses and variable conductivity, that is adjusted. Finally, the one-dimensional models are stitched together to form a three dimensional conductivity distribution.

1.4 Structure of this thesis

This thesis follows the subsequent structure: first, the two site-specific inversion approaches for quantitative interpretation of magnetic gradiometry data are described. I begin with the inversion approach tailored for the Chalcolithic site Maidanetske in Ukraine (Pickartz et al., 2019). The remains of the houses are dense layers of daub, i.e. burned clay, in a distinct depth range. Therefore, we restrict the magnetization to the depth range of this layer and determine the magnetization distribution in this depth range with inversion calculations. Additional excavation data on the mass distribution of daub and pottery allows to set up a linear relation between magnetization and magnetized masses. Finally, the magnetization distribution of non-excavated buildings as well as their total mass are determined with the inversion approach and the linear relationship. The distribution of the total mass in comparison with the areal size of the houses give a first tentative indication for different construction types.

The second site-specific inversion approach targets house-accompanying pits at the Linearbandkeramik site Vráble (Pickartz et al., in review). The pits are the remains of the houses and were dug at their long side. Two-dimensional susceptibility distributions are derived from densely spaced downhole measurements of the magnetic susceptibility. These image the cross-sections of house-accompanying pits and are used to calculate arising magnetic anomalies. It is shown that a significant remanent magnetization must be taken into account. We parameterize the remanent magnetization with the Koenigsberger ratio and determine the ratio with inversion calculations. Taking laboratory analyses of soil and sediment samples into account, the source of remanent magnetization is determined as an increased amount of ferrimagnetic iron compounds in the pits originating from magnetotactic bacteria.

Finally, geophysical methods are applied in the course of an excavation at the site

Vráble to document the archaeological features within the archaeological trench (Pickartz et al., forthcoming 2020). It is described, which kind of archaeologically observed feature can be documented by which geophysical method. Furthermore, we examined how consistent the archaeological and geophysical documentations are. By combining the results of ground-penetrating radar and electromagnetic induction measurements, we derive the bottom of the house-accompanying pits and consequently a three-dimensional image of the archaeological features. Geophysical measurements during ongoing excavations can identify areas of special interest while documenting the archaeological record and therefore guide the excavation process.

Chapter 3 summarizes the results of these studies and a comprehensive conclusion is given. In chapter 4, I outline possible subsequent studies and possible methodical improvements for both targeted sites.

Chapter 2

Publications

2.1 List of publications

The following publications are part of this cumulative dissertation and can be found in the appendix:

Paper I Pickartz, N., Hofmann, R., Dreibrodt, S., Rassmann, K., Shatilo, L., Ohlrau, R., Wilken, D., Rabbel, W., 2019: Deciphering archeological contexts from the magnetic map: Determination of daub distribution and mass of Chalcolithic house remains. *The Holocene*, **29**(10), 1637-1652.
DOI: 10.1177/0959683619857238

Paper II Pickartz, N., Rabbel, W., Rassmann, K., Müller-Scheeßel, N., Furholt, M., Müller, J., Cheben, I., Wilken, D., Wunderlich, T., Dreibrodt, S., submitted. What over 100 drillings tell us: A new method for determining the Koenigsberger ratio of soils from magnetic mapping and susceptibility logging. *Archaeological Prospection*.

Paper III Pickartz, N., Corradini, E., Kahn, R., Panning, D., Rassmann, K., Müller-Scheeßel, N., Furholt, M., Wilken, D., Wunderlich, T., Rabbel, W., forthcoming 2020. Extending archaeological documentation from 2D to 3D: The benefits of geophysical on-site measurements in excavations. In Furholt, M., Cheben, I., Müller, J., Bistáková, A., Wunderlich, M. and Müller-Scheeßel, N. (eds.), *Archaeology in the Žitava valley I - The LBK and Želiezovce settlement site of Vráble*. Leiden, Sidestone Press.
ISBN: 9789088908972

2.2 Contributions

Paper I I contributed to this paper the implementation of all calculations, all Figures and the initial version of the manuscript (except section 'Tripolye megasites and the site Maidanetske').

Paper II I contributed to this paper planning and supervision of the drilling campaign, the initial idea for the study, implementation and execution of all calculations, concept of all Figures (except Fig. 2) and the initial version of the manuscript (except sections 'The archaeological site of Vráble 'Farské'', 'What is the origin of the remanence?').

Paper III I contributed to this paper planning and supervision of the *in situ* measurements, the initial concept for the paper, supervision of the EMI Inversion, concept of all Figures (except Fig. 3 and 9) and the initial version of the manuscript (except sections 'Methods - Ground Penetrating Radar', 'Results - Ground Penetrating Radar').

Chapter 3

Summary and conclusions

This thesis was focused on the development of quantitative interpretation approaches of geophysical measurements at archaeological sites and excavations with emphasis on magnetic gradiometry data. The aim of quantitative interpretation approaches is to use the full potential of magnetic data beyond image interpretation. This means to determine the magnetic parameters of the source body as summarized in the following. We showed that our results derive additional data that is relevant for the archaeological interpretation of the site or even the whole archaeological landscape.

For the site Maidanetske (Pickartz et al., 2019), we developed an inversion approach that determines the spatial distribution of the magnetized remains of non-excavated buildings, basically daub. Based on this, the total mass of the daub layer is determined. We showed that these masses in comparison to the total area of each building can indicate different construction types. An application of this interpretation approach to the complete site yields the database for statistical analysis of mass, size and relative location of the buildings. This is the base for an improved understanding of settlement structure and population estimations. Moreover, this interpretation scheme can be applied to other sites of the Cucuteni-Tripolye culture and as well sites of other cultures with archaeological features consisting of a strongly magnetized layer in a distinct depth range. For both cases, the areal distribution of the depth range of this layer and site-specific mass-magnetization relationship need to be determined by the correlation of measured mass distributions in excavations and calculated magnetization distributions. This provides the basis for gaining the same kind of results as in the presented case study.

For the site Vráble, we demonstrated how to derive a three-dimensional image of the house-accompanying pits as part of excavation documentation with multi-method measurements (Pickartz et al., forthcoming 2020). Secondly we show that a significant remanent magnetization is present in the fillings of the pits resulting from an increased amount of ferrimagnetic iron compounds created by magnetotactic bacteria (Pickartz et al., in review). The aim for further studies is to combine the available information

and results to derive an inversion approach that determines the susceptibility distribution and therefore the geometry of the the house-accompanying pits (cf. section 4.2 in the following chapter). It is assumed that the pits were formed during clay extraction for house construction (e.g. Winkelmann et al., forthcoming 2020; Pickartz et al., forthcoming 2020). Function and filling process of the pits are still a matter of research (e.g. Wolfram, 2013; Květina and Řídký, 2017), however the filling is related to the respective house (e.g. Allard et al., 2013; Müller-Scheeßel et al., in press). Estimation of the volume of pits while considering erosion can therefore be used to evaluate whether or not the pits could have supplied all clay for the respective building (Winkelmann et al., forthcoming 2020). Moreover, the erosion could yield to older pits being more shallow. Therefore, a depth estimation could be related to a chronological order. And possibly, the microtopography of the bottom of the pits could be related to their function. In summary, a determination of the pits' geometry and the comparison to archaeological data can possibly be used to determine a chronological order and to clarify the function of the pits[1].

The presented studies are each based on a combination of geophysical and archaeological fieldwork including magnetic gradiometry as well as excavations, downhole measurements and *in situ* multi-method investigations of archaeological key targets. The magnetic data yield a site-covering database. The key target investigations yield structural and physical characteristics of the archaeological targets that are essential as *a priori* information for the development of site-specific inversion approaches. Since *a priori* information limit the inherent ambiguity of magnetic data and restrict the possible solutions of in the inversion problem. For Maidanetske this is the depth range of the magnetized layer that is determined by archaeological excavations and corings and used as constraint. For Vráble the susceptibility distribution is derived in downhole measurements and is used as subsurface model to infer the magnetization.

This means that an appropriate set of *a priori* information is necessary for an efficient site-specific inversion approach. This enables a magnetically guided upscaling of key target information to the complete site and a quantitative interpretation of large-area magnetic data.

[1]Many thanks to Nils Müller-Scheeßel for the fruitful discussion about the archaeological interpretation of the pits' volume.

Chapter 4

Outlook

In this chapter I outline further research ideas that extend the approaches of this thesis. The chapter is divided into two sections to address the archaeological targets with different characteristics.

4.1 Ideas concerning Maidanetske

Aspects for further research at the site Maidanetske or with the interpretation approach are:

(a) Automatization e.g. with computer aided object detection

(b) Application to complete site followed by a statistical analysis of mass, size and relative location of the buildings

(c) Reevaluation of mass-magnetization relation when additional data of masses from other buildings is available

(d) Application of interpretation scheme to other sites of the Cucuteni-Tripolye culture e.g. Taljanky and Dobrovody in the vicinity of Maidanetske (e.g. Rassmann et al., 2016)

The integration of computer-aided object detection (e.g. Verdonck et al., 2019) into the inversion approach for the detection of anomalies of buildings can lead to an automatization of the complete quantitative inversion approach without manual object selection. There might be the need to develop a highly specified algorithm, since the anomalies of the buildings show also individual patterns apart from rotation and size despite their overall similarities. These individual characteristics might be related to different burning conditions, different degrees of preservation or a different inventory of movable items (e.g. pottery, tools). In any case, a fully automated quantitative interpretation routine can not only be applied to the complete site Maidanetske but also to other sites of the Cucuteni-Tripolye culture, that comprise burned house remains which can be approximated by a magnetized layer (e.g. Rassmann et al., 2014; Mischka et al.,

2016; Müller et al., 2016; Ţerna, 2016). When applying the interpretation approach to other sites, it must be evaluated if the magnetization-mass relation holds also for these sites or if it must be replaced by a site-specific relationship.

Apart form the assumption of negligible magnetization in the layers above and below the thermoremanent magnetized layer, the only *a priori* information included in this inversion approach (Pickartz et al., 2019) are depth and thickness of the magnetized layer. So far we used depth information based on corings or excavations that were extrapolated to anomalies of other buildings in the vicinity. However, the site is located at a slope and the thickness of the sediments above the magnetized layer is variable due to erosion and agricultural activities. Therefore, a simple extrapolation of the depth information to greater distances is not reliable. Consequently, a valuable addition to the existing interpretation scheme are reliable depth information of the magnetized layer, i.e. the daub layer. However, due to the ambiguity of potential field data, magnetization and depth information of the magnetic source can not be inferred simultaneously. There are several methods published (e.g. Nabighian et al., 2005; Li and Nabighian, 2015) that allow a depth estimation of the magnetic source body based on solely magnetic prospection data. Desvignes et al. (1999) tested four methods in the context of archaeological prospection and concluded that the Euler deconvolution with a structural index of 2 yields good results. A next step could be to test the Euler deconvolution for synthetic data representing anomalies of the house remains. If these tests yield positive results an application to features with known depth range can reveal the feasibility for the actual field data.

If the tests fail that are based solely on the magnetic data, the integration of additional data can be considered. With regard to the size of the site and the huge number of buildings, it is favorable to derive the depth of the layer with a prospection method that is feasible to cover large areas in reasonable time. It was not possible to detect the houses with first, unpublished tests of GPR measurements. However, some could be detected in ERT measurements and in the in-phase component of EMI measurements. Since the survey speed is much faster for EMI surveys than for ERT measurements, I propose to include the evaluation of EMI measurements in the interpretation scheme. For example, Benech et al. (2002) and Pétronille et al. (2010) present two studies of joint interpretation of magnetic prospection and EMI data. However, the depth of the source is also estimated via Euler deconvolution but crosschecked with the two independent data sets.

If the joint interpretation of EMI and magnetics also does not yield satisfying results, ERT and corings with downhole susceptibility measurements can be applied. It is plausible that the daub layer produces an interface in the same depth in both, the susceptibility and resistivity distribution. This can be expected since the daub is a dense material, that does not absorb moisture in the same manner as the surrounding material. Since the resistivity is also dependent on the water content, the boundaries can be in similar

depths. However, it needs to be evaluated if the resolution of ERT measurements is sufficient to resolve the layer thickness. This can be analyzed with modeling studies (e.g. Wunderlich et al., 2015). Advantageous of ERT can be the examination of more than one building with a single profile (dependent on the profile length) and depth information from the house remains along cross-sections. Latter can be used to calculate an average value for depth and thickness for each building. For corings with downhole measurements, one advantage is the direct observation of respective layer in undisturbed cores. Another advantage is the direct measurement of susceptibility depth functions as subsurface property that is directly related to the magnetic gradiometry. When the analysis of the complete site relates on ERT or corings, a systematic field procedure needs to be developed, most probably incorporating interpolation of the depth information.

Apart from determining the depth range of the daub layer throughout the site, another possibility can be to determine the thickness of the surface layer (~ plowing layer) that approximately reaches the top of the daub layer. For this purpose also modeling studies are necessary to evaluate the resolution and the best configurations for the measurements. An advantage of this approach is that a varying thickness of the surface layer can be determined and interpolated. Moreover, this approach is independent of the difficulty to detect the lower boundary of an anomalous body. This can be challenging as shown by e.g. Wunderlich et al. (2015). However, this approach does not determine the vertical extension of the daub layer.

Summarizing, there are several possibilities to gain depth information about the magnetized layer that are more elaborated than simple average values of existing ground truth data. Further tests need to be conducted to find the most suitable method.

4.2 Ideas concerning Vráble

Concerning the site Vráble and the related studies, following points could be part of further research:

(a) Combination of pit geometry derived from multi-method *in situ* measurements, together with susceptibility data and remanence as three-dimensional model for gradiometry forward calculations; model adjustment based on comparison of model response and measurements

(b) Alteration of parametrization of Koenigsberger ratio (e.g. more thresholds; experimental relationship between susceptibility and Koenigsberger ratio)

(c) Development of an inversion scheme to derive susceptibility distribution of house-accompanying pits and quantify pits' volume (ideally including automatization e.g. with computer aided object detection; cf. section 4.1)

(d) Application of interpretation approaches to settlements in the Žitava valley with magnetic gradiometry data (cf. Müller-Scheeßel et al., 2020)

The *in situ* documentation of the house-accompanying pits during the excavation yielded a three-dimensional image of their geometry (Pickartz et al., forthcoming 2020). The susceptibility distribution of these and other pits are know from downhole, *in situ* and laboratory measurements. In addition, the range of the Koenigsberger ratio was determined by Pickartz et al. (in review). The combination of these information fully describes the magnetic source and enables detailed forward modeling. Since the susceptibility distribution of the documented pit is not measured throughout the complete pit, adjustments of the starting model are going to be necessary. The final susceptibility distribution can be compared to the archaeological documentation of the pit filling to evaluate possible relations. The microtopography of the pit is related to the step by step extension of the pit. This could be connected to different uses of the single pits and reflected in different susceptibility or magnetization ranges.

The evaluation of the inversion results for determining the Koenigsberger ratio (Pickartz et al., in review) showed that a difference between measured data and calculated data remains for some profiles. This could indicate that the parametrization is not complex enough to enable a fit between modeled and observed data. Consequently, an improvement of this inversion approach would incorporate a more complex distribution of the remanent magnetization. One possibility would be to determine a Koenigsberger ratio for each model cell. In this case further constraints are needed to reduce the number of possible solutions and to avoid overfitting. It could be tested if as part of the inversion also an empirical relation between susceptibility values and Koenigsberger ratio can be found for the site. This might be a reasonable approach since Tabbagh (1984) states that features with remanent magnetization also have a high susceptibility. Another possibility would be to increase the number of thresholds t in the susceptibility values κ and the number of related Koenigsberger ratio values Q. Adding one additional range for the Koenigsberger ratio with the constraints

$$\begin{aligned} & \kappa \leq t_1: && Q = 0 \\ t_1 < & \kappa \leq t_2: && Q = Q_1 \\ t_2 < & \kappa : && Q = Q_2 \end{aligned}$$

with $1 < Q_1 < Q_2$ and $t_1 < t_2$ increases the number of parameters by two. The resulting zones of different Koenigsberger ratio values can be interpreted as a zone with no remanent magnetization (~ undisturbed Loess), a zone with intermediate Koenigsberger ratio (~ pit fill with increased amount of aligned ferrimagnetic iron compounds) and a zone with high Koenigsberger ratio (~ material with thermoremanent magnetization). Of course more zones can be added if necessary. A refined parametrization of the Koenigsberger ratio can improve the fit between calculated and observed magnetic data. Besides this, possible relations between the archaeological record or post-depositional process can be detected.

In the last chapter, I outlined that the volume or geometry of the pits can be related to their chronological order or their function. Consequently, main aim of further research

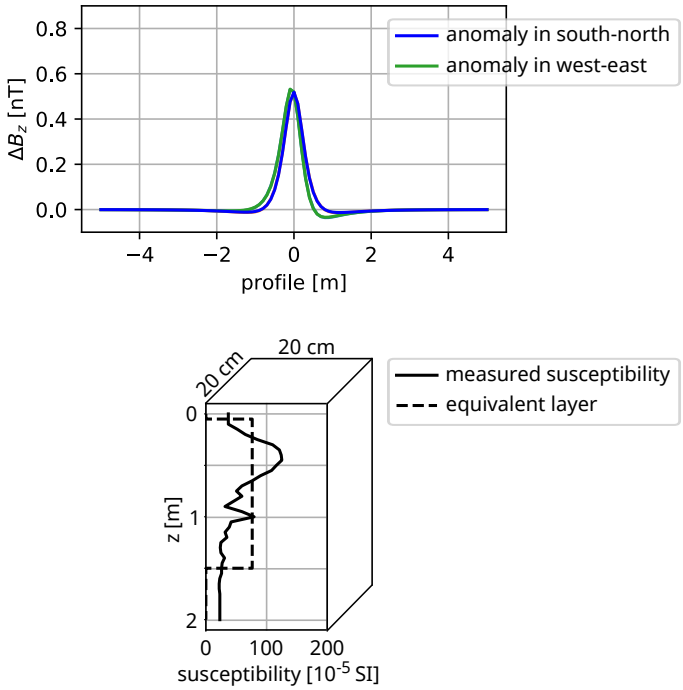

Figure 4.1: Measured susceptibility depth curve (solid line) and respective equivalent layer (dashed line) models (bottom), that both yield the same gradiometry anomaly (top).

should be the development of an inversion approach that quantifies the volume of the pits. First, very preliminary tests including an artificial neural network[1] (ANN) were conducted. The idea consists of the following steps:

1. Every measured susceptibility depth function is represented by an equivalent layer in fixed depth range. The susceptibility of the equivalent layer is chosen in a manner, that both subsurface models produce the same magnetic anomaly (see Fig. 4.1).

2. Inversion of the gradiometry data under the assumption of an equivalent layer (same depth extension as above). This yields a two-dimensional distribution of susceptibilities for the equivalent layer.

3. Train an ANN the mapping between susceptibility of the equivalent layer and the respective measured susceptibility depth curve.

4. Use the ANN to find a susceptibility depth curve for each susceptibility from the equivalent layer inversion. This yields a three-dimensional susceptibility distribution as a base to quantify the volume of the pits.

[1] `https://scikit-learn.org/stable/modules/generated/sklearn.neural_network.MLPRegressor.html`

The first tests were promising, however optimum parameters for the equivalent layer and the set up of the ANN still need to be found. Furthermore, it needs to be evaluated if the training set is large enough. If the tests with this approach fail, the algorithm by Li and Oldenburg (1996) seems promising as it successfully derives three-dimensional susceptibility models .

Bibliography

Allard, P., Hamon, C., Bonnardin, S., Cayol, N., Chartier, M., Coudart, A., Dubouloz, J., Gomart, L., Hachem, L., Ilett, M., Meunier, K., Monchablon, C. and Thevenet, C. (2013) Linear Pottery domestic space: Taphonomy, distribution of finds and economy in the Aisne valley settlements. In *The domestic space in LBK settlements. Nanterre (France), 7-8 October 2010* (eds. C. Hamon, P. Allard and M. Ilett), 9–28. Rahden/Westf.: M. Leidorf.

Benech, C., Tabbagh, A. and Desvignes, G. (2002) Joint inversion of EM and magnetic data for near-surface studies. *Geophysics*, **67**, 1729–1739.

Bevan, B. (2005) Geophysics in Excavations. *Tech. Rep. 11*, Geosight, Weems, VA, USA.

Breiner, S. (1973) *Applications manual for portable magnetometers*. Geometrics Sunnyvale, California.

Cheyney, S., Fishwick, S., Hill, I. A. and Linford, N. T. (2015) Successful adaptation of three-dimensional inversion methodologies for archaeological-scale, total-field magnetic data sets. *Geophysical Journal International*, **202**, 1271–1288.

Desvignes, G., Tabbagh, A. and Benech, C. (1999) The determination of the depth of magnetic anomaly sources. *Archaeological Prospection*, **6**, 85–105.

Eder-Hinterleitner, A., Neubauer, W. and Melichar, P. (1996) Reconstruction of archaeological structures using magnetic prospection. *Analecta Praehistorica Leidensia*, **28**, 131–137.

Evans, M. E. and Heller, F. (2003) *Environmental Magnetism: Principles and Applications of Enviromagnetics*. San Diego: Academic Press.

Everett, M. E. (2013) *Near-Surface Applied Geophysics*. New York: Cambridge University Press.

Fassbinder, J. W. (2015) Seeing beneath the farmland, steppe and desert soil: magnetic prospecting and soil magnetism. *Journal of Archaeological Science*, **56**, 85–95.

Gaffney, C. (2008) Detecting Trends in the Prediction of the Buried Past: A Review of Geophysical Techniques in Archaeology. *Archaeometry*, **50**, 313–336.

Herwanger, J., Maurer, H., Green, A. and Leckebusch, J. (2000) 3-D inversions of magnetic gradiometer data in archeological prospecting: Possibilities and limitations. *Geophysics*, **65**, 849–860.

Hulin, G., Prilaux, G. and Talon, M. (2014) Intégration de la géophysique à un projet archéologique d'envergure. L'exemple du projet canal Seine-Nord-Europe. *Revue archéologique de Picardie*, **1**, 245–260.

Kainz, J. (2016) An Integrated Archaeological Prospection and Excavation Approach at a Middle Neolithic Circular Ditch Enclosure in Austria. In *Digital Methods and Remote Sensing in Archaeology* (eds. M. Forte and S. Campana), 371–403. Cham: Springer International Publishing.

Květina, P. and Řídký, J. (2017) Neolithic settlement space waste, deposition and identity. In *Archaeologies of waste: encounters with the unwanted* (eds. D. Sosna and L. Brunclíková), 127–144. Oxford: Oxbow Books.

Li, Y. and Nabighian, M. (2015) Tools and Techniques: Magnetic Methods of Exploration – Principles and Algorithms. In *Treatise on Geophysics - Volume 11* (ed. G. Schubert), 335–391. Amsterdam: Elsevier.

Li, Y. and Oldenburg, D. W. (1996) 3-D inversion of magnetic data. *Geophysics*, **61**, 394–408.

Linford, N. (2006) The application of geophysical methods to archaeological prospection. *Reports on Progress in Physics*, **69**, 2205–2257.

Mischka, C., Mischka, D. and Rubel, A. (2016) Geomagnetic survey of Cucuteni-Settelments in Moldova – Results of the FAU – Campaign 2015. *Arheologia Moldovei*, **XXXIX**, 333 – 345.

Moskowitz, B., Jackson, M. and Chandler, V. (2015) Geophysical Properties of the Near-Surface Earth: Magnetic Properties. In *Treatise on Geophysics - Volume 11* (ed. G. Schubert), 139–174. Amsterdam: Elsevier.

Müller, J., Rassmann, K. and Videiko, M. (2016) *Trypillia Mega-sites and European Prehistory: 4100-3400 BCE*. London and New York: Routledge.

Müller-Scheeßel, N., Cheben, I., Filipović, D., Hukelová, Z. and Furholt, M. (in press) The LBK site of Vráble in Southwestern Slovakia: Selected results of the excavation season 2016. *Bericht der Römisch-Germanischen Kommission*, **97**.

Müller-Scheeßel, N., Müller, J., Cheben, I., Mainusch, W., Rassmann, K., Rabbel, W., Corradini, E. and Furholt, M. (2020) A new approach to the temporal significance of house orientations in European Early Neolithic settlements. *PLOS ONE*, **15**, e0226082.

Nabighian, M. N., Grauch, V. J. S., Hansen, R. O., LaFehr, T. R., Li, Y., Peirce, J. W., Phillips, J. D. and Ruder, M. E. (2005) The historical development of the magnetic method in exploration. *Geophysics*, **70**, 33ND–61ND.

Neubauer, W. and Eder-Hinterleitner, A. (1997) 3D-interpretation of postprocessed archaeological magnetic prospection data. *Archaeological Prospection*, **4**, 191–205.

Pickartz, N., Rabbel, W., Rassmann, K., Müller-Scheeßel, N., Furholt, M., Müller, J., Cheben, I., Wilken, D., Wunderlich, T. and Dreibrodt, S. (in review) What over 100 drillings tell us: A new method for determining the koenigsberger ratio of soils from magnetic mapping and susceptibility logging. *Archaeological Prospection*.

Pickartz, N., Corradini, E., Kahn, R., Panning, D., Rassmann, K., Müller-Scheeßel, N., Furholt, M., Wilken, D., Wunderlich, T. and Rabbel, W. (forthcoming 2020) Extending archaeological documentation from 2d to 3d: The benefits of geophysical on-site measurements in excavations. In *Archaeology in the Žitava valley I - The LBK and Želiezovce settlement site of Vráble* (eds. M. Furholt, I. Cheben, J. Müller, A. Bistáková, M. Wunderlich and N. Müller-Scheeßel). Leiden: Sidestone Press.

Pickartz, N., Hofmann, R., Dreibrodt, S., Rassmann, K., Shatilo, L., Ohlrau, R., Wilken, D. and Rabbel, W. (2019) Deciphering archeological contexts from the magnetic map: Determination of daub distribution and mass of Chalcolithic house remains. *The Holocene*, **29**, 1637–1652.

Pétronille, M., Thiesson, J., Simon, F.-X. and Buchsenschutz, O. (2010) Magnetic signal prospecting using multiparameter measurements: the case study of the Gallic Site of Levroux. *Archaeological Prospection*, **17**, 141–150.

Rassmann, K., Korvin-Piotrovskiy, A., Videiko, M. and Müller, J. (2016) The New Challenge for Site Plans and Geophysics: Revealing the Settlement Structure of Giant Settlements by Means of Geomagnetic Survey. In *Trypillia Mega-sites and European Prehistory: 4100-3400 BCE* (eds. J. Müller, K. Rassmann and M. Videiko). London and New York: Routledge.

Rassmann, K., Ohlrau, R., Hofmann, R., Mischka, C., Burdo, N., Videjko, M. Y. and Müller, J. (2014) High precision Tripolye settlement plans, demographic estimations and settlement organization. *Journal of Neolithic Archaeology*, **16**, 96–134.

Schneider, M., Linzen, S., Schiffler, M., Pohl, E., Ahrens, B., Dunkel, S., Stolz, R., Bemmann, J., Meyer, H.-G. and Baumgarten, D. (2014) Inversion of Geo-Magnetic SQUID Gradiometer Prospection Data Using Polyhedral Model Interpretation of Elongated Anomalies. *IEEE Transactions on Magnetics*, **50**, 1–4.

Tabbagh, A. (1984) On the Comparison between Magnetic and Electromagnetic Prospection Methods for Magnetic Features Detection. *Archaeometry*, **26**, 171–182.

Tarantola, A. (2005) *Inverse Problem Theory and Methods for Model Parameter Estimation*. Philadelphia: Society for Industrial and Applied Mathematics.

Trinks, I., Hinterleitner, A., Neubauer, W., Nau, E., Löcker, K., Wallner, M., Gabler, M., Filzwieser, R., Wilding, J., Schiel, H. and et al. (2018) Large-area high-resolution ground-penetrating radar measurements for archaeological prospection. *Archaeological Prospection*, **25**, 171–195.

Verdonck, L., De Smedt, P. and Verhegge, J. (2019) Making sense of anomalies: Practices and challenges in the archaeological interpretation of geophysical data. In *Innovation in Near-Surface Geophysics* (eds. R. Persico, S. Piro and N. Linford), 151–194. Amsterdam: Elsevier.

Winkelmann, K., Bátora, J., Kalmbach, I. H. J., Müller-Scheeßel, N. and Rassmann, K. (forthcoming 2020) Revealing the general picture. Magnetic prospection on the multiperiod site Fidvár/Veľké Lehemby/Farské near Vráble (Slovakia). In *Archaeology in the Žitava valley I - The LBK and Želiezovce settlement site of Vráble* (eds. M. Furholt, I. Cheben, J. Müller, A. Bistáková, M. Wunderlich and N. Müller-Scheeßel). Leiden: Sidestone Press.

Wolfram, S. (2013) Two sides of the coin: ceramic taphonomy and domestic space in the Linear Pottery settlements Hanau-Klein-Auheim and Eythra (Germany). In *The domestic space in LBK settlements. Nanterre (France), 7-8 October 2010* (eds. C. Hamon, P. Allard and M. Ilett), 79–90. Rahden/Westf.: M. Leidorf.

Wunderlich, T., Wilken, D., Andersen, J., Rabbel, W., Zori, D., Kalmring, S. and Byock, J. (2015) On the Ability of Geophysical Methods to Image Medieval Turf Buildings in Iceland: Geophysical Imaging of Turf Buildings. *Archaeological Prospection*, **22**, 171–186.

Ţerna, S. (2016) Geomagnetic surveys of the Neolithic and the Copper Age sites from the Republic of Moldova (1968-2016): main results, current state and future perspectives. *Raport*, **11**, 187–225.

Eidesstattliche Erklärung

Hiermit versichere ich, die vorliegende Arbeit selbstständig verfasst und keine anderen als die angegebenen Quellen und Hilfsmittel benutzt sowie die Zitate deutlich kenntlich gemacht zu haben.
Ich erkläre weiterhin, dass die vorliegende Arbeit in gleicher oder ähnlicher Form noch nicht im Rahmen eines anderen Prüfungsverfahrens eingereicht wurde.
Die Arbeit entstand unter Einhaltung der Regeln guter wissenschaftlicher Praxis der Deutschen Forschungsgemeinschaft.
Desweiteren wurde mir kein akademischer Grad entzogen.

Kiel, den 15. Juni 2020 Natalie Marie Pickartz

Appendix A

Publications

A.1 Paper I

Published in *The Holocene*, Vol. 29, Issue 10, Pages 1637–1652.

Deciphering Archaeological Contexts from the Magnetic Map: Determination of Daub Distribution and Masses of Chalcolithic House Remains

Natalie Pickartz[1,2], Robert Hofmann[1,3], Stefan Dreibrodt[1,4], Knut Rassmann[5], Liudmyla Shatilo[1,3], René Ohlrau[3], Dennis Wilken[1,2], and Wolfgang Rabbel[1,2]

[1]Collaborative Research Center 1266, Kiel University, Kiel, 24118, Germany
[2]Institute of Geosciences, Kiel University, Kiel, 24118, Germany
[3]Institute of Pre- and Protohistoric Archaeology, Kiel University, Kiel, 24118, Germany
[4]Institute of Ecosystem Research, Kiel University, Germany
[5]Römisch-Germanische Kommission, German Archaeological Institute, Germany

Abstract

The unique size and development of the prehistoric megasites of the north Pontic Cucuteni-Tripolye Chalcolithic groups (4100-3600 BCE) challenges modern archaeology and palaeoecology. The extremely large number of houses (about 3000, mostly burned) necessitates the development of multidisciplinary technologies to gain a holistic understanding of such sites. In this contribution, we introduce a novel geophysical methodology and a detailed analysis of magnetic data - including evolved modelling techniques - to provide critical information about the setup of findings, enabling the thorough understanding of the settlement dynamics apart from invasive excavation techniques. The case study is based upon data from magnetic field maps and distribution maps of the find categories daub and pottery. This information is used to infer magnetic models for each find category to numerically calculate their magnetic fields for comparison with the archaeological data. The comparison quantifies the sensitivity of the magnetic measurements with respect to the distribution of the different find categories. Next, via inversion computation, the characteristic depth functions of soil magnetization are used to generate maps of magnetization from the measured magnetic field maps. To validate the inverted soil magnetization maps the magnetic excavation models are used, providing an interpretational frame for the application to magnetic anomalies outside excavated areas. This joint magnetic and archaeological methodology allows estimating the find density and testing hypotheses about burning processes of the houses. In this paper we show internal patterns of burned houses comparable to archaeological house models and their calculated masses as examples of the methodology. An application of the new approach to complete megasites has the potential to enable a better understanding of the settlement structure and its evolution, to improve the quality of population estimations and thus calculating the human impact on the forest steppe environment and addressing questions of resilience and carrying capacity.

Keywords: Cucuteni-Tripolye, daub, inversion, magnetics, magnetization, modeling, prehistoric sites, quantification, tripolye megasites, Ukraine

1 Introduction

Since the 1980s magnetic surveys have found increasing acceptance as a prospecting method for mapping archaeological sites. This trend was caused by the advantages of the method: it allows rapid data acquisition – especially if motorized – and reveals the location and contours of subsurface findings such as buildings, pits and ditches situated in a variety of geological set-ups if they show a magnetization contrast to the surrounding soil (e.g. Gaffney, 2008; Linford, 2006; Fassbinder,

2015; Cheyney et al., 2015). Usually, as a final product, the measured magnetic data are depicted in form of maps, basically areal greyscale images of the magnetic field strength. These images are usually visually interpreted, the findings are located and excavations or drillings can be planned. Magnetic maps are typically used to answer three questions: Which kind of finding? Where is it located? What horizontal extent does it have?

In Tripolye giant-settlements magnetic prospections have been conducted already since the 1970s, initially by Soviet and Ukrainian Archaeologists and since 2009 by Ukrainian-British and Ukrainian-German teams (Дудкин, 1978; Кошелев, 2004; Дудкін, 2007; Chapman et al., 2014; Rassmann et al., 2014; Videiko and Rassmann, 2016). In combination with air photography and numerous excavations, in particular magnetic surveys contributed decisively to the realization of the unique character of these settlements. Not only their size of up to 320 ha and their centripetal spatial layout is extraordinary but also the extremely good visibility of thousands of pits and predominantly burned residential houses and communal buildings.

Prime objective of the research conducted in the frame of the Collaborative Research Center 1266 'Scales of Transformations' is to gain a better understanding of the nature of the at European Scale unique settlements. Which social or political transformations triggered the agglomeration of thousands of people in Tripolye megasites between 4200 and 3600 BCE and how was the social and economic space organized within these settlements? Is there a measurable reflection of such processes within the archaeo-magnetic record? How can we understand the development in the Tripolye areas in a trans-regional perspective, for example in relation to neighbouring cultures in the Caucasus and the Carpathian Basin and which social, environmental or economic factors caused and influenced their decline?

In addressing these and other questions geophysical methods, in particular magnetic prospections, are of crucial importance. The considered site of the Cucuteni-Tripolye culture consist of several thousands of buildings covering several hundred hectares. Therefore, extensive invasive research is neither feasible nor admissible. Yet, the question of the internal distribution of findings arises for a thorough understanding of the settlement dynamics. Inevitably, this is directly related to the question of how much preserved archaeological material in a particular depth range exists. Transferring this to the interpretation of magnetic data, the question is: Can we determine the spatial extension of the archaeological material from its magnetic properties and the observed magnetic anomalies?

This result cannot be achieved from the analysis of magnetic measurements alone because different subsurface settings, involving depth, size and magnetization of magnetic bodies, exist, which may produce similar magnetic anomalies. Constraining information about the subsurface is necessary to overcome the ambiguity. Constraints can be gained through other geophysical prospection methods as well as through exemplary drillings and excavations.

Here, we present a novel concept of quantitative interpretation of magnetic prospection data focusing on excavation and drilling results as interpretational constraints to overcome this substantial methodical problem. Thus, our paper has the following prime objectives:

1. develop a method to derive the spatial distribution of the magnetic sources,
2. develop a method to derive the masses of the magnetic sources,
3. exemplarily apply the new interpretation approach to the Chalcolithic site Maidanetske with the goal to extrapolate results of excavations to the whole settlement area in the sense of a magnetically guided upscaling.

2 Tripolye Megasites and the site Maidanetske

Between about 4150 and 3600 BCE up to 320 ha large settlements emerged in the Southern Bug-Dnieper interfluve with very distinct concentric spatial layout, central free spaces, public buildings and thousands of mostly burned dwellings (Menotti and Korvin-Piotrovskiy, 2012; Müller et al., 2016c). The Chalcolithic settlements were termed 'Tripolye megasites' during their intensive

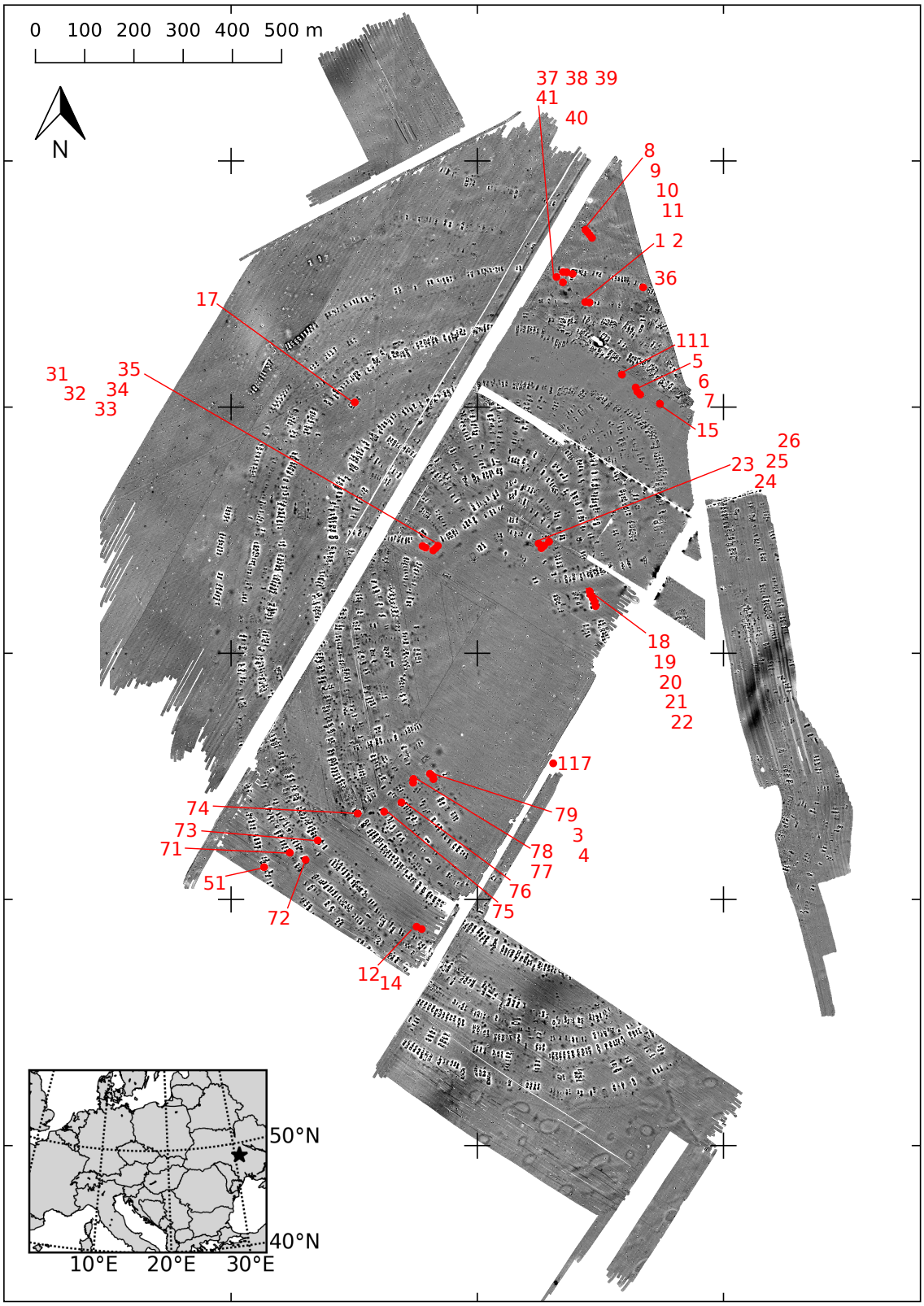

Figure 2.2.1: Magnetic map of the site Maidanetske (white: -10 nT, black +10 nT). The examined buildings and trenches are marked. Especially, the three completely excavated buildings are house 44 (here in trench no. 51), house 54 (here marked with consecutive number no. 33) and the megastructure (here in trench no. 111). In the lower left corner the location of Maidanetske is marked with a star.

archaeological investigation of more than 100 years (Videiko and Rassmann, 2016). Already since Soviet times advanced research techniques such as aerial photography, extensive magnetic surveys and large-scale excavations are used to investigate these sites (Шишкін, 1985; Дудкин, 1978). It is discussed partly controversially, if these sites represent proto-Urban settlements, large nucleated villages or meeting places used seasonally only (Шмаглий and Видейко, 2005; Chapman and Gaydarska, 2016; Chapman, 2017; Müller et al., 2018).

The subsistence in these 'giant settlements' was based on the cultivation of cereals and other crop plants and livestock farming mainly of cattle (Журавльов, 2008; Kirleis and Dal Corso, 2016; Dal Corso et al., 2018). Higher levels of craft specialization are indicated by highly developed and standardized ceramic vessels and kilns of a technologically advanced type (Korvin-Piotrovskiy et al., 2016). Models of cattle-drawn sledges prove the adaption or invention of new transportation techniques which probably made such population agglomerations possible (Shatilo, 2017).

Beside the large settlements of Talianki (48°48' 17.8" N, 30°31' 56.0" E), Nebelivko (48°38' 21.1" N, 30°33' 38.5" E) and Dobrovody (48°45' 29.0" N, 30°22' 45.6" E), the site Maidanetske (48°48' 25.9" N, 30°41' 05.8" E) (Figure 2.2.1), with a size of about 200 ha, represents one of the largest megasites which belongs to the Tomashivka regional group and the advanced stage of Tripolye-development (Tripolye C1). This site is in the focus of a Ukrainian-German cooperation. It attempts to gain a better understanding of the nature of these so-called 'megasites' based on reconstructions of the site development, environmental conditions, subsistence and economic strategies, socio-political organisation and underlying population processes (Відейко et al., 2015a; Müller and Videiko, 2016; Müller et al., 2017). For Maidanetske a significantly longer chronological range of settlement activities of 300–350 years between about 3950 and 3650 BCE is suggested by additional radiocarbon dates, in contrast to earlier chronological models, which assumed for Tripolye sites very short occupations of clearly less than 100 years (Müller et al., 2016a; Ohlrau, 2018).

Different types of architecture are known through surveys and excavations: Thousands of domestic dwellings of the Tomashivka regional group show specific constructive characteristics and a high degree of standardisation (Chernovol, 2012). Most striking are massive, originally uplifted platforms in the houses consisting of wooden sub-constructions and partly thick covering layers of chaff-tempered and un-tempered clay. Relatively lightweight walls of the upper storage supported rounded roofs which can be identified in Chalcolithic house models (Shatilo, 2016). The houses showing a very standardized internal division in mostly two and sometimes three rooms, internal furnishing with ovens, installations, grinding stones and numerous ceramic vessels preserved at the place of their use. 'Standard houses' with anteroom and main room are distinguished from longer and rarer 'extended houses' with one additional chamber for workshops (cf. Figure 2.2.7).

Another category of buildings are so-called 'megastructures' which are interpreted as communal facilities due to their highly visible positioning in the public space of the settlement (Ohlrau, 2015; Burdo and Videiko, 2016; Chapman et al., 2016; Müller et al., 2016b). In contrast to domestic dwellings such buildings do not show an elevated platform but only a simple floor applied on the underlying terrain surface (Korvin-Piotrovskiy et al., 2016). Frequently, in the magnetic map of megastructures, in particular the debris of relatively lightweight constructed external walls is visible while, in contrast, the internal surface either appears largely empty or shows varying masses of debris from collapsed walls.

The vast majority of houses in Tripolye settlements show traces of burning in varying intensity. In Maidanetske almost 80 % of the buildings are clearly burned while the condition of the remaining ones is less clear. Findings of clearly burned domestic dwellings usually consist mainly of the highly fired and dropped down platform. On top of this platform are found: daub remains of the internal wall, separating anteroom and main room, foundation remains of an oven, a central clay installation, a podium on the longitudinal side, and sometimes storage bins (cf. Fig. 2.2.7). In addition there are grinding stones and larger quantities of ceramic vessels. Together with the overlying daub of the external wall, these remains form a dense package of highly magnetized materials.

Weak visible house remains which are usually classified as 'partly burned', 'eroded', 'unburned' or 'maybe burned' house remains, represent the most frequent (20 %) deviation from standard

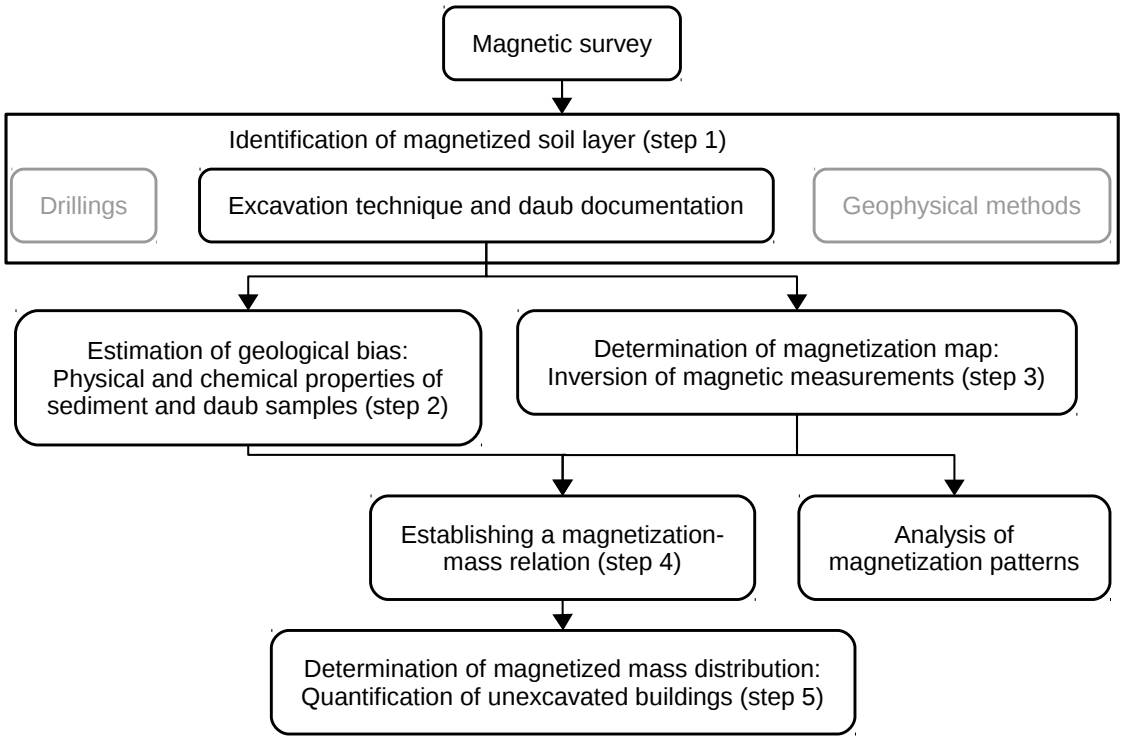

Figure 2.2.2: Flowchart of the novel interpretation scheme with the steps 1 - 5 (cf. 'Methodical details').

houses. Two of such objects were excavated in Nebelivko. Indeed they contained a normal amount of partly secondary burned pottery and some burned installations. Yet, very few and fragmented daub, that was partly vitrified was unearthed (Відейко et al., 2015b). Based on these observations, the excavators interpret the features as remains of houses which consisted mainly of wood and only low amount of daub. Assuming the deliberate character of the house burning, insufficient addition of fuel and resulting lower burning temperatures was suggested as alternative explanation (Chapman, 2017). Further scenarios take into account the character of these buildings as non-residential storage buildings or as dwellings which were abandoned during the occupation of the settlement (Diachenko, 2016).

3 Methodical development and data acquisition

3.1 Interpretation concept for magnetic data of large settlements

The archaeological investigation of a settlement with the dimension of Maidanetske needs an appropriate excavation design based on well-defined research questions. Taking the enormous size of the settlement into account only very small excavation windows can be opened. Minimizing the size of the excavation areas is not only an aspect related to the research strategy, it is also a necessary condition for respecting heritage management guidelines and to protect the archaeological archives.

The vast majority of houses needs to be identified and classified on the basis of areal magnetic measurements alone. Whereas locating house remains on a magnetic map is straightforward, a joint effort combining geophysical computation with soil and find analyses is needed to perform a quantitative interpretation of the magnetic field data.

In this respect we develop an approach allowing to answer the questions (1) how the magnetized

material associated with each house is spread out in depth and horizontally, and (2) how much of this material is present.

Before getting into the details of the analysis procedure we present an overview of its components and of how they interfinger in this section. Because of its principal ambiguity, magnetic model development can only be performed under certain given preconditions. First, we explain the assumptions on which the novel interpretation approach is based, followed by an outline of the concept itself. Next, the methodical details for every step are described.

In the then following section 'Numerical modelling of magnetic anomalies' we investigate how different find categories contribute to generating magnetic field anomalies. We use the digitally documented spatial distribution of daub and pottery of a megastructure which was excavated in 2016. This data is converted into a magnetic subsurface model, for which synthetic magnetic data are computed. The comparison of the observed and modelled data illustrates the model quality, the spatial correlation of each digitally documented find category is shown by the model itself.

Having identified the magnetically most significant material (which is daub in our case) we follow the interpretation scheme illustrated in Figure 2.2.2. It consists of the following steps:

Step 1 Identification of depth and thickness of the magnetized soil layer: Given the magnetic field data the depth and depth range of soil layer containing the magnetic material has to be identified by exemplary drillings and excavations. This information serves as a numerical constraint under which the distribution of the magnetized material is determined by a so-called inversion computation from the magnetic data. This is necessary because the spatial distribution of magnetic material cannot be found from magnetic mapping alone since the magnetic anomalies are ambiguous with respect to shape, depth and volume-specific magnetization of subsurface materials. Alternatively to drilling and excavation, these depth constraints could also be gained through depth-sensitive geophysical methods if the depth functions of the respective physical soil parameters correlate with magnetization. In the present case, we can limit the magnetic layer to a specific depth range, which is justified by the excavations at the Cucuteni-Tripolye sites. They showed that the remains of the buildings form a dense layer with a high fraction of daub in a specific depth range. The horizons above and beneath this archaeological layer show a homogeneous solely induced magnetization and can therefore be neglected in the calculations.

Step 2 Estimation of geological bias: Since the procedure of mass determination relies on the applicability of a general, though location-specific, mass-magnetization relation (step 3) it has to be checked if bias exists in form of a spatial variability of potentially magnetic geological layers. To investigate this, daub samples, soils and sediments were investigated considering their elemental composition and magnetic susceptibility. Since the source material of the daub is the local loess, the variability of the loess was also determined for enabling a respective assessment.

Step 3 Determination of magnetization map: Using the depth information from step 1 the areal distribution of magnetization is determined inside the magnetic layer from the magnetic survey data by an inversion. This results in a map showing the magnetization distributionthat is in accordance with the measured magnetic field strength.

Step 4 Establishing a magnetization-mass relation: For converting the volume-specific magnetization determined in step 3 into the mass of magnetized material an empirical calibration curve is needed, which can then be applied to quantify the magnetic masses of not excavated buildings. For determining a calibration curve, the excavation of key targets is needed, including a documentation of the archaeological materials with respect to spatial distribution and weight. In the presented case, the masses of daub and pottery per square meter were weighed (cf. 'excavation technique and daub documentation') during the excavation of three buildings. From this data an average calibration curve is computed which allows also to numerically assess the uncertainties of the resulting mass estimates.

Step 5 Determination of magnetized mass distribution: In a next step the calibration curve of step 4 is applied to the magnetization map determined in step 3 resulting in a map of magnetized masses. This map can then be analyzed with respect to archaeological criteria such as bulk mass or shape of house remains.

In summary, the magnetic map is transferred firstly into a map of magnetization and then into a map of masses of daub and pottery. This introduces new possibilities for the archaeological interpretation of magnetic measurements at archaeological sites with an almost uniform basement geology. The distribution of magnetization respectively the concentration of daub and pottery can be interpreted in terms of different internal layouts of buildings (cf. 'Analysis of magnetization patterns'). The application of the outlined methodology to a whole settlement or even a complete area of settlements can reveal different types of buildings possibly related to ancient societal transformations. It may contribute to a better understanding of the settlement structure, to population estimations and thus to calculating the human impact on the forest steppe environment.

3.2 Magnetic survey

Since 2011, magnetic surveys have been conducted at the site Maidanetske using the FGM650 gradiometers by Sensys. Most of the total 185 ha have been surveyed motorized with 25 cm sensor distance (crossline) and 35 cm sensor height. With survey speed between 12 to 16 km/h and a sample rate of 20 readings per second the inline point distance results in about 30 cm. Details on the processing can be found in Rassmann et al. (2016).

3.3 Excavation technique and Daub documentation (step 1)

For this study the results from two completely excavated burned dwellings 44 and 54 (excavation in 2013 and 2014), of one burned megastructure (excavated in 2016), and of 23 small test trenches in the area of burned dwellings (excavated in 2013, 2014, and 2016) are available which provide a clear picture of the stratigraphical variability in the settlement area (Müller and Videiko, 2016; Müller et al., 2017; Ohlrau, 2018). Additionally, also other object categories like pits, remains of pottery kilns and ditches have been archaeologically investigated in a systematic way.

After removal of the Chernozem top layer, the architectural remains (packages of daub and pottery) of dwellings and the megastructure were removed layer by layer. During this excavation process the position and masses of archaeological finds and daub were systematically documented with point coordinates and ordered in a grid of 1 m × 1 m cell size. The documentation of daub includes not only recording of masses differentiated according to material properties but also registration and mapping of type, direction and dimensions of wood negatives (Müller et al., 2017).

3.4 Physical and chemical properties of sediments and daub samples (step 2)

The density of 33 samples (14 from the megastructure, 19 from house 44) was determined by dividing the dry weight of selected pieces (between 1 and 2.5 cm in diameter) by its volume (calculated via volume of replaced water). For 75 daub pieces (26 from the megastructure, 49 from house 44) the mass specific magnetic susceptibility was measured after homogenization $<$ 2 mm following the procedure of Dearing (1999) using a Bartington MS2B susceptibility meter (resolution $2 \cdot 10^{-6}$ SI, measuring range $1 - 9999 \cdot 10^{-5}$ SI, systematic error 10%). Three samples of each piece were measured and a standard sample (1% Fe_3O_4) was measured after each three measurements to check for device drift and to calibrate the results.

The elemental composition of 92 daub pieces (38 from the megastructure, 53 from house 44) was carried out on a ped-xrf device, namely a Niton XL3t900-ed-XRF. The dried samples (one week at 35 °C) were ground in a mortar and homogenized in an agate mill before measurements. For the measurements the He-flotation in the measurement chamber was used. The measurement

mode was the "mining-mode, Cu/Zn", total measurement time was 300 seconds: main filter, 40 kV, 50 μA- 60 seconds; high filter, 50 kV, 40 μA- 60 seconds; low filter, 20 kB, 100 μA- 60 seconds; light filter 6 kV, 100 μA- 120 seconds. The semi-quantitative results were converted into quantitative percentages per weight according to Dreibrodt et al. (2017). The mass specific susceptibility and the total iron content of the loess and the soil developed within that deposit were determined in 16 soil profiles (157 samples in total) at different parts of the settlement area in the same manner as described for the daub above.

3.5 Numerical modelling of magnetic anomalies

The terms 'numerical modelling' and 'forward calculation' describe the calculation of synthetic measurement data based on a numerical model of the subsurface in terms of physical parameters. In the present case study, the given spatial distribution of the archaeological finds is the base to calculate the theoretically resulting anomalies of the vertical component of the magnetic field. We approximate the archaeological structures by polygonal bodies, that allow to calculate the magnetic fields using the formula of Plouff (1976). The computations were performed with a python code using the library 'Fatiando a Terra' by Uieda et al. (2013). The total magnetization is assumed parallel to the magnetic field at the time of the survey according to the 'International Geomagnetic Reference Field' (IGRF) (Thébault et al., 2015). The magnetic field anomaly is calculated with unit magnetization. It represents a normalized anomaly that can be adjusted to the field data by multiplication with the actual magnetization magnitude.

3.6 Inversion of magnetic measurements (step 3)

The inversion computation leading to the areal distribution of soil magnetization is based on fitting synthetic to measured magnetic data. To achieve this we define thickness and depth of the magnetic soil layer according to the depth and thickness of the daub layer as inferred from excavations and drillings. We assume that the observed magnetic anomalies are mainly caused by the magnetization of the burned clay, compared to which the magnetization of the surrounding unburned soil can be neglected. Also, we assume that the magnetization direction of the daub is parallel to the direction of the ambient earth's magnetic field. Next, we divide the magnetic layer into regular grid cells with given constant depth and thickness but unknown magnetization.

Each model cell i is attributed an unknown magnetization M_i, which contributes to the magnetic field anomaly. In our case, the M_i can be assumed to be scalar values because the direction of magnetization is assumed to be given. The linear superposition of the magnetic fields of all grid cells represents the anomalous magnetic field at the observation points j. The relative field contribution of magnetized cell i to the magnetic field observed at point j is described by the elements A_{ji} of matrix A in equation (1). The synthetic data d_j^{syn} at point j, in our case the difference in the vertical component of the magnetic field, is accordingly expressed by

$$d_j^{syn} = \sum_{i=1}^{n} A_{ji} \cdot M_i. \tag{1}$$

In the present study d_j^{syn} represents the difference of of the vertical components of the magnetic field as measured at the heights of the sensors of the differential magnetometer applied in the field. We computed the relative field strengths at positions j of the magnetized cells at positions i with the formula of Bhattacharyya (1964) (implemented in the python library 'Fatiando a Terra' by Uieda et al., 2013). We applied the ambient magnetic field values according to the IGRF at the time of the magnetic survey (B = 49867.1 nT, I = 65.8918°, D = 6.6206°).

The cost function, which is minimized by the inversion computation is:

$$L = \sum_{j=1}^{m} w_j (d_j^{obs} - d_j^{syn})^2 + w_0 \sum_{i=1}^{n} (2M_i - M_{i,N} - M_{i,E})^2 \tag{2}$$

Here, the sum of the squared residuals between the observed d_j^{obs} and synthetic data are weighted with $w_j = 1$. The second term represents a smoothness-constraint, where $M_{i,\mathrm{N}}$ and $M_{i,\mathrm{E}}$ denote the northern and eastern neighbours of M_i, respectively. This term is weighted with the constant $w_0 = |\max(A_{ji})|$. The weight w_0 is dependent on the depth and thickness of the magnetized layer and varies for our examples between 1.3 and 5.0.

The M_i values are determined through minimizing L under the constraint $M_i > 0$. The M_i values have to be positive scalars because the direction of magnetization - parallel to the ambient magnetic field - is contained implicitly in the matrix elements A_{ji} and because burned daub is not diamagnetic (diamagnetic materials would have negative M_i values).

Computationally, we solved the minimization and inversion problem by applying a so-called subspace trust region interior reflective (STIR) algorithm (Branch et al., 1999), which is a well established and robust method for non-linear constrained and unconstrained optimization problems. In a first step, an initial estimate of the M_i values is obtained by solving the problem in a least-squares sense without positivity constraints. Next, using these starting values, the STIR algorithm is applied in an iterative way, in which the constraints $M_i > 0$ are considered through Kuhn-Tucker conditions. Details of the method can be found in Coleman and Li (1996) and Branch et al. (1999). For the computations we applied an open-source Python script (scipy.optimize.least_squares) of the scipy library (Jones et al., 2001).

3.7 Establishing a magnetization-mass relation (step 4)

In order to determine the masses of daub and pottery of not excavated buildings, a relation between magnetization of the grid cells, determined through the inversion computation, and the masses of the causative magnetic material must be established. It can be derived from the excavations of the Maidanetske site (house 44, house 54 and megastructure) where the masses of daub and pottery have been documented per square meter. Under the assumption that density and volume-specific magnetization of the collected finds are almost constant, this relation is linear.

In principle, it can be determined by a bivariate regression between the daub masses, pottery masses and magnetization of the grid cells. However, in all excavations the found masses of daub were much higher than the pottery masses so that the regression coefficient of the pottery could not reliably be determined. Therefore, the masses of burned material were summed and treated as an entity.

Equation (3) describes the linear relation between the mass of burned material m_A and the mean magnitude of magnetization $\overline{|M|}$ in the volume V of one grid cell:

$$a_1 \cdot m_A \cdot V^{-1} + a_2 = \overline{|M|} \tag{3}$$

The coefficients a_1, a_2 are determined by orthogonal distance regression (ODR) (e.g. Boggs and Rogers, 1990) because both mass of burned material and magnetization are prone to statistical errors.

Since the regression coefficients $a_1^{(1)}$, $a_1^{(2)}$, $a_1^{(3)}$ obtained for the three excavated buildings do not agree exactly, we use the middle of the interval

$$a_1^\star = (a_1^{\max} + a_1^{\min})/2 \tag{4}$$

as a representative value of a_1, where $a_1^{\min}$ and $a_1^{\max}$ are minimum and maximum of the determined $a_1^{(1)}$, $a_1^{(2)}$, $a_1^{(3)}$. We use the extrema $a_1^{\max}$ and $a_1^{\min}$ as an estimate of the uncertainty of $a_1^\star$.

The application of equation (4) is motivated by the small number of only 3 excavations ('samples'), from which no meaningful average and standard deviation of a_1 can be computed. With the chosen way we assume that the samples bound the possible interval of a_1 in the sense of a generalized Gaussian of order ∞ (box distribution) such as underlying the ℓ_∞-norm. This normalized probability density function is centered at the mid-range (4) and the uncertainty is given by half of the bandwidth. A more reliable value of a_1 can be obtained when data of more excavated houses are available.

The variable a_2 represents an average magnetization offset, which is independent of the recorded find masses. It is caused by the background magnetization of the soil enriched by small grains of daub and ceramics, too small to be collected. Since these values may be quite variable we made no attempt to define a representative a_2-value. Instead the magnetization offset was determined independently for each investigated building by determining a representative magnetization value of the cells surrounding it.

For this purpose, the following procedure was developed and tested at the three example excavation sites:

- The visibly magnetized area of each dwelling is circumscribed with a 2 m wide polygonal stripe.
- A cumulative magnetization histogram is determined for the cells of this stripe.
- The 75 % mark is then used as representative local a_2-value.

The application of the approximate coefficient $a_1^\star$ and local a_2-value determined as described to the three example sites showed that the gathered find masses could be recovered with an accuracy of ± 11%.

3.8 Quantification of burned masses of not excavated buildings (step 5)

The procedure described in the previous paragraph was exemplarily applied to 45 non-excavated house, listed in Table 1. These house were selected according to the following criteria:

Main selection criterion for the set of objects was the availability either of direct information on the depth range from test trenches, excavations and drilling cores or the existence of depth information from adjacently located excavations or test trenches. Another intention was to test the method on a variety of different types of dwellings which were classified in the categories 'burned', 'unburned/eroded' and 'megastructure' as well as belonging to different phases of the site.

4 Results

Before we start explaining the results obtained from magnetic mapping on the exemplary masses and mass distribution of houses, we focus on the laboratory measurements of the daub and sediment samples to show that no significant geological bias was observed.

4.1 Physical and chemical properties of sediments and daub samples

The medians of the densities (cf. Fig. 2.2.3 B) of daub pieces of house 44 and the megastructure were not significantly different with respect to their 25 % and 75 % quartile levels. The same applies to the medians of the mass-specific magnetic susceptibility (cf. Fig. 2.2.3 C). Moreover, as a main source of magnetism, the total iron content (cf. Fig. 2.2.3 A) of the daub samples is not differing significantly between the two objects. These findings are important because they justify indirectly also the assumption of homogeneity of daub magnetization underlying the interpretation procedure.

The total iron content (cf. Fig. 2.2.3 D-H) in the soils and sediments displays a mean of 2.28 %.. The measured range spans from a minimum of 1.94 % by weight to a maximum of 2.86 % by weight (whereas the latter is considered an outlier). Measurements of low frequency mass-specific susceptibility on soil profiles through and beside houses and the megastructure are given in Figure 2.2.3 I-M. They show little background variability in the Chernozem that overlays the cultural layer (around $100 \cdot 10^{-8}\mathrm{m}^3/\mathrm{kg}$) with a peak in the depth of the archaeo-deposits (around $200 \cdot 10^{-8}\mathrm{m}^3/\mathrm{kg}$). Note that in the profiles 76a, 77b, 78a-c, and 110 the archaeological record is reflected by higher susceptibility values.

Table 1: Information on examined buildings. The locations are given in Figure 2.2.1 with the ID. The buildings are divided into the categories burned (b), 'unburned/eroded' (u/e) and megastructure (m).

ID	Intercept a_2 (A/m)	Max. magnetization (A/m)	Mass (t)	Min. mass (t)	Max. mass (t)	Area (m^2)	Mass/area (kg/m^2)	Category	Trench	House ID	Contextual information/remarks
1	0.39	3.48	1.6	1.4	1.8	85.1	18.7	b	110	71	Burned floor but no platform, partly excavated 2016
2	0.02	0.25	0.1	0.1	0.1	57.6	1.6	u/e			Settlement 2
3	0.05	0.2	0.1	0	0.1	43.9	1.3	u/e			Settlement 2
4	0.09	0.34	0	0	0	44.4	0.8	u/e			Settlement 2
5	0.25	1.59	0.4	0.3	0.4	62.4	6.1	u/e			Settlement 1
6	0.23	1.98	0.6	0.6	0.7	89.3	7.1	u/e			Settlement 1
7	0.3	1.95	0.4	0.4	0.5	63.4	6.5	u/e			Settlement 1
8	0.38	1.16	0.1	0.1	0.1	48.1	2.2	u/e			Settlement 1
9	0.41	2.11	0.6	0.5	0.7	99.8	6.3	b			Settlement 1
10	0.36	4.13	0.8	0.7	0.9	92.5	8.2	b			Settlement 1
11	0.39	1.81	0.2	0.2	0.2	64.3	3.2	u/e			Settlement 1
12	0.15	0.44	0.1	0.1	0.1	61	2.1	u/e			Settlement 2
14	0.09	0.38	0.2	0.2	0.3	94	2.4	u/e			Settlement 2
15	0.33	3.56	1.7	1.5	1.9	219	7.6	m			Settlement 2, empty interior space
17	0.52	2.94	5.9	5.2	6.7	431.5	13.6	m			Settlement 2, interior space overbuild
18	0.24	1.34	0.6	0.5	0.7	69.3	8.3	b			Settlement 2
19	0.14	2.07	2.9	2.5	3.3	124	23.3	b			Settlement 2
20	0.02	1.04	0.9	0.8	1	80.4	11	b	96	66	Settlement 2
21	0	2.48	3.2	2.8	3.7	130.4	24.7	b	96	65	Settlement 2
22	0.2	3	6.8	6	7.8	166.3	41.1	b			Settlement 2
23	0.14	1.95	0.6	0.6	0.7	53.7	11.8	b			Settlement 2
24	0.25	3.63	1.6	1.4	1.8	66.5	23.5	b			Settlement 2
25	0.27	3.87	1.5	1.3	1.7	64.9	23.4	b			Settlement 2
26	0.22	1.16	0.2	0.2	0.3	54.3	4.2	b			Settlement 2
31	0.55	2.51	1.2	1	1.3	75.9	15.5	b			Settlement 2
32	0.51	3.76	3.2	2.8	3.7	94.6	33.7	b	91	58	Settlement 2
33	0.62	4.1	1.9	1.7	2.2	71.9	26.5	b	92	54	Settlement 2
34	0.65	2.67	0.6	0.5	0.7	71.6	8.7	b			Settlement 2
35	0.18	1.59	0.8	0.7	0.9	64.7	12.7	b			Settlement 2
36	0.33	2.8	1.4	1.2	1.6	64	21.5	b	103	70	Settlement 2
37	0.19	3.77	2.5	2.2	2.9	79.5	31.8	b	100	67	Settlement 2
38	0.16	1.53	0.3	0.3	0.4	41.2	7.8	u/e			Settlement 2
39	0.81	3.85	5.2	4.5	5.9	204.9	25.2	b			Settlement 2
40	0.24	2.82	1.3	1.1	1.4	73.2	17.1	b	99		Settlement 1
41	0.1	1.77	0.8	0.7	1	71.8	11.6	b			Settlement 1
51	0.46	5.06	3.9	3.4	4.4	110	35.2	b	51	44	Settlement 2
71	0.89	3.83	1	0.8	1.1	39	24.5	b	71	45	Settlement 2
72	0.68	3.7	1.5	1.3	1.7	85.8	16.9	b	72	46	Settlement 2
73	0.88	5.15	2	1.8	2.3	61.1	33.1	b	73	47+48	Settlement 2
74	0.46	3.48	2.6	2.3	3	137.3	18.8	b	74	49	Settlement 2
75	0.34	4.92	3.1	2.8	3.6	85.2	36.8	b	75	50	Settlement 2
76	0.6	3.99	2.1	1.8	2.4	72.8	28.4	b	76	51	Settlement 2
77	0.81	4.88	1.9	1.7	2.2	68.7	27.8	b	77	52	Settlement 2
79	0.14	2.74	2.4	2.1	2.7	108.2	22.1	b	79	53	Settlement 2
111	0.2	1.72	1.8	1.6	2	262.4	6.8	m	111		Settlement 2, interior space partly overbuild

4.2 Results of numerical modelling study

In this section we verify the relative contributions of the different find categories to the magnetic patterns of houses by numerical modelling. The basis of this computation are the geo-referenced finds of the megastructure, which are not the entirety of finds but can be considered as representative regarding the spatial frequency distribution and location of find categories within the building. Figure 2.2.4 A shows the distribution of the single objects which have been digitally recorded for the find categories of daub from walls and floor and of pottery from the megastructure (cf. location: no. 111 in Fig. 2.2.1, magnetic measurements: Fig. 2.2.4 F). Figure 2.2.4 B, C and D show the relative synthetic anomalies of these objects, Figure 2.2.4 E the superposition of

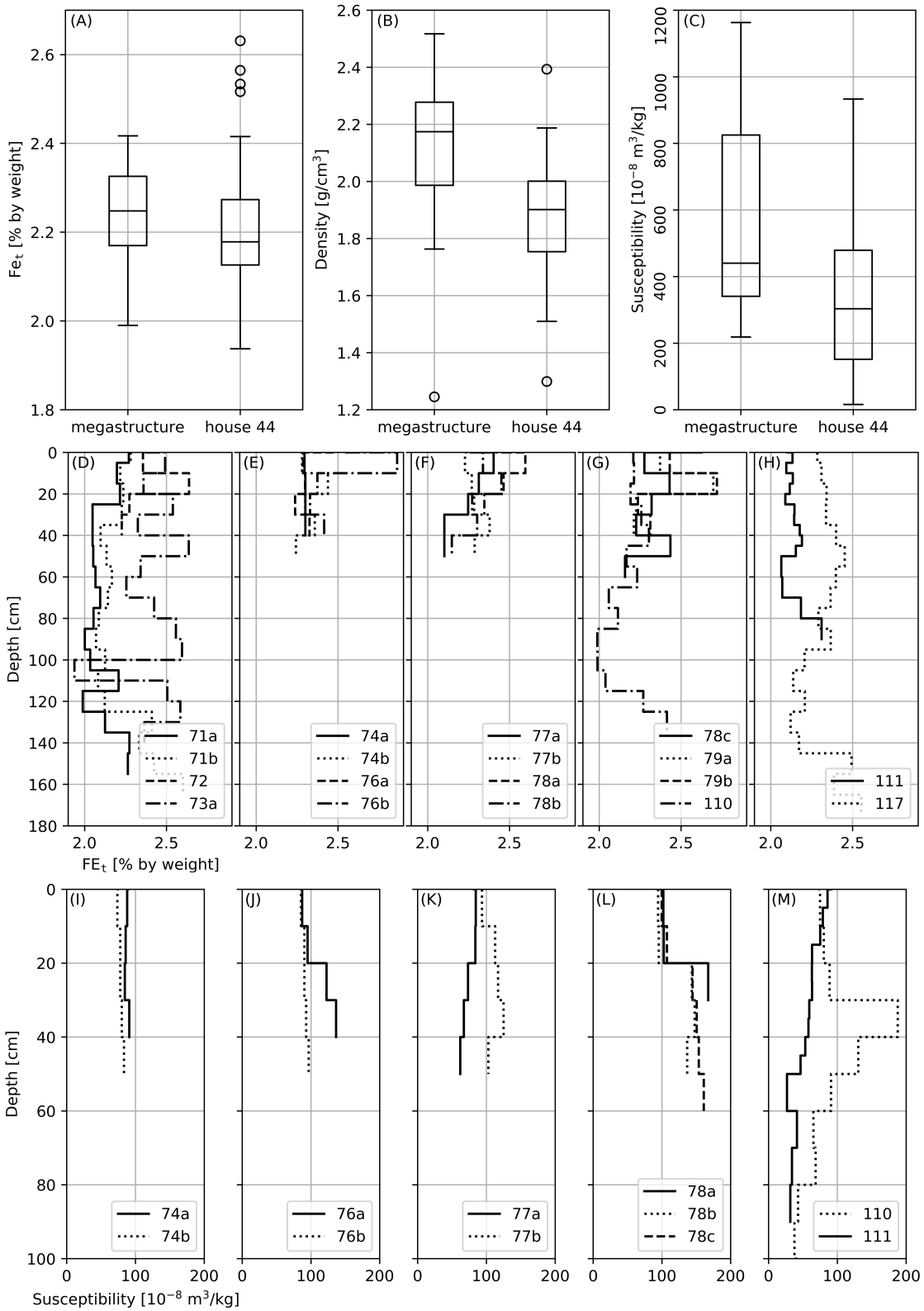

Figure 2.2.3: Results of laboratory measurements: Total iron content by weight (A), density (B) and mass-specific susceptibility (C) of daub samples from the megastructure and house 44. (D-H): depth dependent total iron content of different profiles. (I-M): depth dependent mass-specific susceptibility of different profiles. The locations of the profiles are given in Figure 2.2.1.

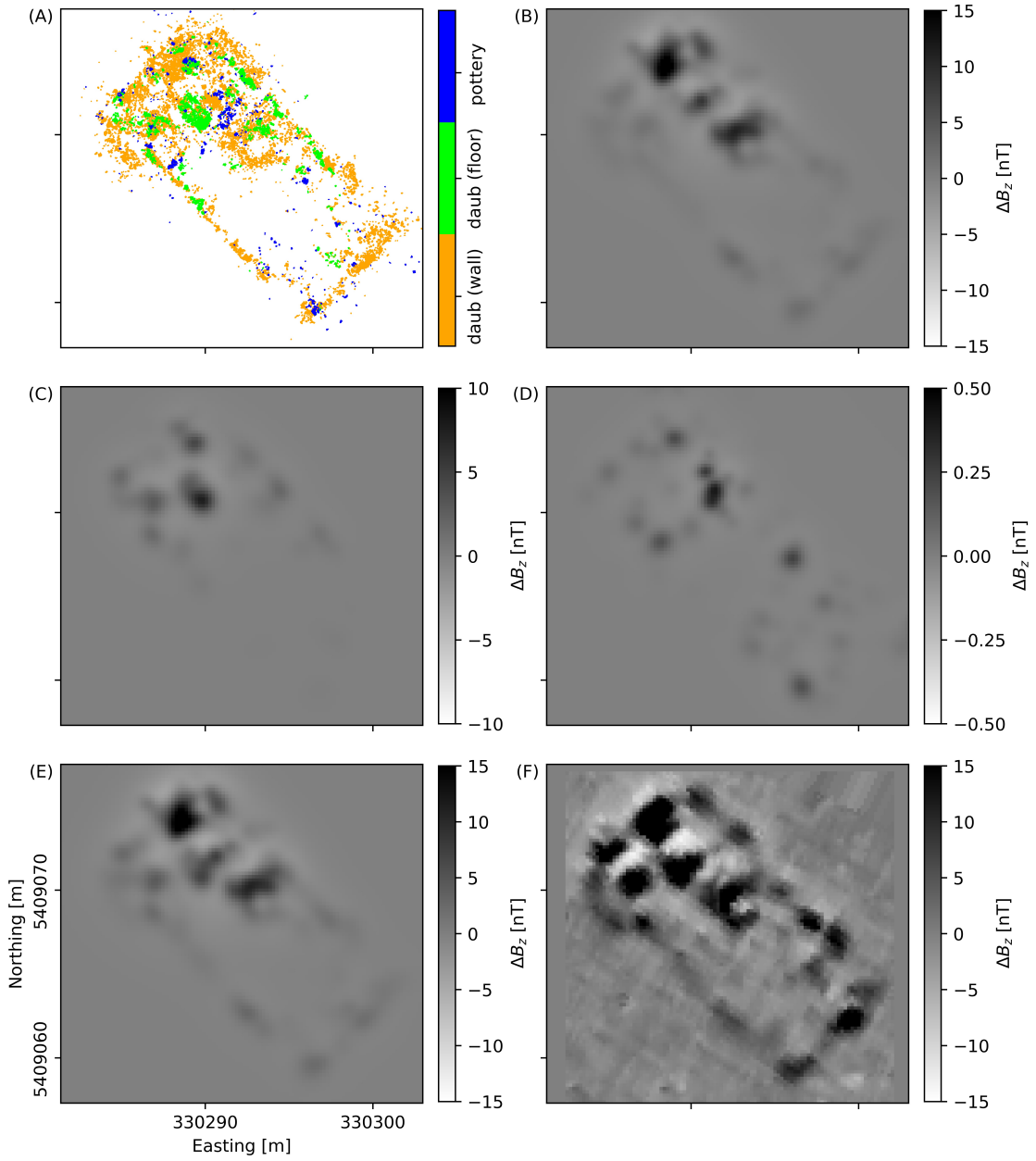

Figure 2.2.4: Exemplary building megastructure: digitally documented finds (A) of the categories daub of walls, daub of floor and pottery, calculated magnetic anomalies for the find categories daub of walls (B), daub of floor (C), pottery (D). The bottom row shows the comparison of the sum of the calculated anomalies (E) and the measured data (F).

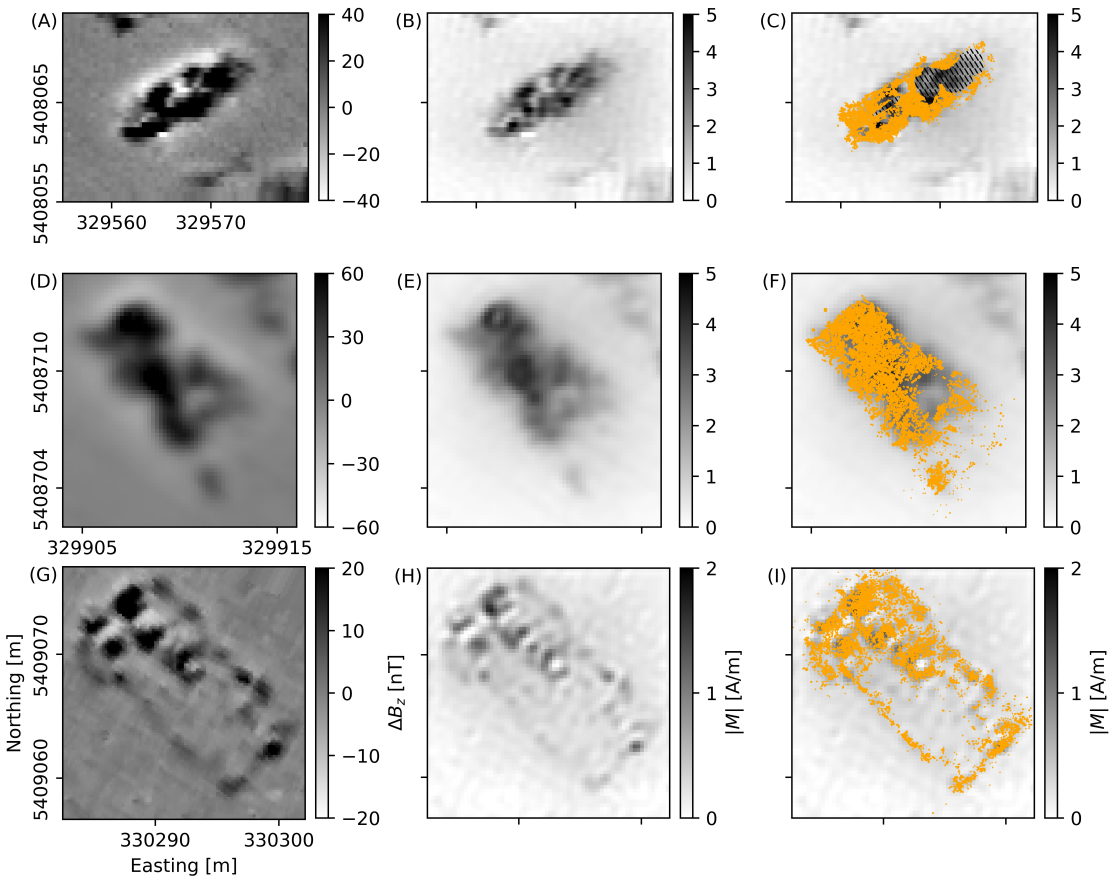

Figure 2.2.5: Comparison of measured magnetic data (left column), calculated magnetization (center) and documented daub in orange (right) for the three excavated buildings: house 44 (top row), house 54 (middle) and megastructure (bottom row). The hatched area in house 44 is disturbed because of illegal looting.

them. Comparing these to the measured data (Fig. 2.2.4 F) we arrive at the following conclusions:

The synthetic anomalies based on the daub assigned to walls (Fig. 2.2.4 B) resemble in their distribution the overall distribution of measured anomalies. Also, the location of local minima and maxima, especially in the northern quarter and the southern outline, correlate. Yet, the apsis-like shape in the western corner is calculated as a faint anomaly. The synthetic anomalies originating from the daub of the floor are shown in Figure 2.2.4 C. They mainly appear in the northern half of the building and the main maxima coincide with maxima in the measured data. In Figure 2.2.4 D the calculated anomalies of the pottery are depicted. The extrema of their amplitudes are around 50 times smaller than those of the daub from walls. Spatially, they are distributed over the complete area of the building with a gap in the central part.

The comparison of the synthetic to the measured data (Fig. 2.2.4 F) shows that the overall pattern of the measured magnetic anomalies is caused by the daub distribution and that the contribution of ceramics in only of minor importance.

4.3 Magnetization intensity of excavated buildings

The inversion yields magnetization maps (Fig. 2.2.5 B, E, H) which show the areal distribution of magnetized soil matter in a more realistic way than the maps of magnetic field strengths (Fig. 2.2.5 A, D, G). A comparison between the distribution of the digitally documented finds of the

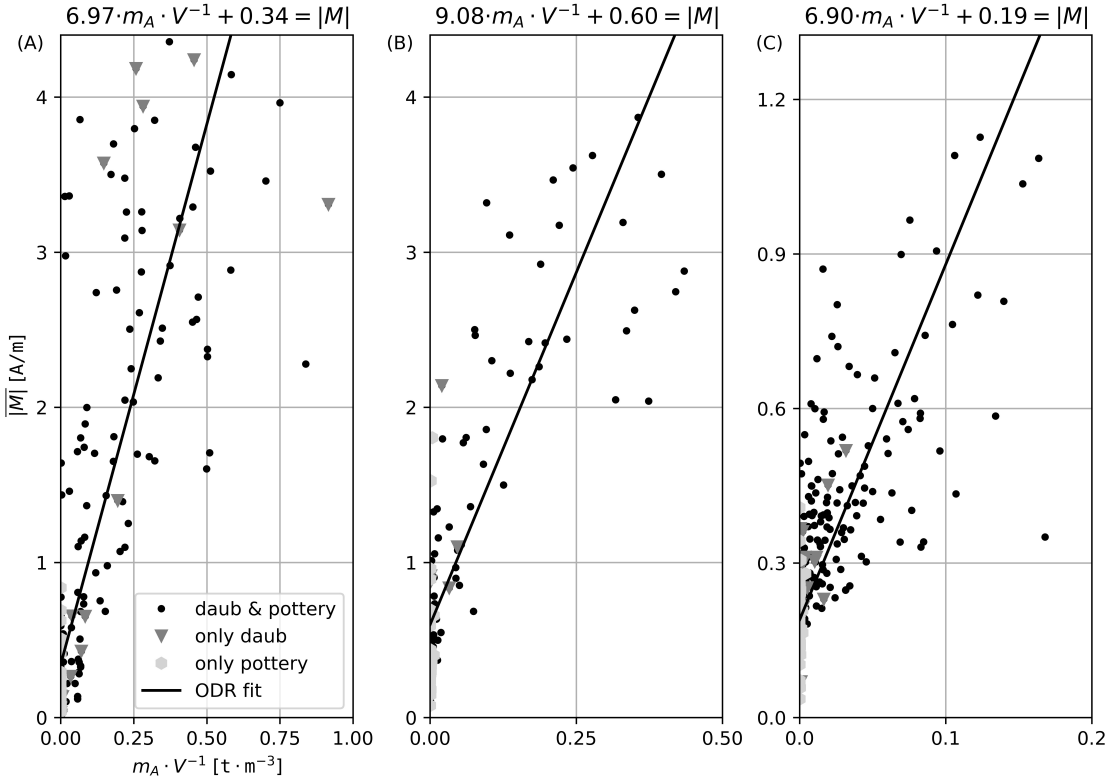

Figure 2.2.6: Mass-magnetization-relation for house 44 (A), house 54 (B) and the megastructure (C). The total masses of daub and pottery m_A per volume V are contrasted with the mean magnetization $\overline{|M|}$.

megastructure (Fig. 2.2.4 A) and the calculated magnetization (Fig. 2.2.5 H) shows that areas with increased magnetization coincide well with the location and frequency of finds. The modelling study of the previous paragraph indicated that the daub of the walls has the largest contribution to the magnetic anomalies. This is confirmed by the comparison of the inverted magnetization to the spatial density of the finds. It shows that the daub of the walls has the highest alignment with areas of increased magnetization.

4.4 Relation between magnetization and magnetized masses

To transfer these results to the unexcavated houses the relation between magnetization and magnetized masses was quantified by linear regression of the inverted magnetizations of the three excavated buildings and the recorded masses per excavation square. To determine the regression coefficients a_1 and a_2 of equation (3) the sum of the masses of pottery and daub are compared with the mean magnetization per excavation square (Fig. 2.2.6). For the megastructure (Fig. 2.2.6 C) these are 392 squares, 200 for house 44 (Fig. 2.2.6 A) and 140 for house 54 (Fig. 2.2.6 B). In Figure 2.2.6, the squares with solely pottery are marked with light gray hexagons (⬡), with solely daub with a gray triangle (▼) and those with both find categories with a point (●). The mass of pottery is small compared to the mass of daub being equal or under 5% of the total mass for all three buildings. This makes a bivariate regression not feasible. The masses per volume range up to 0.2 t/m^3 for the megastructure and up to 1 t/m^3 (0.5 t/m^3) for the house 44 (54) and the mean magnetizations up to 1.2 A/m respectively up to 4.5 A/m (4.0 A/m). The clear differences in the data ranges are also reflected in the different total masses of archaeological material of 1.7 t for the megastructure and 4.4 t for the house 44. The regression coefficients deduced for the three

Table 2: Comparison of observed and estimated masses of the three completely excavated buildings.

Building	Observed mass (t)	Estimated mass (t)	Difference (%)
house 44	4.4	3.9	11
house 54	1.7	1.9	11
megastructure 111	1.7	1.8	6

excavated buildings are given in Figure 2.2.6.

In Table 2, the observed and estimated masses of the three excavated buildings are listed. They were calculated with the local coefficient a_2 (cf. Table 1) and $a_1^\star = 8.0$, resulting in a maximum difference of 11% between the measured and estimated masses.

4.5 Classification of houses from their magnetization patterns

To explore the archaeological potential of the suggested interpretation concept we applied it exemplarily to a total number of 45 dwellings. Three of them are megastructures, 12 are classified as 'unburned/eroded' and 30 as burned houses according to their appearance in the magnetic plan.

Comparing the patterns of the magnetization different categories can be identified. The dwellings classified prior to the inversion as 'unburned/eroded' and megastructures remain in their own groups. In one megastructure (no. 15 in Fig. 2.2.1) areas with high magnetization are found only for the exterior walls. In contrast, in the other two examples (no. 17 and 111 in Fig. 2.2.1) also the interior space shows partly or complete areas with increased magnetization. Dwellings classified a-priori as 'unburned/eroded' have in general low values of magnetization but show patches of increased magnetization not higher than 2 A/m (per inversion cell). Their diverse patterns make a further subcategorization not feasible.

After the inversion, the group of burned dwellings can be further subdivided based on patterns in the magnetization. Figure 2.2.7 shows exemplary buildings divided into three subgroups. For a better comparability, the magnetization in each subfigure is scaled to its maximum, which is given in Table 1. Moreover, the houses are uniformly reoriented in the figure according to patterns described in the following. The largest subgroup (Fig. 2.2.7, group 1) with 20 specimens show a roughly rectangular area of increased magnetization with one or two local maxima and a local minimum. Referring to the orientation of the standardized floor plan after Chernovol (2012), one local maximum is located at the back end. Moving from there to the front end, on the left side of the house the local minimum can be seen in the central part. Further towards the front side, a local maximum is located. After that the area of increased magnetization ends rather sharply. From here until the front end of the object, follows commonly a zone of slightly increased magnetization.

To test the regularities of the observed patterns, we consider additionally the location of the pit which is usually associated with each house. For 15 of the 20 houses the pit is situated on the backside. For the remaining five objects the pit is on the opposite side. Moreover, there are five more houses with an insecure association to this group of houses.

A second group (Fig. 2.2.7, group 2) is defined for houses, which are larger than the houses of group 1. It includes three specimens. The basic pattern is identical with the pattern of the houses of group 1. In comparison though, they show a larger extent and a slightly increased magnetization at the front.

Three buildings are considered as a subgroup (Fig. 2.2.7, group 3), which show non-uniform patterns in the magnetization. The left building (no. 37 in Fig. 2.2.7) seems to show the magnetization pattern of the standard houses, yet at the front side an area of increased magnetization is found. The central building no. 79 sticks out because the areas of increased magnetization form its outlines whereas the complete central part has low magnetizations. The third dwelling of this group (no. 39 in Fig. 2.2.7) is the largest examined house.

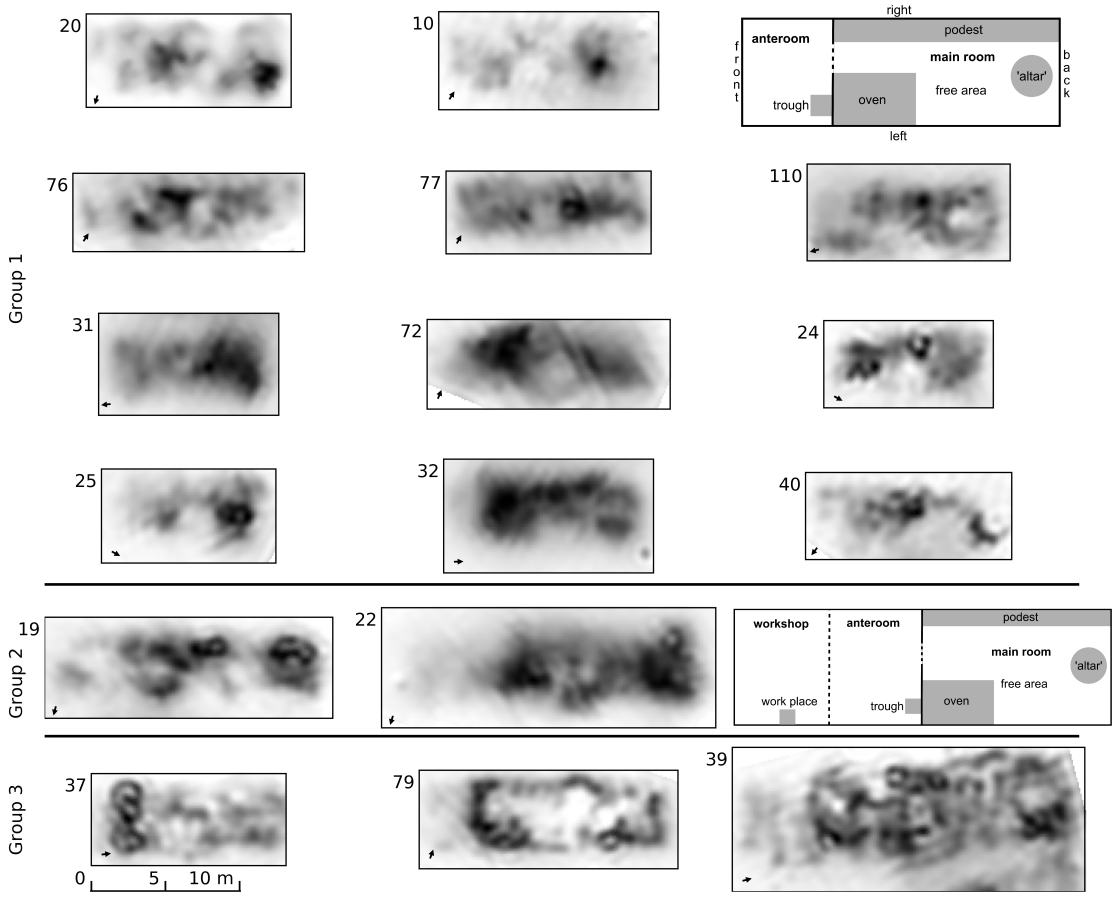

Figure 2.2.7: Magnetization maps (all to scale) of not excavated buildings (white: 0 A/m, black: maximum magnetization). The maximum magnetization is given in Table 1. North is indicated in the lower left corner of each plot. For comparison, the schematic floor plans by Chernovol (2012) for the standard house (upper) and extended standard house (lower) are shown (not to scale). Group 1 are examples for the standard house, group 2 for the extended standard house and the examples of group 3 show individual patterns.

4.6 Daub masses of not excavated buildings

From the previous results it can be concluded that the house masses, determined in in the final step of the interpretation sequence, are basically daub masses. The results of the mass determination are summarized in Table 1. In Figure 2.2.8 A the masses determined for the 45 selected non-excavated houses are shown in comparison to the area of each dwelling. Figure 2.2.8 B depicts the estimated total masses of the dwellings versus their total mass per area. The minimum and maximum of the regression coefficient ($a_1 \in [6.97, 9.08]$) have been used to calculate minimum and maximum estimates of the total mass (cf. Table 1) and consequently the total mass per total area. The masses range up to 7 t and the mass per area up to 41 kg/m^2. The house groups, classified from the magnetic map, can be identified also as groups in the mass diagrams. The 'unburned/eroded' buildings (•) have the lowest masses and are smaller than 100 m^2 (Fig. 2.2.8 A). In Figure 2.2.8 B they lie nearly on a straight line reaching from the origin to 0.6 t and 8 kg/m^2. The burned buildings (▲) approximately follow that line, too, up to values of 2 t and 20 kg/m^2.

In both graphs of Figure 2.2.8, the group of burned buildings separates apparently into two subsets indicated tentatively by dashed and dotted grey lines. For the area-versus-mass-plot, each

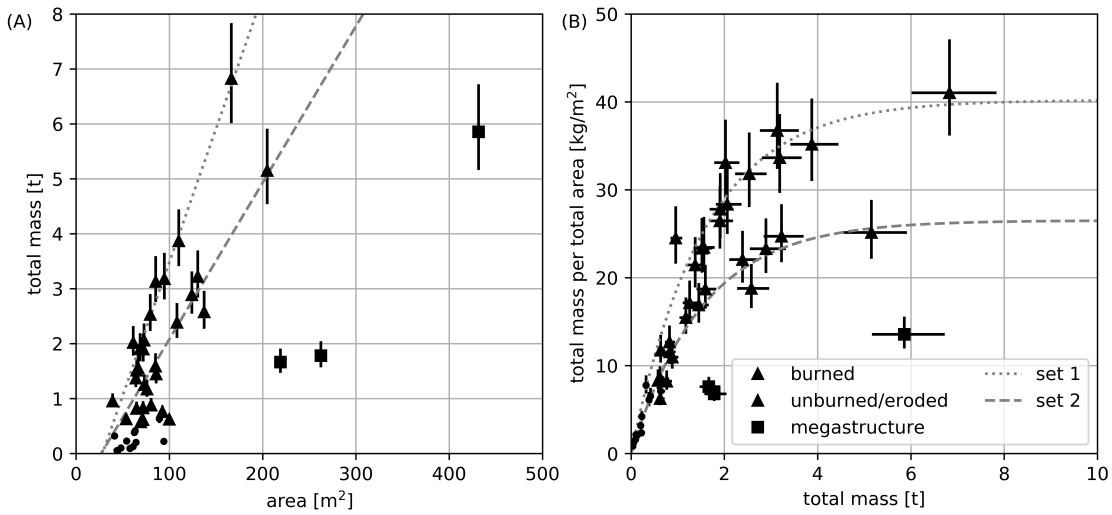

Figure 2.2.8: (A) Estimated total masses of examined buildings versus their area. (B) Estimated total mass per area versus total mass.

subset follows a linear relation. Figure 2.2.8 B shows the bulk mass per area of each building plotted versus its bulk mass. In this diagram the tentative regression curves of the two subsets are non-linear and seem to converge to a constant maximum value with increasing mass. Subset 1 consists of dwellings with an overall increased magnetization, whereas subset 2 consists of buildings showing only patches of increased magnetization. Compared to the houses the megastructures (■) are larger in size and have lower masses and lower masses per area.

5 Methodical discussion

In this section we focus on the discussion of mainly methodical aspects. The archaeological implications of the study are outlined in the next section.

5.1 In how far does the presented interpretation approach differ from previously published magnetic interpretation methods?

During the last decades a large number of studies, targeting the quantitative interpretation of archaeological magnetic prospection data, have been published. The general problem of magnetic data inversion is the principle ambiguity of magnetic source models that can explain observed magnetic anomalies. Attempts have been made to reduce this ambiguity, for example, by applying weight functions regarding the magnetic field decay with depth (Argote et al., 2009), by making certain assumptions on the magnetic susceptibility (Eder-Hinterleitner et al., 1996; Neubauer and Eder-Hinterleitner, 1997; Herwanger et al., 2000), or by constraining positive and negative ranges of allowed susceptibility contrasts (Cheyney et al., 2015). Compared to these approaches our computational scheme is quite simple, as it is basically a variant of the well-known equivalent-layer approach (e.g. Blakely, 1995), the realization of which is straightforward and merely a question of available computer power. It can be applied here, because we are able to impose quite strict constraints on depth and thickness of the major magnetic layer and to evaluate the results by drilling and excavations. The 'new' aspect of our approach lies therefore in the systemized coaction of geophysical, geoarchaeological and archaeological investigations, and not its single components.

5.2 What are the causes of the observed spatial variation of soil magnetization?

The presented magnetic interpretation is based on the assumption that the volume-specific magnetization of daub is almost homogeneous so that variations in magnetization can be translated into variation of magnetized mass. Alternatively, it might be considered that the soil, from which the houses were constructed, could have been heterogeneous from the beginning, especially in its iron content. In this regard, it has to be emphasized that the analysis of the physical and chemical properties of the daub pieces from houses and megastructure did not show any statistically significant differences. This implies that the measured properties cannot explain the variability observed in magnetization data. The total iron content of the sediments and soils at Maidanetske is slightly varying from sample site to sample site, but main differences, especially in maximum and minimum total iron contents, are a result of few outliers and not statistically significant. Taking into account that the depth profiles (Fig. 2.2.3) were taken from three different parts of the site, the results probably reflect a small-scale variability within the parent material (loess). A comparison of the total iron contents of soil and sediment with that of the daub pieces clearly implies that the former was the material used by the Tripolye settlers to produce the latter. Thus, the variability of the parent material is also improbable to explain the observed variability within the magnetization data of the site.

5.3 How does the surrounding soil influence the determination of daub mass from magnetization?

Equation (3) describes the relation between magnetized masses and magnetization. Regarding our idealized subsurface model, where non-zero magnetization is allowed only for the daub layer, an intercept a_2 of zero would be expected, whereas a non-zero intercept is observed. This intercept can be interpreted as the sum of the magnetizations of the hosting sediments and of all fragments of daub and pottery that were not recorded during the excavations. This is evident from investigations of excavation cells without any recorded daub or pottery in comparison to cells outside the buildings. The differences range from 0.01 A/m to 0.09 A/m, whereas differences would be close to zero if non-recorded fragments would not be present. At the present stage of investigation this 'diffuse' magnetic background signal cannot be further interpreted. In future investigations, however, this aspect should be addressed by special sampling and onsite measurements.

6 Archaeological implications of magnetization patterns and house masses

6.1 Analysis of magnetization patterns

The calculated magnetization enables a more distinct insight into the structures of the dwellings. This creates the potential for further examinations on the internal setup of the houses. For comparison, the floor plan of the 'standard' and 'extended standard' house by Chernovol (2012) is shown in Figure 2.2.7 beside the examples of calculated magnetization distributions. Additionally, in group 3 also other constructive types of houses can be identified which seem not recorded in current classifications. Especially, house 79 which resembles because of its empty internal space megastructures without an elevated platform.

For most inverted houses, the main room is characterized by two maxima and is distinguishable from the anteroom which is characterized by a slightly increased magnetization at the front of the dwellings. Since several excavation reports (e.g. Kruts et al. 2001: 25; Kruts et al. 2013: 12 and 15) note a thinner layer of daub for the anteroom (respectively 'porch'), this indicates a difference in construction. This lighter type of construction can explain the relatively lower magnetizations compared to the main room. Moreover, for the majority of the dwellings the area of slightly increased magnetization is on the opposite side than the pit which is associated with

each dwelling. The pit was supposingly used to gather the construction material and is located at the back side of the house.

Aside of their fuzziness the displayed magnetization patterns resemble the floor plans with the areas of increased magnetization belonging to the immovable interior elements. Yet, because of the fuzziness and the small number of excavated buildings a clear assignment of spots of increased magnetization to immovable interior remains insecure. For the excavated houses 44 and 54 no clear assignment can be made. However, for megastructure 15 the location of the central installation can be determined reliably.

Still, it is not clear if the local minimum of the magnetization distributions located mostly at the 'left' side of the buildings originates from the oven or the 'usable area' towards the 'backside' of the building. In favour of the first possibility is the observation that in excavated examples of the houses 44 and 54 the location of the oven coincides roughly with areas of lower magnetization. Additionally, it could be frequently shown by excavations that the oven was removed or destroyed. This observation gave rise to the assumption of 'ritual demolitions' of ovens during the process of house abandonment (Круц, 2003: 76; Chernovol, 2012: 186).

Facing the unsecure assignment of local maxima and immoveable interior elements we need to take into account the possibility of other factors for the location of the local maxima than immovable interior components. For example, the collapsed material of the backend gable wall or the partition wall between ante and main room might be the source of local maxima in the magnetization patterns. Moreover, a microtopography as well as variations in the thickness of the daub layer can result in local extrema due to shorter distances between sensor and magnetized material. Furthermore, different positioning of parts of the immovable interior could also explain these deviations. Finally, the burning conditions are unknown and can vary not only among the buildings but also inside each building. This can influence the formation of durable daub as well as the composition of (ferri-) magnetic minerals.

6.2 Masses of not excavated buildings

The masses of the excavated buildings are estimated with a maximum difference of 11 %, which shows that the calculated masses are reliable estimates of the known masses. However, to our knowledge no study is published aiming to quantify the mass of daub using geophysical methods.

The determined masses provide important new arguments for the discussion on houses with low magnetization which are currently frequently classified as potentially 'unburned' or 'eroded' dwellings. It is an important result that these objects contain low amounts of daub and do not represent completely unburned objects. According to our results of magnetic data interpretation, these remnants contain masses of daub and pottery in a range between 0.05–0.6 t at the lower end of the determined scale (cf. Fig. 2.2.8/ Table 1).

Similar results were obtained through the excavation of such a building place at the giant settlement Nebelivko (Рудь, 2015; Відейко et al., 2015b; Burdo and Videiko, 2016: 107-110). This feature was composed of small sized, partly vesicular vitrified daub, one locally limited clay installation and larger quantities of pottery. Daub was distributed in a thin veil but also showed clusters at some places. Remains of installations like the oven, the central installation and the podium which are usually arranged on the top of the platform were missing. The building contained a pottery assemblage of at least nineteen vessels which showed clear traces of secondary firing. The vitrified daub and the secondary fired pottery might indicate that the firing happened at high temperatures.

We conclude that the labels 'unburned' or 'eroded' represent wrong interpretations. Therefore we suggest to specify by the expression 'houses with low amount of daub'. Far reaching social and demographic interpretations of such buildings should be avoided as long as the structural reasons for the low masses of daub is not understood from archaeological side (e.g. Nebbia et al., 2018). Concerning the interpretation of buildings with low magnetization different scenarios have already been discussed (e.g. Diachenko, 2016): The missing characteristic elements of dwellings like ovens and podiums may indicate a non-residential use. The low quantity of partly vitrified daub might among other things be explained through the use of only small amounts of clay to construct such

buildings (Відейко et al., 2015b). Furthermore, the partly removal of daub from burned houses cannot be excluded as large amount of burned debris in pits show (e.g. Müller et al., 2017: 51-56). Due to the above described difficulties in the interpretation, it remains still very difficult to judge how such buildings should be interpreted with regard to demographic reconstructions. The considerable number of pits and ditches which are filled with daub, indicate that the house were not only burned at the end of Tripolye settlements but already during the use of the sites. Thus, it surely falls short to interpret houses with low magnetization as dwellings which were abandoned already during the life of a settlement.

A further tentative approach for an interpretation of the area-mass-plot and the mass-mass per area-plot is given in the following. After Chernovol (2012) the dwellings show a high degree of standardization, yet the area-mass-plot indicates a house sizes between 50 to 200 m^2. Idealizing the standardization and assuming identical burning conditions, a house of smallest size and mass should exist, because a dwelling even smaller would be unusable. If all components of the building and the immovable inventory would scale proportional with the size of the house, the relation between the size and the mass should be linear. Our data differs from this idealized image for several reasons: It is most probable that the burning conditions differ for each building and due to movable and immovable interior that might vary also inside each building. Furthermore, there are some variations in the floor plan of the houses possible, like a second 'altar' (increase of total mass) in different locations of the building (Chernovol, 2012). Moreover, buildings with and without a platform, on which the buildings rests, exists (respectively increase or decrease of total mass). It is rather unlikely that the constructional elements and the immovable interior scale proportional to the size of the building (e.g. thickness of walls). Also, the free, usable area might grow (decrease of total mass). Some excavations (Круц, 2003: 76; Chernovol, 2012: 186) showed, that the oven was removed from the dwelling resulting in a decrease of total magnetized mass. However, also the size of the buildings is an estimate based on the remains producing the magnetic anomaly, yet also an under- or overestimation is possible. The anteroom is constructed in a lighter way (e.g. Kruts et al., 2001: 25; Kruts et al., 2013: 12 and 15), resulting in an uncertainty whether it is visible in the magnetic or magnetization map. The differences in the total mass for set 1 and set 2 (cf. Figure 2.2.8 A) for dwellings of same size, are in the order of a tonne or more for buildings larger than 100 m^2. This difference seems to be too large to be explained by the existence or not of an oven. Summarizing, the tentative split in the two subsets resulting in different slopes for a linear relation between area and mass, most probably results from different types of construction and/or burning conditions. Thus, a general model of intentional house burning after abandonment suggested by Johnston et al. (2018) seems improbable. Either, the inhabitants did not have equal access to wood to burn their houses, or the houses burned down under varying conditions. Since palaeoecological results imply a proper wood delivery of the settlement throughout its inhabitation time (Dal Corso et al., in review), the latter might be more probable.

In the mass per area versus total mass plot (Figure 2.2.8 B) the two subsets of burned houses become also visible. Since for masses higher than 4 t only a few examples exist, deliberately a curve of an asymptotic saturation can be seen. As tentative interpretation, houses at the saturation level might be burned completely, so that all building material is transformed into durable daub. The two different levels could then represent houses with and without a platform in the construction. For more differentiated interpretation a larger number of inverted houses ideally accompanied by additional examinations are needed, including measurements of the magnetic properties of daub and the determination of burning conditions.

7 Conclusion

Based on constraints from excavations and drillings magnetic gradiometer measurements of the Chalcolithic Maidanetske settlement could be converted into an areal distribution of magnetization intensity by application of a rather simple inversion algorithm.

The resulting magnetization maps display the magnetized remains of the buildings in clearer images than the gradiometer measurements. This enables a distinct examination of patterns in

the magnetization. A comparison with existing floor plans of excavated houses showed common structures, yet a clear identification of immovable interior was not possible. However, in most cases the orientation of the building could be identified. The comparison with the existing floor plans showed also that there might be buildings which do not fall into the existing classification.

Based on three excavated buildings an empirical relation between the calculated magnetization and magnetized masses was found and applied to determine the masses of not excavated buildings from magnetization maps. Based on test computations for excavated buildings the accuracy of the derived masses is of the order of about ± 10 %. Masses of up to 0.6 t of daub are determined for buildings that were initially classified as 'unburned/eroded'. Hence, a rephrasement as 'houses with low amount of daub' is suggested. Houses with higher masses can be grouped into two subsets if their ground areas are considered. These subsets might be a result of different burning conditions or construction types.

The interpretation scheme can be applied directly without modification to sites where the magnetic sources are confined to one distinct soil layer of approximately constant depth and thickness. If the thickness or depth of this layers varies significantly, site specific modifications need to be incorporated, for example, using interpolated depths and thicknesses based on a densified grid of drillings.

The application of the novel interpretation scheme to the complete settlement can form the basis for a profound statistical analysis, including cluster analysis, of the size, mass and relative location of the buildings. Our tentative archaeological interpretation can then be reevaluated, and the analysis of the settlement as a whole will lead to an improved understanding of settlement structure, population estimations and human impact on the forest steppe environment.

8 Funding

We are grateful to the Deutsche Forschungsgemeinschaft (DFG, German Research Foundation - Projektnummer 2901391021 – SFB 1266) for funding the presented research and to two anonymous reviewers for their constructive critical comments that helped to improve the paper.

References

Argote DL, Tejero A, Chávez RE, López PA and Bravo R (2009) 3d modelling of magnetic data from an archaeological site in north-western Tlaxcala state, Mexico. *Journal of Archaeological Science* 36(8): 1661–1671.

Bhattacharyya BK (1964) Magnetic Anomalies due to prism-shaped bodies with arbitrary polarization. *Geophysics* 29(4): 517–531.

Blakely RJ (1995) *Potential theory in gravity and magnetic applications.* Cambridge [England]/New York: Cambridge University Press.

Boggs P and Rogers J (1990) Orthogonal Distance Regression. In: Brown P and Fuller W (eds.) *Statistical analysis of measurement error models and applications: proceedings of the AMS-IMS-SIAM joint summer research conference held June 10-16, 1989.* pp. 186–194.

Branch MA, Coleman TF and Li Y (1999) A Subspace, Interior, and Conjugate Gradient Method for Large-Scale Bound-Constrained Minimization Problems. *SIAM Journal on Scientific Computing* 21(1): 1–23.

Burdo N and Videiko M (2016) Nebelivka: From Magnetic Prospection to New Features of Mega-Sites. In: Müller J, Rassmann K and Videiko M (eds.) *Trypillia Mega-Sites and European Prehistory 4100-3400 BCE.* London/New York: Routledge Taylor and Francis Group, pp. 95–116.

Chapman J (2017) The Standard Model, the Maximalists and the Minimalists: New Interpretations of Trypillia Mega-Sites. *Journal of World Prehistory* 30(3): 221–237.

Chapman J and Gaydarska B (2016) Low-Density Urbanism: The Case of Trypillia Group of Ukraine. In: Fernández-Götz M and Krause D (eds.) *Eurasia at the Down of History. Urbanization and Social Change*. New York: Cambridge University Press, pp. 81–105.

Chapman J, Gaydarska B and Hale D (2016) Nebelivka: Assembly Houses, Ditches, and Social Structure. In: Müller J, Rassmann K and Videiko M (eds.) *Trypillia Mega-Sites and European Prehistory 4100–3400*. London/New York: Routledge Taylor and Francis Group, pp. 117–131.

Chapman J, Videiko M, Hale D et al. (2014) The Second Phase of the Trypillia Mega-Site Methodological Revolution: A New Research Agenda. *European Journal of Archaeology* 17(3): 369–406.

Chernovol D (2012) Houses of the Tomashovskaya Local Group. In: Menotti F and Korvin-Piotrovskiy A (eds.) *The Tripolye Culture Giant-Settlements in Ukraine. Formation, Development and Decline*. Oxford and Oakville, pp. 183–209.

Cheyney S, Fishwick S, Hill IA and Linford NT (2015) Successful adaptation of three-dimensional inversion methodologies for archaeological-scale, total-field magnetic data sets. *Geophysical Journal International* 202(2): 1271–1288.

Coleman T and Li Y (1996) An Interior Trust Region Approach for Nonlinear Minimization Subject to Bounds. *SIAM Journal on Optimization* 6(2): 418–445.

Dal Corso M, Hamer W, Hofmann R et al. (in review) Modelling Landscape Transformation at the Chalcolithic Tripolye Mega-site of Maidanetske (Ukraine): Wood Demand and Availability. *The Holocene* .

Dal Corso M, Out W, Ohlrau R et al. (2018) Where are the cereals? Contribution of phytolith analysis to the study of subsistence economy at the Trypillia site Maidanetske (ca. 3900–3650 BCE), central Ukraine. *Journal of Arid Environments* 157: 137–148.

Dearing JA (1999) *Environmental magnetic susceptibility: using the Bartington MS2 system.* 2nd edition. Bartington Instruments.

Diachenko A (2016) Demography Reloaded. In: Müller J, Rassmann K and Videiko MY (eds.) *Trypilla Mega-Sites and European Prehistory 4100–3400 BCE*, Themes in Contemporary Archaeology. London/New York: Routledge Taylor and Francis Group, p. 181–193.

Dreibrodt S, Furholt M, Hofmann R, Hinz M and Cheben I (2017) P-ed-XRF-geochemical signatures of a 7300 year old Linear Band Pottery house ditch fill at Vráble-Ve'lké Lehemby, Slovakia - House inhabitation and post-depositional processes. *Quaternary International* 438(Part B): 131–143.

Eder-Hinterleitner A, Neubauer W and Melichar P (1996) Reconstruction of archaeological structures using magnetic prospection. *Analecta Praehistorica Leidensia* 28(2): 131–137.

Fassbinder JW (2015) Seeing beneath the farmland, steppe and desert soil: magnetic prospecting and soil magnetism. *Journal of Archaeological Science* 56: 85–95.

Gaffney C (2008) Detecting Trends in the Prediction of the Buried Past: A Review of Geophysical Techniques in Archaeology. *Archaeometry* 50(2): 313–336.

Herwanger J, Maurer H, Green A and Leckebusch J (2000) 3-D inversions of magnetic gradiometer data in archeological prospecting: Possibilities and limitations. *Geophysics* 65(3): 849–860.

Johnston S, Diachenko A, Gaydarska B, Nebbia M, Voke P, Bondar K, Litkevych V and Chapman J (2018) The experimental building, burning and excavation of a two-storey Trypillia house. *PAST (Newsletter of the Prehistoric Society)* 89: 13–15.

Jones E, Oliphant T, Peterson P et al. (2001) SciPy: Open source scientific tools for Python. URL `http://www.scipy.org/`. [Online; accessed 23.11.2018].

Kirleis W and Dal Corso M (2016) Trypillian Subsistence Economy: Animal and Plant Exploitation. In: Müller J, Rassmann K and Videiko M (eds.) *Trypillia Mega-Sites and European Prehistory 4100-3400 BCE*. London/New York: Routledge Taylor and Francis Group, pp. 195–205.

Korvin-Piotrovskiy A, Hofmann R, Rassmann K et al. (2016) Pottery Kilns in Trypillian settlements. Tracing the division of labour and the social organisation of Copper Age communities. In: Müller J, Rassmann K and Videiko M (eds.) *Trypillia Mega-Sites and European Prehistory 4100-3400 BCE*, Themes in Contemporary Archaeology. London/New York: Routledge Taylor and Francis Group, pp. 221–252.

Kruts BA, Korvin-Piotrovskiy AG, Chabanyuk VV and Shatilo LA (2013) *Talianki - settlement-giant of the tripolian culture. Investigations in 2012*. Kiev.

Kruts V, Korvin-Piotrovskiy AG and Rizhov SN (2001) *Talianki – settlement giant of the Tripolian culture. Investigations in 2001*. Kiev: Institute of Archaeology of the National Academy of Science of Ukraine.

Linford N (2006) The application of geophysical methods to archaeological prospection. *Reports on Progress in Physics* 69(7): 2205–2257.

Menotti F and Korvin-Piotrovskiy AG (2012) *The Tripolye culture giant-settlements in Ukraine: formation, development and decline*. Oxford: Oxbow Books.

Müller J, Hofmann R, Brandtstätter L, Ohlrau R and Videiko MY (2016a) Chronology and Demography: How Many People Lived in a Mega-Site? In: Müller J, Rassmann K and Videiko M (eds.) *Trypillia Mega-Sites and European Prehistory 4100-3400 BCE*. London/New York: Routledge Taylor and Francis Group, pp. 133–170.

Müller J, Hofmann R, Kirleis W et al. (2017) *Maidanetske 2013: New excavations at a Trypilia mega-site*. Bonn: Habelt, R.

Müller J, Hofmann R and Ohlrau R (2016b) From Domestic Households to Mega-Structures: Proto-Urbanism? In: Müller J, Rassmann K and Videiko M (eds.) *Trypillia Mega-Sites and European Prehistory 4100-3400 BCE*. London/New York: Routledge Taylor and Francis Group, pp. 253–268.

Müller J, Hofmann R, Ohlrau R et al. (2018) The social constitution and political organisiation of Tripolye mega-sites: hierarchy and balance. In: Meller H, Gronenborn D and Risch R (eds.) *Surplus without the State – Political Forms in Prehistory: 10th Archaeological Conference of Central Germany October 19–21, 2017 in Halle (Saale)*. Halle (Saale): Landesamt für Denkmalpflege und Archäologie Sachsen Anhalt – Landesmuseum für Vorgeschichte, pp. 247–260.

Müller J, Rassmann K and Videiko M (2016c) *Trypilla Mega-Sites and European Prehistory 4100–3400 BCE*. London/New York: Routledge Taylor and Francis Group.

Müller J and Videiko M (2016) New Facts of a Mega-Site. In: Müller J, Rassmann K and Videiko M (eds.) *Trypillia Mega-Sites and European Prehistory 4100-3400 BCE*. London/New York: Routledge Taylor and Francis Group, pp. 71–93.

Nebbia M, Gaydarska B, Millard A and Chapman J (2018) The making of chalcolithic assembly places: Trypillia megasites as materialized consensus among equal strangers? *World Archaeology* 50(1): 41–61.

Neubauer W and Eder-Hinterleitner A (1997) 3D-interpretation of postprocessed archaeological magnetic prospection data. *Archaeological Prospection* 4(4): 191–205.

Ohlrau R (2015) Trypillia Großsiedlungen - Geomagnetische Prospektion und architektursoziologische Perspektiven. *Journal of Neolithic Archaeology* (17): 17–99.

Ohlrau R (2018) *Maidanets'ke. Development and decline of a Trypillian mega-site in Central Ukraine*. PhD Thesis, Christian-Albrechts-Universität zu Kiel, Germany.

Plouff D (1976) Gravity and magnetic fields of polygonal prisms and application to magnetic terrain corrections. *Geophysics* 41(4): 727–741.

Rassmann K, Korvin-Piotrovskiy A, Videiko M and Müller J (2016) The New Challenge for Site Plans and Geophysics: Revealing the Settlement Structure of Giant Settlements by Means of Geomagnetic Survey. In: Müller J, Rassmann K and Videiko M (eds.) *Trypillia Mega-Sites and European Prehistory 4100-3400 BCE*. London/New York: Routledge Taylor and Francis Group, pp. 29–54.

Rassmann K, Ohlrau R, Hofmann R, Mischka C, Burdo N, Videjko MY and Müller J (2014) High precision Tripolye settlement plans, demographic estimations and settlement organization. *Journal of Neolithic Archaeology* 16: 96–134.

Shatilo L (2016) Roofs of Tripolian Houses. Reconstruction: Sources and Problems. In: Preoteasa C and Ciprian-Dorin N (eds.) *Cucuteni Culture within the European Neo-Eneolithic Context. Proceedings of the International Colloqium "Cucuteni 130" 15-17 October 2014, Pietra Neamţ, Romania. In Memoriam Dr. Dan Monah. In Memoriam Dr. Gheorghe Dumitroaia*. Pietra Neamţ, pp. 725–740.

Shatilo L (2017) Ornaments and Signs on the Sledge Models from Talianki (Excavation 2012) – Art Decor or a source of information? In: Ursu CE, Poruciuc A and Lazarovici CM (eds.) *Papers presented at the international symposium "From Symbols to Signs. Signs, Symbols, Rituals in sanctuaries" Suceava, Romania, 9–11 September 2016. In Memoriam Gheorge Dumitroaia*. Suceava: Editura Karl. A. Romstorfer, pp. 177–185.

Thébault E, Finlay C, Beggan C et al. (2015) International Geomagnetic Reference Field: the 12th generation. *Earth, Planets and Space* 67(1): 67–79.

Uieda L, Oliveira VC Jr and Barbosa VCF (2013) Modeling the Earth with Fatiando a Terra. In: van der Walt S, Millman J and Huff K (eds.) *Proceedings of the 12th Python in Science Conference*. pp. 96–103.

Videiko M and Rassmann K (2016) Research on Different Scales: 120 Years of Trypillian Large Sites Research. In: Müller J, Rassmann K and Videiko M (eds.) *Trypillia Mega-Sites and European Prehistory 4100-3400 BCE*. London/New York: Routledge Taylor and Francis Group, pp. 17–28.

Відейко МЮ, Мюллєр Й, Бурдо НБ, Хофманн Р and Церна С (2015a) Дослідження у централній частині Майданецького. *Археологія* 1: 71–78.

Відейко МЮ, Чепмэн Дж, Бурдо НБ, Гайдарска Б, Церна СВ, Рудь ВС and Киосак ДВ (2015b) Комплексные исследования оборонительных сооружений, производственных комплексов и остатков построек на трипольском поселении у села Небелевка. *Stratum Plus* 2.

Дудкін ВП (2007) Магнітометричні дослідження поселень трипільської цивілізації. In: Кот С and Відейко М (eds.) *Трипільська культура. Пошуки. Відкриття. Світовий контекст*. Київ: Спадщина ЛТД, pp. 57–70.

Дудкин ВП (1978) Геофизическая разведка крупных трипольских поселений. In: Генинг ВФ (ed.) *Использование методов естественных наук в археологии*. Киев: Наукова думка, pp. 35–45.

Журавльов ОП (2008) *Тваринництво та мисливство у трипільських племен на території України*. Київ: Націона́льна акаде́мія нау́к Украї́ни. Інститут археології.

Кошелев ИН (2004) *Памятники трипольской культуры (по данным магнитной разведки)*. Киев: Самиздат.

Круц ВА (2003) Трипольские площадки - результат ритуального сожжения домов. In: Корвин-Пиотровский А Г, Круц ВА and Рижов СМ (eds.) *Трипільські поселення-гіганти. Материали міжнародної конференції. Tripolian Settlements-Giant. The international symposium materials*. Київ: Корвин Пресс, p. 74–76.

Рудь В (2015) Дослідження залишків жител на розкопі 5 поселення Небелівка. In: Відейко М Ю, Чапман Дж and Козир І А (eds.) *На східній межі Старої Європи. Матеріали міжнародної наукової конференції, Кіровоград, Небелівка, 12-14 травня 2015 року*. Кіровоград, pp. 26–28.

Шишкін КВ (1985) Планування трипільських поселень за даними аерофотозйомки. *Археологія* 52: 72–76.

Шмаглий Н М and Видейко Ю М (2005) *Майданецкое - трипольский протогород*. Киев.

A.2 Paper II

The following version was submitted to the Journal *Archaeological Prospection* on November 25th, 2019. The latest version is accepted for publication.

What over 100 drillings tell us: A new method for determining the Koenigsberger ratio of soils from magnetic mapping and susceptibility logging

Natalie Pickartz[1,2], Wolfgang Rabbel[1,2], Knut Rassmann[3], Nils Müller-Scheeßel[4], Martin Furholt[5], Johannes Müller[4,2], Ivan Cheben[6], Dennis Wilken[1,2], Tina Wunderlich[1,2], and Stefan Dreibrodt[7,2]

[1]Institute of Geosciences, Kiel University, Kiel, 24118, Germany
[2]Collaborative Research Center 1266, Kiel University, Kiel, 24118, Germany
[3]Romano-Germanic Commission, German Archaeological Institute, Frankfurt a. M., 60325, Germany
[4]Institute of Pre- and Protohistoric Archaeology, Kiel University, Kiel, 24118, Germany
[5]Department of Archaeology, Conservation and History, University of Oslo, Oslo, 0316, Norway
[6]Archaeological Institute of Slovak Academy of Sciences, Nitra, 949 21, Slovakia
[7]Institute for Ecosystem Research, Kiel University, Kiel, 24118, Germany

Abstract

We investigate the relative fractions of remanent and induced magnetization of the fillings of neolithic longpits in order to develop remanent magnetization as an additional parameter for the archaeological interpretation of magnetic maps. We determine the Koenigsberger ratio – the ratio between induced and remanent magnetization intensities - for key targets by combining magnetic mapping with downhole measurements of magnetic susceptibility, numerical modelling and inversion computations. The susceptibility data were acquired in drill holes along profiles crossing the targets identified by magnetic mapping. The targets of this exemplary study are house-accompanying pits at the Linearbandkeramik site Vráble 'Farské'. For this purpose we conducted auger drillings with a point distance of 25 cm and measured the magnetic susceptibility with a downhole susceptometer. The resulting two-dimensional susceptibility distributions were used to calculate synthetic magnetic anomalies corresponding to the case of solely induced magnetization. The comparison to the observed magnetic data showed a considerable discrepancy that can only be explained with remanent magnetization. To determine the Koenigsberger ratio we developed a new interpretation approach, in which parts of the measured susceptibility distribution serve as a basis function for determining the Koenigberger ratio. The free parameters of this numerical problem are determined by non-linear inversion. We applied the novel approach to six exemplary profiles and found Koenigsberger ratios between 1.6-10.5 with the majority of the values being smaller than 4. These values apply to soil volumes with susceptibility values larger than $27-160\cdot10^{-5}$ SI. Laboratory measurements on soil samples were used to examine the possible causes of the observed magnetization. The analyses suggest that the increase in susceptibility and remanent magnetization in the house-accompanying pits is caused by an increase of the population of magnetotatic bacteria and by the alignment of the ferrimagnetic iron compounds in the waterlogged environment of the pits.

Keywords: Koenigsberger ratio, magnetic susceptibility, inversion, forward modelling, Linearbandkeramik (LBK) longpits, magnetotatic bacteria

1 Introduction

The title of this paper suggests two questions, which guide the present study: Why should we want to determine the Koenigsberger ratio in an archaeological context? And how can we determine it

from field measurements?

The Koenigsberger ratio Q is the ratio between remanent and induced magnetization. It characterizes the relative importance of the remanent magnetization to be considered in a quantitative interpretation of magnetic anomalies and can be regarded as a parameter of archaeological relevance (Fassbinder, 2015). However, the contribution to the observed magnetic anomalies resulting from remanent magnetization is often neglected in field studies if effects of remanence are not obvious in the magnetic map. In this context, exceptionally strong amplitude anomalies and signif icant azimuthal deviations of the magnetic field vector from the ambient field may be regarded as "obvious" indications, such as resulting from thermoremanent magnetization of kilns, ovens and displaced bricks.

Case studies often approach a quantitative interpretation of magnetic anomalies using the assumptions of a simplified source geometry and induced-only magnetization. To explain the observed data, the susceptibility contrast between the source and the surrounding subsurface matrix is then determined for this geometry by linear inversion. (e.g. Schneider et al., 2014; Wilken et al., 2015; Miller et al., 2019).

In archaeomagnetic and archaeological case studies, the Koenigsberger ratio is usually determined via measurements of the magnetic susceptibility and the natural remanent magnetization (NRM) of samples. To our knowledge, these studies have always been conducted in the laboratory on samples from archaeological sites that had been exposed to heating (e.g. Carrancho et al., 2009; Catanzariti et al., 2008; Ertepinar et al., 2016; Gómez-Paccard et al., 2006; Herries et al., 2008; Hunt et al., 2013; Jordanova et al., 2004; Kapper et al., 2014b,a; Linford and Canti, 2001; Schnepp and Pucher, 1998; Schnepp et al., 2004). For example, Q varies between values of 0.1 for granite and 100 for mud-bricks (Ertepinar et al., 2016), between 0.1 and 100 for different kind of kilns, baths, hypocausts and furnaces (Gómez-Paccard et al., 2006; Schnepp et al., 2004) or 0.7 and 10 with values up to 250 in the context of combustion levels (Kapper et al., 2014a). Kapper et al. (2014b) found values between 0.1 and 10 for burned cave sediments.

Jrad et al. (2014) presented a comparison of measurements of the magnetic properties of palaeohearths and an experimental hearth. For the experimental hearth, they derived values of Q between 0.3 and 3.5 by susceptibility and NRM measurements, where the highest values were reached in the first cm below the surface. They could reproduce the observed magnetic anomaly of two paleaohearts with a subsurface model consisting of four layers (ash, base, soil, limestone pebbles). The derived values for Q turned out to be in the same range as the measured ones.

Apart from thermoremanent magnetization, detrital or depositional remanent magnetization (DRM) can occur in the context of archaeological pits and ditches or more general in ground depressions. The anomalies are rather weak but detectable (Fassbinder, 2015). DRM develops trough the alignment of remanent magnetized particles in direction of the earth's magnetic field if they are mobile in the pore water (e.g. Evans and Heller, 2003; Fassbinder, 2015).

In this paper, we show the importance of remanent magnetization for the magnetization of soils. This is a case where magnetic maps usually do not show obvious evidence of a contribution of remanent magnetization because the anomalies of soil-filled pits are usually only low or moderate in amplitude and only little, if at all, deviated from the present declination. We present a novel approach to determine the Koenigsberger ratio from magnetic prospection data and downhole susceptibility measurements. In this approach neither sampling nor NRM measurements are necessary. Our study targets magnetic anomalies arising from long-pits that accompany houses belonging to the neolithic Linear Pottery culture at the site Vráble 'Farské'. We base our study on susceptibility-depth sections crossing the magnetic anomalies that were gathered with dense downhole measurements. These two-dimensional susceptibility distributions clearly show the cross-section of the pits and are used as empirical subsurface models to calculate related synthetic magnetic anomalies. A comparison of the synthetic and observed magnetic data shows a discrepancy that can be explained with an additional remanent magnetization. From the susceptibility distribution we derive spatial basis functions for an inversion calculation, by which the Koenigsberger ratio is determined. Additional laboratory analyses are conducted to determine low and high frequency magnetic susceptibility, iron content, loss on ignition (LOI), soil color, X-Ray Fluorescence (XRF) and X-Ray Diffraction (XRD). These enable an understanding of the mea-

sured susceptibility distributions as such and of environmental and archaeological factors related to the site formation.

This paper is structured as follows: First, general information on the archaeological example site and the house-accompanying pits as the actual investigation targets are given. Second, the physical background, the applied measurement methods and our approach for the determination of the Koenigsberger ratio are explained. Then, we present the inversion results for one drilling profile in detail and a comparative overview including five more profiles. In addition, the results of the laboratory analyses of the samples are given. In the discussion section, we first examine methodical aspects and then give an interpretation regarding the magnetic history of the site.

2 The Archaeological Site of Vráble 'Farské'

2.1 General Information

The site of Vráble is located in the valley of the upper Žitava River, one of the many north-south running tributaries of the Danube. At about 140 m a.s.l., the site is situated in a slightly hilly environment on a fertile soils developed on a loess plateau above the river. Research at this site started in 2009 with large-scale magnetic prospections and excavations as well as geoarchaeological research were conducted in ensuing years (Furholt et al., 2014; Müller-Scheeßel et al., in press; Dreibrodt et al., 2017). They have shown that the site actually consisted of three co-existent settlements (see Fig. 1) of the Linearbandkeramik (LBK). Each settlement encompassed a size of 10–15 ha and, at their peak, they probably incorporated up to 60 houses with about 500 inhabitants (Müller-Scheeßel et al., accepted). The settlements of Vráble as a whole date between c. 5250 and 4950 cal BCE (Meadows et al., 2019) and belong to the late local phase of the LBK (Želiezovce group) (Furholt et al., 2014).

2.2 Characteristic of House-accompanying Pits

The house-accompanying pits usually run along the full length of both sides of the respective houses (10–30 m). They measure about 2–3 m in width and their bottom is 0.8–1.5 m below today's surface. The varying depth of the bottom may point to the fact that they were dug out in sections and not in one go. The microtopography was also documented with electromagnetic induction and ground-penetrating radar measurements on the stripped surface (approximately 60 cm below the present surface) during the course of an excavation (Pickartz et al., submitted). In most instances, the fill of the pits is very homogeneous and consists of dark brown soil (Munsell color 10YR3/3-3/4), mixed with few archaeological finds like ceramics, stone tools and animal bones (Figure 2). In many cases towards the top, but sometimes also near the bottom, a thin layer consisting of a higher amount of daub is found. However, as seen in Figure 1 these layers do not always produce a distinctly strong signal to be characterized as (thermo-)remanent feature. Divergent fillings, especially encountered at the southern ends, like checkered or ashy soil might point to special activities having taken place there.

It is usually taken for granted that the long pits flanking LBK houses were used as clay extraction pits and subsequently filled with waste, whereas their function and the filling processes are still debated (e.g. Wolfram, 2013; Květina and Řídký, 2017). However, recent research (e.g. Allard et al., 2013) as well as our own excavations (Müller-Scheeßel et al., in press) have shown that the debris is patterned and thus obviously reflects activities having taken place during the existence of the respective house. Therefore, we expect that material coming from undisturbed layers of lateral pits belong to the accompanying house.

3 Physical Background and Methods

In this section, we present first the theoretical framework for this study, followed by a description of the methods for data acquisition in the field and laboratory. Finally, we present the inversion

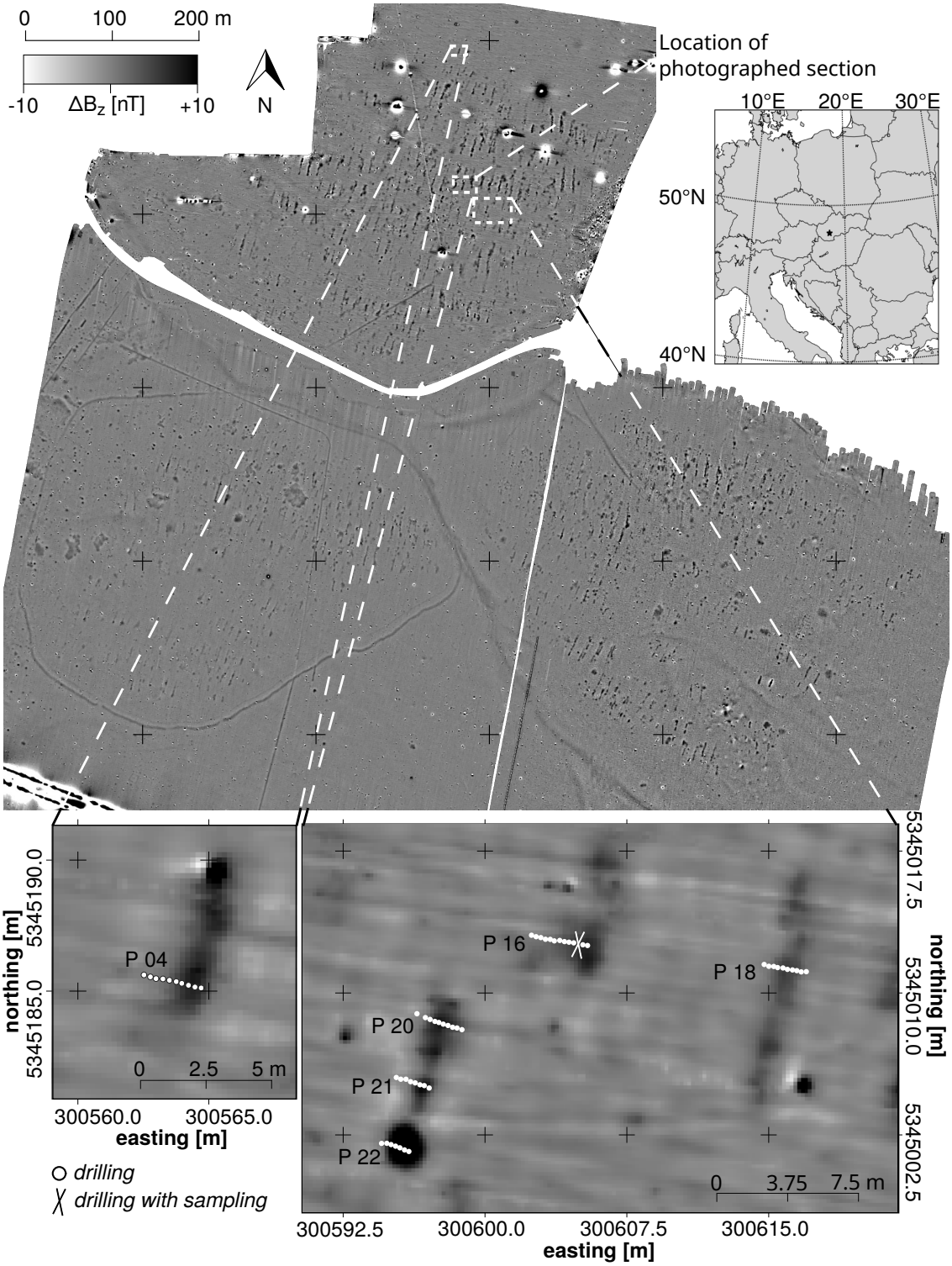

Figure 1: Magnetic map of the site Vráble and its location in Slovakia (upper right inlet). The detailed views show the location of the drilling profiles with the single drillings marked with a white dot. From one drilling (marked with a cross), samples were taken and analyzed in the laboratory.

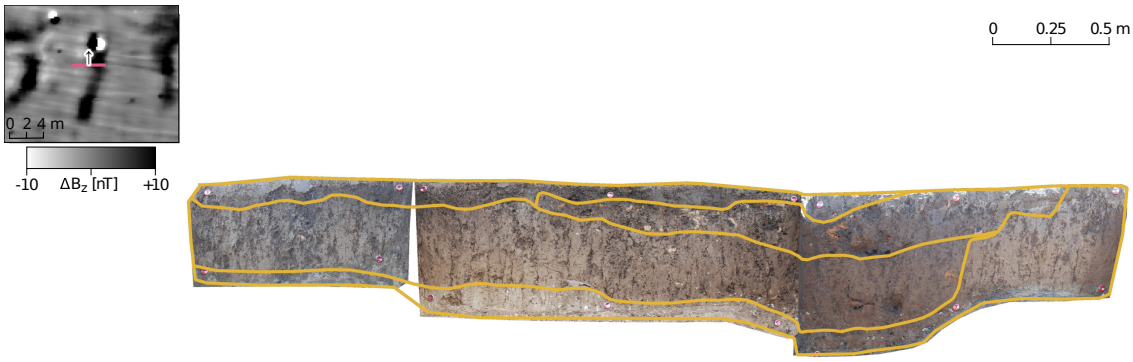

Figure 2: Photogrammetry of a section of the eastern long pit of house 245 (trench 8, 2014). The pit is composed of several layers with humous material and inclusions of daub and pottery.

algorithm that we used to estimate the Koenigsberger ratio.

3.1 Physical Background

Magnetic anomalies mapped in archaeological prospection arise from spatial variations of the 'total' magnetization of the soil $\vec{M}_T$. The total magnetization is the sum of a remanent $\vec{M}_R$ and induced $\vec{M}_I$ component:

$$\vec{M}_T = \vec{M}_R + \vec{M}_I \tag{1}$$

$$= \vec{M}_R + \kappa \cdot \vec{H}, \tag{2}$$

where κ denotes the isotropic volume susceptibility and $\vec{H}$ the vector of the ambient earth's magnetic field. The Koenigsberger ratio is the ratio of remanent to induced magnetization

$$Q = \frac{|\vec{M}_R|}{|\vec{M}_I|} \tag{3}$$

and is independent of the magnetization directions.

The magnetic susceptibility can be measured at different frequencies of an artificially generated exciting magnetic field to determine the frequency dependence of the material (e.g. Kainz and Cotter, 2018). The device used in the present study, a MS3 with MS2B sensor by Bartington, is an inductor coil instrument that is tuned to resonance. Hereby, the relative permeability μ_r of the sample modulates the frequency of oscillation (Evans and Heller, 2003). It is related to the magnetic susceptibility by

$$\kappa = \mu_r - 1. \tag{4}$$

The magnetic grain size distribution can be investigated by measuring the susceptibility at two (or more) different frequencies in the laboratory. The used device performs low-frequency measurements κ_{lf} at 0.465 kHz and high-frequency κ_{hf} measurements at 4.65 kHz. From this data the frequency dependent susceptibility is computed in percent by

$$\kappa_{fd} = (\kappa_{lf} - \kappa_{hf})/\kappa_{lf} \times 100\,\% \tag{5}$$

which is used to estimate the grain size distribution.

3.2 Data Acquisition

3.2.1 Magnetic Field Measurements

Between 2010 and 2012, the area of the site Vráble was extensively surveyed (Furholt et al., 2014) by the Romano-Germanic Commission of the German Archaeological Institute. The surveys were

conducted with the FGM650 gradiometers by Sensys GmbH in a 16-sensor array. The distance between the lower and upper sensor is 65 cm. In the array, the sensors have a distance of 25 cm cross-line and are mounted 35 cm above the ground. The survey speed of 12 km/h to 16 km/h results in in-line point distances of 30 cm with a sample rate of 20 readings per second.

Each magnetic profile was filtered with a third-order butterworth low-pass filter (cut-off wavenumber at 0.5 m^{-1}) to remove short-wavelength random noise and apply a gentle smoothing. Also the linear trend was removed from each profile.

3.2.2 Field Susceptibility Measurements

The drilling points were placed along linear profiles crossing the house accompanying pits orthogonally with a spacing of 25 cm (Fig. 1). The boreholes were drilled with an auger corer of 22 mm diameter to a maximum depth of 2 m (if feasible). For the susceptibility measurements we used the MS3 device by Bartington Instruments Limited in combination with the MS2H sensor. Starting at a depth of 10 cm, the probe was lowered in 5 cm steps to the maximum depth of 2 m or until no further lowering was possible. For each hole, the measurements were preceded and followed by drift measurements in the air. Each susceptibility depth curve was manually edited to remove a systematic increase of the susceptibility in the depth range from 1.00 m to 1.15 m because of soil compaction due to drilling. In addition, the topsoil susceptibility was measured with the same device using the MS2K sensor at the selected drilling points. The susceptibility values of the topsoil were averaged along the profile and the resulting mean value was attributed to the uppermost 10 cm of the soil column.

3.2.3 Sediment Analyses

To characterize the sediments under investigation and elucidate the possible sources of magnetization, samples from drill location P16_175 (Fig. 1) were taken for additional laboratory analysis. The following paragraphs describe the methods that were used to characterize the sediment with laboratory analysis.

Sample Preparation Samples were taken in the field from the auger corer (P16_175, see Fig. 1 and Fig. 9). Because of the small diameter of the corer (22 mm), sample material had to be gathered over depth intervals of 20 to 30 cm in order to provide sufficiently large soil volumes for the lab analysis. Some material was lost or displaced during the coring process. All samples were dried at 35 °C for at least 3 weeks and disintegrated with mortar and pestle. Following standard procedures of pedology and geoarchaeology, the fraction > 2 mm was separated via dry sieving.

Laboratory Susceptibility Measurements The magnetic susceptibility was measured on 10 ml of the < 2 mm, homogenized samples using a MS3 meter by Bartington Instruments Limited with the MS2B probe. Measurements were carried out at both low (0.465 kHz) and high (4.65 kHz) frequency. A reference sample consisting of 1 % Fe_3O_4 (magnetite) was measured repeatedly and the samples' susceptibility values were calibrated using this reference before converting them to mass-specific susceptibility. Finally, low and high frequency measurements were used to calculate the percentage of frequency dependent susceptibility (see sec. 3.1). The measurements were repeated with the whole sample - including particles > 2 mm - to check their influence on the values and ensure comparability with field measurements.

Iron content The content of dithionite soluble iron (Fe_d) indicating the formation of goethite and maghemite/magnetite during soil formation processes was determined according to Blakemore et al. (1987). Via this method a reducing reactant ($Na_2S_2O_4$) at a stable pH-value dissolves non-crystalline to badly crystalline oxides of iron, and their concentration was measured on an atomic absorption spectroscopy in the supernatant. The dithionite soluble fraction of iron is typical for products of soil formation processes.

Soil color The color of the samples was measured using a Voltcraft Plus RGB-2000 Color Analyzer set to display in a 10-bit Red, Green, and Blue (RGB) color space (Rabenhorst et al., 2014; Sanmartín et al., 2014). This digital device has integrated LED lighting and an external sensor with a 45°/0°measuring geometry to ensure the minimization of specular reflection. It has a spectral range of 400 to 700 nm and measures with a precision of < 3 for the RGB color model. In this system Red, Green, and Blue vary from 0 to 1023 with 0, 0, 0 representing black and 1023, 1023, 1023 representing white.

XRF - X-Ray Fluorescence The total elemental content of the samples was measured with a portable electron dispersive X-ray fluorescence device (ped-xrf) (Niton XL3t900-ed-XRF). For this purpose the <2 mm fraction was first homogenized in an Agate mill and then placed in a plastic tube covered by a 4 μm film. These were then measured in a lead-mantled measurement chamber with He-flotation using the "mining, Cu/Zn" settings for 300 s. The instrumentally determined values for Fe, Mn, Ti, Ca, K, Si, Al, P, Zr, Sr, and Rb were finally corrected using the published equations (Dreibrodt et al., 2017).

XRD - X-Ray Diffraction The mineral assemblage of the samples of core P16_175 was studied by X-ray diffractometry (xrd) measurements using a Philips diffractometer PW1710 (Cu radiation, 40 kV, 25 mA). Conventional powder samples were measured on ground samples of the fine earth fraction < 2 mm ($2 \cdot \vartheta$: 2°to 80°, step size: 0.02°, time: 2 s).

LOI - Loss On Ignition Loss on ignition (LOI) values were measured to estimate the organic matter and carbonate contents of the sediments (Dean, 1974). First the samples were dried at 105 °C overnight. The contents of organic matter and carbonates were then determined from the weight losses caused by heating the samples for each 2 h at 550 °C and 940 °C, respectively. F inally, the LOI values were converted into contents of soil organic matter and carbonates based on empirically determined site specific factors by linear regression.

3.3 Magnetic Data Interpretation

The next sections describe the components of the magnetic data interpretation. The interpretation starts with model calculations assuming solely induced magnetization and the susceptibility distributions determined in situ. The resulting synthetic data deviate strongly from the measured magnetic field data, which motivated the introduction of a model for remanent magnetization. Based on this model a representative Koenigsberger ratio is finally determined with an inversion calculation for each profile.

3.3.1 Magnetic Forward Calculation

To determine the portion of the magnetic anomalies that is caused by induced magnetization we performed magnetic model computations based on two-dimensional subsurface susceptibility models such as sketched in Figure 3. The subsurface below the drilling profile is divided in a regular grid with 0.125 m horizontal and 0.05 m vertical cell size. Between two drilling locations the susceptibility data are interpolated and smoothed. To avoid a boundary effect from the bottom model boundary, the susceptibility values were tapered with a cosine to zero. This extends the model to 3.0 m depth. To avoid boundary effects from the sides of the drilled section we extrapolated the susceptibility depth curves of the two outermost drilling locations to the sides and tapered them to an average susceptibility depth curve. This background curve represents the arithmetic mean of curves measured outside the pits in surrounding undisturbed soils (Figure 4 (B)). The length of the horizontal tapering interval l was held variable and tuned later by the inversion computation. Finally, to avoid boundary effects from the sides of the model, the susceptibility depth curve of the background was tapered to zero over a length of 10.0 m.

The forward calculations were carried out in Python using the library 'Fatiando a Terra' (Uieda et al., 2013). From this package we used the implementation of the formula by Plouff (1976) for

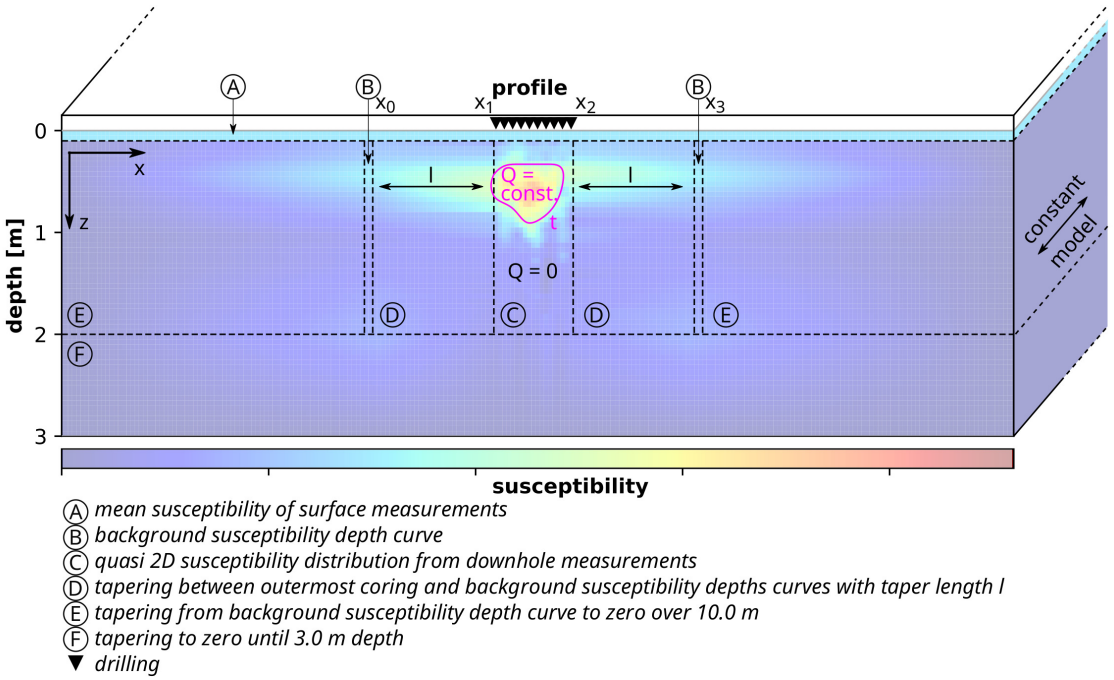

Figure 3: Sketch of a susceptibility model with the three inversion parameters Q (Koeningsberger ratio), t (threshold) and l (taper length).

each model cell to calculate the difference in the vertical component of the resulting magnetic field $\Delta B_z^{syn,\,i}$ as measured by the differential fluxgate sensors at each observation point $i = 1, ..., N$. For the modelling we applied the orientation and field strength of the present ambient earth magnetic field according to the 'International Geomagnetic Reference Field' (IGRF) as described by Thébault et al. (2015), i.e. the following values: declination $D = 3.87°$, inclination $I = 64.63°$ and magnetic field strength $B = 48626.3$ nT.

3.3.2 Remanent Magnetization Model

To determine the remanent soil magnetization in a representative way, we assumed that the Koenigsberger ratio is an unknown constant along each profile, the value of which is to be determined by the inversion calculation (see sec. 3.3.3). The remanent magnetization is thought to occur only above an unknown threshold t in the measured susceptibility (see Fig. 3), where the numerical value of the threshold would again be determined by inversion computation. This concept was implemented by defining trial values for the threshold and by attributing remanent magnetization only to grid cells with a measured susceptibility above these thresholds. By applying this threshold we imply that the surrounding loess matrix has a negligible remanent magnetization compared to the filling of the pits.

As to the orientation of the remanent magnetization vector, we assume that the change in the orientation of the ambient magnetic field since the filling of the pits is neglectable with respect to the resolution of the inversion computation. Indeed, palaeomagnetic studies have shown that the changes in declination since the 5th millenium BC are of the order of 5 °only (see Fig. 10 based on Pavón-Carrasco et al., 2010). Therefore, we applied the orientation of the recent earth's magnetic field according to the IGRF. This simplification is justified by a synthetic model study that is presented in appendix B.

3.3.3 Inversion of magnetic field data

We invert the magnetic data of each profile with respect to three variables: a representative constant Koenigsberger ratio Q, a susceptibility threshold t identifying the remanently magnetized cells and the length of the horizontal tapering interval l limiting the extrapolation of the drilled section to the sides. The inversion is performed by least-squares fitting of synthetic to field data.

To describe the horizontal tapering outside the drilled profile, let x_1 and x_2 be the location of the outermost left and right downhole measurement. Moreover, let x_0 and x_3 describe the locations of the background susceptibility depth curve $\kappa_{BG}(z)$, so that $x_1 - x_0 = x_3 - x_2 = l$ (see Fig. 3). Then, the taper $f(x)$ along the profile x is

$$f(x) = \begin{cases} \cos\left(\frac{l-(x-x_0)}{l}\frac{\pi}{2}\right), & \text{for } x_0 \le x \le x_1 \\ \cos\left(\frac{(x-x_2)}{l}\frac{\pi}{2}\right), & \text{for } x_2 \le x \le x_3. \end{cases} \tag{6}$$

The susceptibility distribution for $x_0 \le x \le x_1$ and $x_2 \le x \le x_3$ is then

$$\kappa(x,z) = \begin{cases} \kappa(x_1,z) + (\kappa(x_1,z) - \kappa_{BG}(z)) \cdot f(x), & \text{for } x_0 \le x \le x_1 \\ \kappa(x_2,z) + (\kappa(x_2,z) - \kappa_{BG}(z)) \cdot f(x), & \text{for } x_2 \le x \le x_3. \end{cases} \tag{7}$$

As described in section 3.3.1, the subsurface is divided into a regular grid where $\kappa_j = \kappa(x_j, z_j)$ denotes the susceptibility in cell $j = 1, ..., M$ at location (x_j, z_j). The calculated magnetic gradiometer data at observation point i resulting from solely induced magnetization is

$$\Delta B_z^{ind,\,i} = \sum_{j=1}^{M} a_{ij}\kappa_j, \tag{8}$$

where a_{ij} is a factor that comprises the information about the relative location of sensors and cells, the earth magnetic field as exciting field and the cell size (Plouff, 1976). Introducing remanent magnetization described by the Koenigsberger ratio Q and occurring only in cells with a susceptibility larger than the threshold t ($\kappa_j > t$), extends equation (8) to

$$\Delta B_z^{syn,\,i} = \sum_{j=1}^{M_t} a_{ij}\kappa_j + Q \cdot \sum_{j=M_t+1}^{M} a_{ij}\kappa_j. \tag{9}$$

We here assume that the cells are in the order from smallest $\kappa_{j=1}$ to highest susceptibility $\kappa_{j=M}$ and that κ_{M_t} is the largest susceptibility value smaller than t.

For $t, l = 0$, equation (9) describes an over-determined system of linear equations for Q. However, for $t, l \neq 0$ equation (9) describes a non-linear system with inversion parameters in the summation index (M_t) and the underlying subsurface model (l).

In least squares sense, the cost function is

$$L(Q,t,l) = \sum_{i=1}^{N} \left(\Delta B_z^{obs,\,i} - \Delta B_z^{syn,\,i}(Q,t,l)\right)^2 \tag{10}$$
$$0 \le Q \qquad 0 \le t \qquad 0 \le l \le l_{max}.$$

Hereby, all three parameters are constraint to be positive. Moreover, l is bound to be smaller than the distance to the next obvious magnetic anomaly on the profile l_{max}. This is always in a few meter distance.

To solve this non-linear optimization problem, we applied a subspace trust region interior reflective (STIR) algorithm (Branch et al., 1999). The idea of a trust region algorithm is to approximate the cost function in a region around the start parameters resp. the current solution of the iterative process. The approximation is then minimized in this trusted region, which is the so called subproblem. The used algorithm restricts the subproblem to two dimensions, in which

s_1 and s_2 span the subspace. The first direction s_1 is determined by the conjugate gradient, the second s_2 either by the direction of a Newton step or a negative curvature vector. If the solution of the subproblem leads to a smaller value of the cost function, this step is accepted and a new current solution is found. Otherwise the trust region is shrunk and all steps are repeated. The complete procedure is iteratively repeated until convergence.

3.3.4 Evaluation of inversion results

To quantify the reliability of the models, we use two statistical approaches. With the first one (A), we test if the single inversion problem (one magnetic profile) is multimodal and if trade-offs between different model parameters exist. For this we use the Gibb's distribution to calculate so-called expected model parameters, standard deviations and co-variances. With the second one (B), we test the influence of different magnetic profiles that are close to the drilling profile. The arithmetic mean and the standard deviation of the inversion parameters for each drilling profile are the final results.

Statistical Evaluation (A) - Gibb's distribution Following the descriptions by e.g. Martińez et al. (2000) and Wilken and Rabbel (2012), a set of expected model parameters can be calculated considering the Gibb's distribution as probability density function. To test whether the inversion result is influenced by the starting parameters, we defined a bounded model parameter space and passed trough this space systematically with the sets of starting parameters. Hereby, each of the three model parameters had five equidistantly spaced starting values. This results in 125 combinations and inversion runs for each magnetic profile. For the statistical evaluation of the inversion problem, we considered not only the final inversion results but also every set of parameters being an intermediate step of the inversion process. This results in a total number of R models for each inversion. Let m_k be a set of model parameters (Q_k, t_k, l_k) with $k = 1, ..., R$ with the respective cost $L_k = L(m_k)$. Then,

$$\xi(m_k) = \exp[-L_k] \tag{11}$$

is the probability of m_k. The expected model is then

$$\langle m \rangle = \frac{1}{P} \sum_{k=1}^{R} m_k \, \xi(m_k) \tag{12}$$

with the normalization factor

$$P = \sum_{k=1}^{R} \exp[-L_k]. \tag{13}$$

The covariance matrix is

$$C_m = \frac{1}{P} \sum_{k=1}^{R} (m_k - \langle m \rangle)(m_k - \langle m \rangle)^T \, \xi(m_k) \tag{14}$$

where the entries on the diagonal are the variances of each parameter. Hence, the standard deviation of the expected model parameters $\langle m \rangle_i$ is $\sigma_i = \sqrt{C_{i,i}}$. To evaluate the correlation or possible trade-off between two parameters, the normalized covariance matrix

$$\tilde{C}_{i,j} = \frac{C_{i,j}}{\sqrt{C_{i,i} \cdot C_{j,j}}} \tag{15}$$

is considered.

Statistical Evaluation (B) - Arithmetic mean The drilled profiles are approximately parallel to the magnetic profiles of the single sensors of the magnetic sensor array and orthogonal to the house-accompanying pits, which can be regarded as quasi two-dimensional structure. Therefore, we repeated the inversion computation for the five single sensor profile lines closest to the drilling profile (Fig. 4 A). The root mean square (RMS) error

$$\delta B_{RMS} = \sqrt{\frac{\sum_{i=1}^{N} \left(\Delta B_z^{obs,\,i} - \Delta B_z^{syn,\,i}\right)^2}{N}}, \tag{16}$$

is used to identify the best fitting model for each of the five magnetic profiles. This results in five best fitting models for each drilling profile and enables an estimation of an arithmetic mean with standard deviation for each inversion parameter and drilling profile.

4 Results

In the first subsection we present the results of the inversion of magnetic field data in two steps: first for one exemplary profile in detail and, next, for the remaining five profiles in form of an overview and table. In the second subsection, we include the results of the laboratory analyses of the samples.

4.1 Results of the inversion of magnetic field data

4.1.1 Example Profile 4

Figure 4 (B) shows the susceptibility depth curves that were measured along profile P 04 and are the base for the inter- and extrapolation of the two-dimensional susceptibility distribution. The susceptibility distribution is shown in Figure 5 (B) with the observed and calculated magnetic data at the top (A). The left column of Figure 4 (B) shows the mean curve for the subsurface outside of archaeological features ('background', 'BG'). The different magnetic profiles that were used for the inversion of the drilling profile P 04 are shown in Figure 4 (A). These are the measurements of single sensors in the gradiometer array.

For the uppermost layer of the topsoil (0.0 - 0.1 m depth) no data from borehole measurements are available. Therefore, we assumed a mean susceptibility of $74.5 \cdot 10^{-5}$ SI for this uppermost part of the surface layer, which is the average of the surface measurements. Susceptibility values deeper than 10 cm were determined in situ (cf. Fig. 4). Between 10 cm and 30 cm depth we found comparatively small susceptibility values between $60 - 70 \cdot 10^{-5}$ SI, which show only little lateral variation and represent the values of the topsoil mixed by ploughing. The susceptibility distribution of the subsoil shows increased values up to $192 \cdot 10^{-5}$ SI found in the central part in 60 cm depth. Below this maximum the susceptibility values decrease to around $25 \cdot 10^{-5}$ SI. Measurements outside the pits suggest that the susceptibility values around $150 \cdot 10^{-5}$ SI can be used as an approximate indicator for the boundary between pit and surrounding soil matrix (see also Fig. 4). Using this criterion the pit cross-section turns out to be a wide-angled V-shape. The top of the pit is found in about 50 cm depth where it is approximately 150 cm wide. The bottom of the pit reaches down to about 75 cm depth. The center of the pit shows the highest susceptibility values.

The measured magnetic anomaly has a maximum of 7.2 nT and a half-width of approximately 1.8 m. Assuming solely induced magnetization, the calculated magnetic data reach a maximum of 1.6 nT (dotted line, Figure 5). This corresponds to only 22% of the observed value or a maximal difference of 5.6 nT at the peak.

The difference along the profile between the measured and calculated magnetic anomaly can only be explained with a significant remanent magnetization. However, test computations have shown that an optimum fit cannot be reached by simply enhancing the susceptibility values of the model by a factor of Q. As shown in Figure 6 the fit improves if a lateral taper with adjustable width l is applied, which serves to grading susceptibility distribution from the pit to the

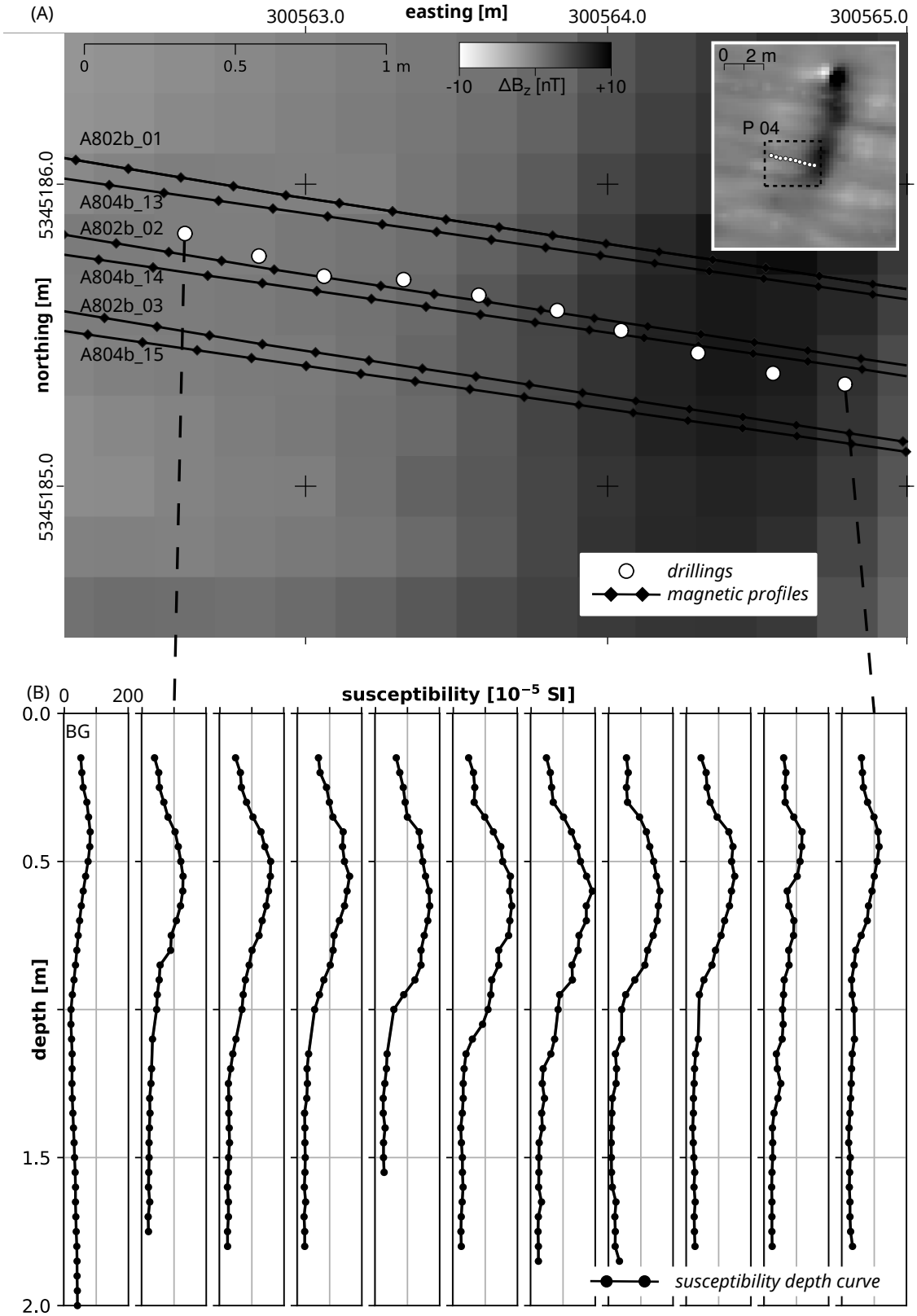

Figure 4: (A) Close-up of profile P 04 with the location of the drilling points and the magnetic sensor traces that were chosen for the inversion. (B) The left column (BG) shows the average 'background' susceptibility depth curve. The remaining columns show the measured susceptibility depth curves of profile P 04.

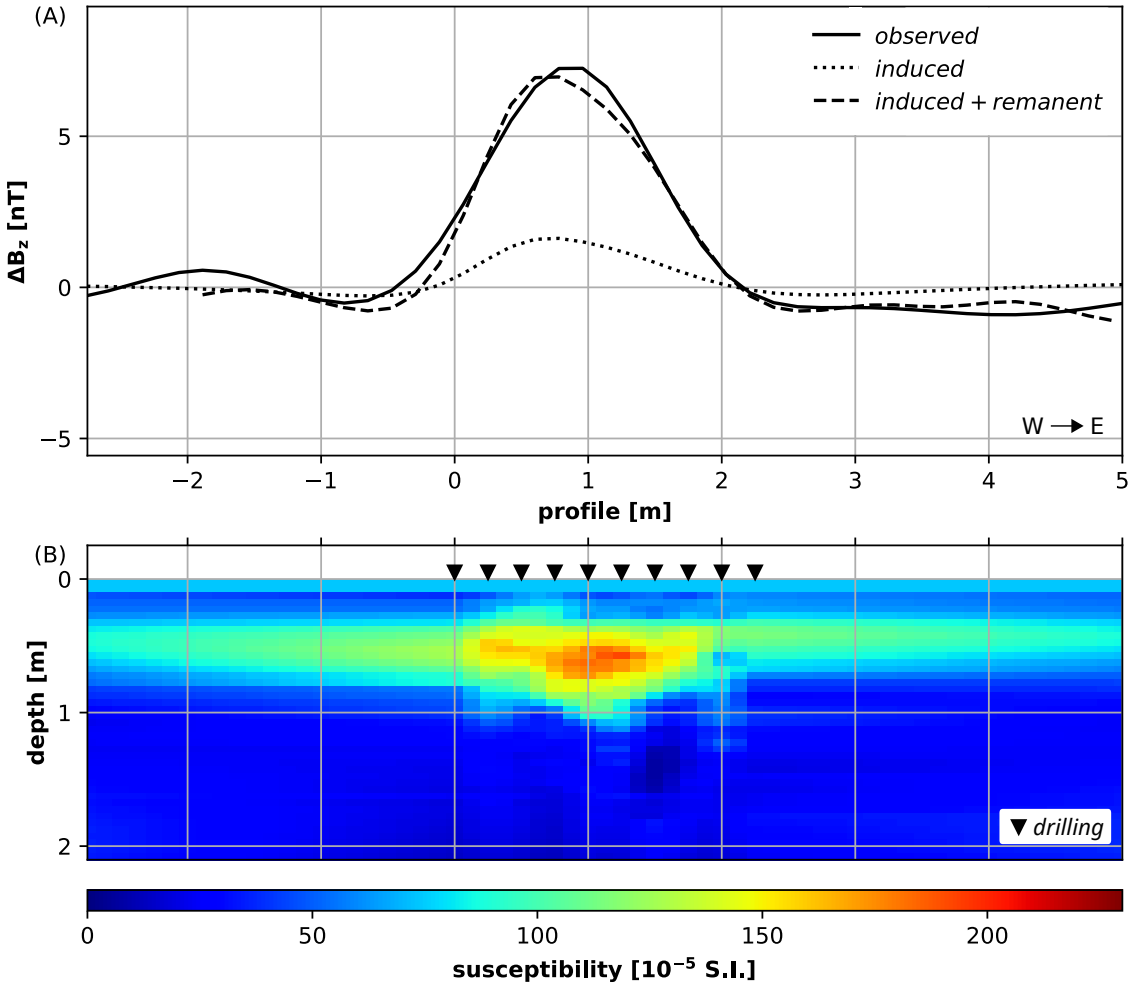

Figure 5: Profile P 04. (A) Measured magnetic profile (vertical component gradiometer data, A802b_03, see Tab. 2 and Fig. 4) and calculated magnetic anomaly assuming induced (doted line) and induced plus remanent (dashed line) soil magnetization. The dashed line shows the optimum fit obtained for a Koenigsberger ratio Q of 2.4 for subsurface points with a susceptibility $\kappa \geq 90 \cdot 10^{-5}$ SI, and $Q = 1$ elsewhere. The underlying 2D susceptibility distribution is shown in (B). Downhole measurements of magnetic susceptibility were performed at the drilling locations indicated by black triangles (cf. Fig. 4). Outside this area the values were extrapolated and tapered to the average κ-depth function of the surrounding soil.

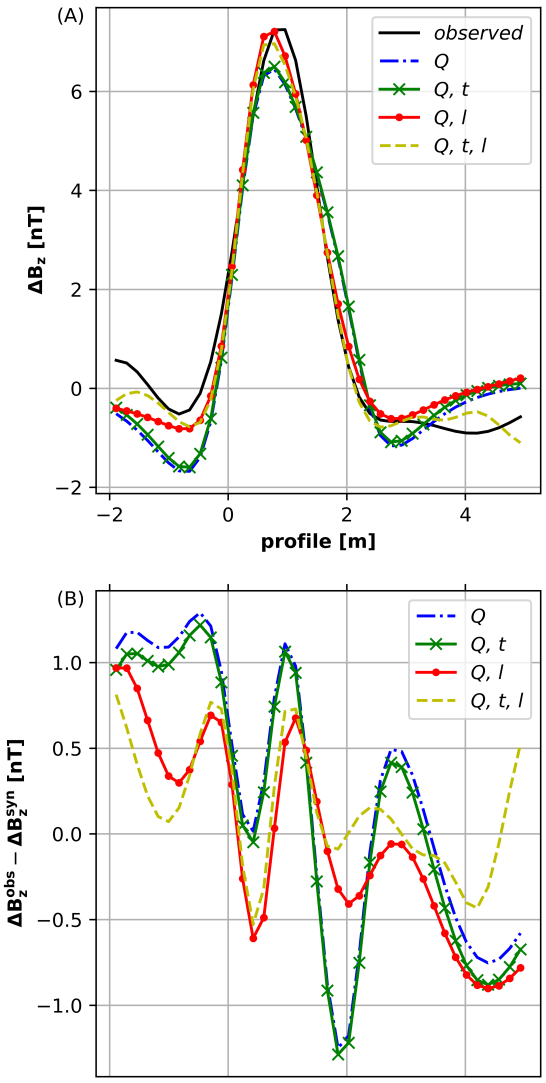

Figure 6: (A) Comparison between observed magnetic anomaly and calculated anomalies with different sets of parameters for profile P 04 (cf. Fig. 5). All model parameters (Koenigsberger ratio Q, threshold t and taper length l) are tuned by the inversion to optimum fit. (B) Difference between the observed magnetic anomaly and the different model responses.

undisturbed surrounding sediment. Obviously, also this additional condition is not sufficient for obtaining a satisfactory fit because the shape of the anomaly function is still not well reproduced in the boundary areas. This can be improved by introducing a threshold that restricts the application of a $Q > 1$ only to soil volumes exceeding a certain minimum susceptibility t. Figure 6 shows that the combination of Q and t is not sufficient as t is basically set to 0 SI by the inversion. The introduction of the variable horizontal taper l is primarily a numerical trick. However, it can be justified by the interpretation that the upper portions of the pit fill may have been smeared to a certain extent to outside the pit by agricultural activity in the past millennia.

The statistical evaluation (A) for drilling profile P 04 and the magnetic profile A802b_03 yields the expected model parameters $Q = 2.4 \pm 0.1\,(2.8\,\%)$, $t = 90 \pm 3 \cdot 10^{-5}\mathrm{SI}\,(3.8\,\%)$ and $l = 3.6 \pm 0.1\mathrm{m}\,(2.8\,\%)$. Figure 7 (A - C) shows the intermediate steps and converged models with the respective cost for all model parameters. The cost function is unimodal for all model parameters, which means it shows one well-defined minimum in the model parameter space (cf. circles in Fig. 7). Also there is no significant trade-off between the model parameters with trade-off values < 0.4 as visible in the covariance matrix in Figure 7 (D).

To evaluate how well the model parameters are resolved, we consider a fit within twice the sensor resolution ($\pm 2 \cdot 0.2\,\mathrm{nT}$) as equally well fitted. Then the synthetic data is $\Delta B_z^{syn,\,i} = \Delta B_z^{obs,\,i} + 2 \cdot 0.2\,\mathrm{nT}$ and for the cost follows $L_{res} = N \cdot (2 \cdot 0.2nT)^2$ where N is the number of observation points. Figure 8 shows the model parameters versus each other and the respective cost values. All models shown in green are equally well fit to the observed data. For Q the variability is small and therefore Q is well resolved. Contrasting to this, l and t show a higher variability. This is also reflected by the higher trade-off between t and l (cf. Fig. 7 D).

The optimum fitting parameters by RMS (statistical elvaluation B) of drilling profile P 04 with magnetic profile A802b_03 (ig. 5) is a Koenigsberger ratio of $Q = 2.4$, applied to soil volumes with a susceptibility of $\kappa \geq 90 \cdot 10^{-5}$ SI and a lateral taper with length $l = 3.7$ m. These are identical to the expected model parameters within their standard deviation. The resulting magnetic anomaly of induced and remanent magnetization has a maximum of approximately 7.0 nT (observed 7.2 nT) and the RMS error is reduced to 0.4 nT. The arithmetic means of the model parameters over the best fitting models for the different magnetic profiles for the drilling profile P 04 are $Q = 2.3 \pm 0.3\,(14.8\,\%)$, $t = 100 \pm 6 \cdot 10^{-5}\mathrm{SI}\,(6.3\,\%)$ and $l = 3.9 \pm 0.9\mathrm{m}\,(22.8\,\%)$. These errors are larger than those of the expected values for the inversions of a single magnetic profile. Therefore, the overall error is determined by the deviation resulting from different magnetic datasets.

4.1.2 Comparison of different magnetic profiles

The results of all drilling profiles are shown in Figure 9. They differ in both, the appearances of the cross-sections of the pits and the related magnetic anomalies. Yet, the underlying susceptibility-depth functions are very similar in their general form: the susceptibility increases until a maximum is reached and then decreases down to around $25 \cdot 10^{-5}$ SI. The location and amplitude of the maximum as well as the slope determine the cross-section of the pits.

Table 1 shows the statistical evaluation (A) of all drilling and magnetic profile combinations. These cases do not depend on the drilling profile but rather on the magnetic profile. For the majority of profile combinations the cost functions have a well-defined minimum for Q. Exceptions of this are profiles 16 and 21, which show considerable trade-offs between the inversion variables.

The best fitting model parameters in terms of RMS errors are shown in Table 2. The arithmetic mean for each drilling profile according to the statistical evaluation (B) is also given in this Table. A comparison of Tables 1 and 2 shows that the expected values and the best fitting values are very similar to each other.

The mean Koenigsberger ratio varies between 1.8 ± 0.2 and 7.0 ± 3.3, in which the mean of all best fitting values is 3.3 ± 2.2. The mean threshold in the susceptibility values, over which remanent magnetization is considered, varies between $27 \pm 3 \cdot 10^{-5}$ SI and $160 \pm 31 \cdot 10^{-5}$ SI with an overall mean of $78 \pm 54 \cdot 10^{-5}$ SI. Considering all best fitting values for the threshold, clusters at approx. 20 - 30 $\cdot 10^{-5}$ SI and 90 - 110 $\cdot 10^{-5}$ SI are found.

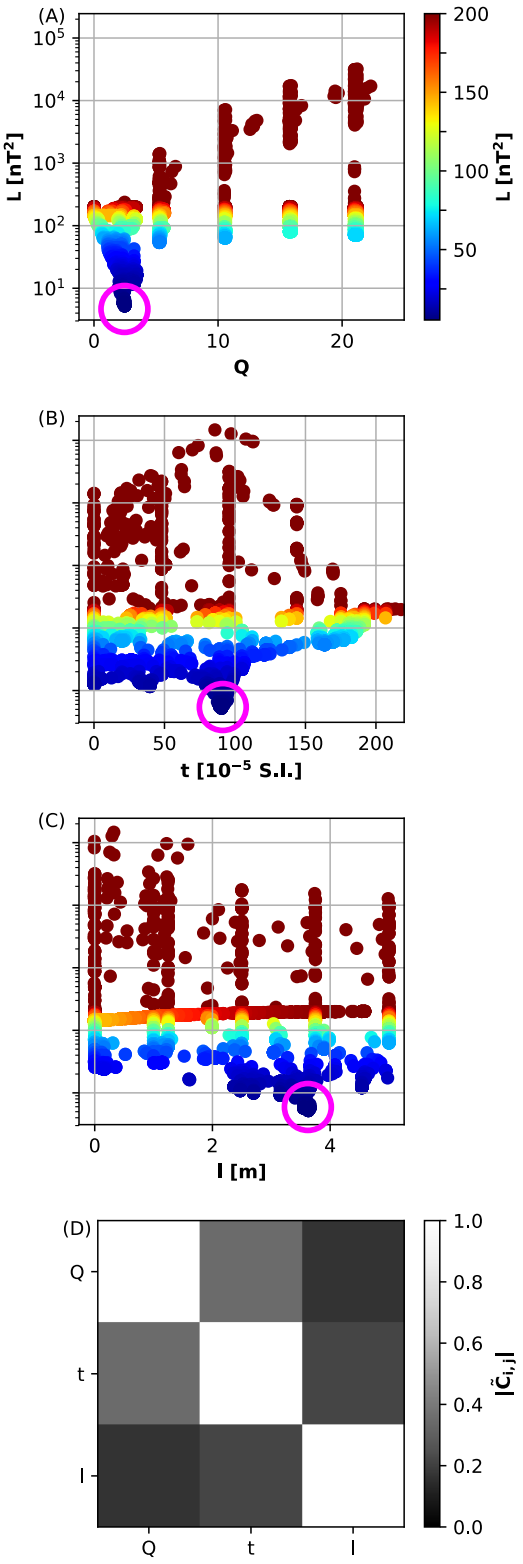

Figure 7: Model parameters (A) Koenigsberger ratio Q, (B) threshold t and (C) taper length l versus cost L for drilling profile P 04 and magnetic profile A802b_03. (D) Correlation matrix for this profile.

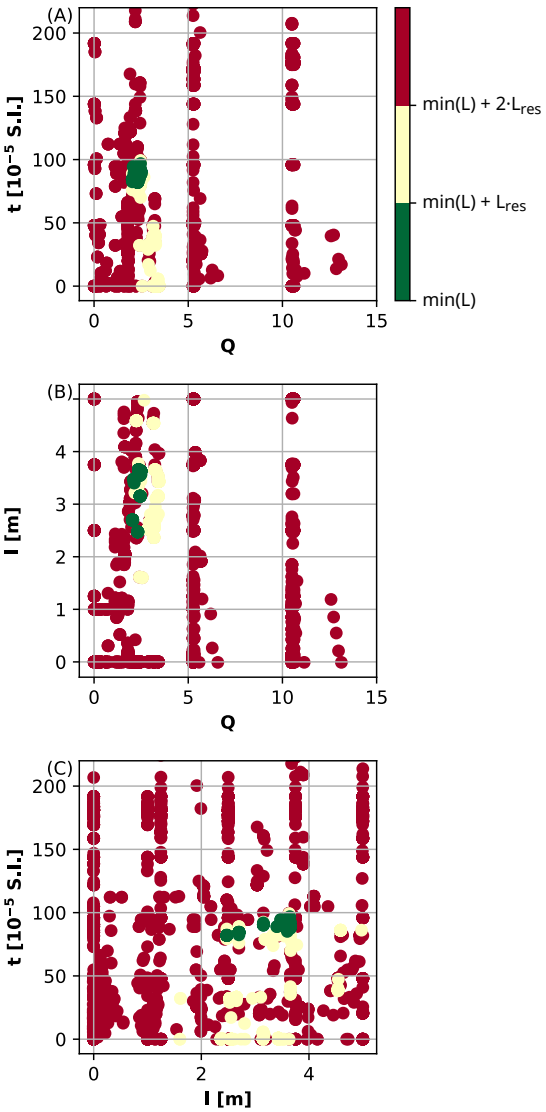

Figure 8: Comparison of model parameters versus each other for drilling profile P 04 and magnetic profile A802b_03. The cost indicates the fit of the respective model response to the observed data with values in green in the interval between the lowest cost and the lowest cost plus L_{res}. (A) Koenigsberger ratio Q versus threshold t, (B) Q versus taper length l, (C) l versus t.

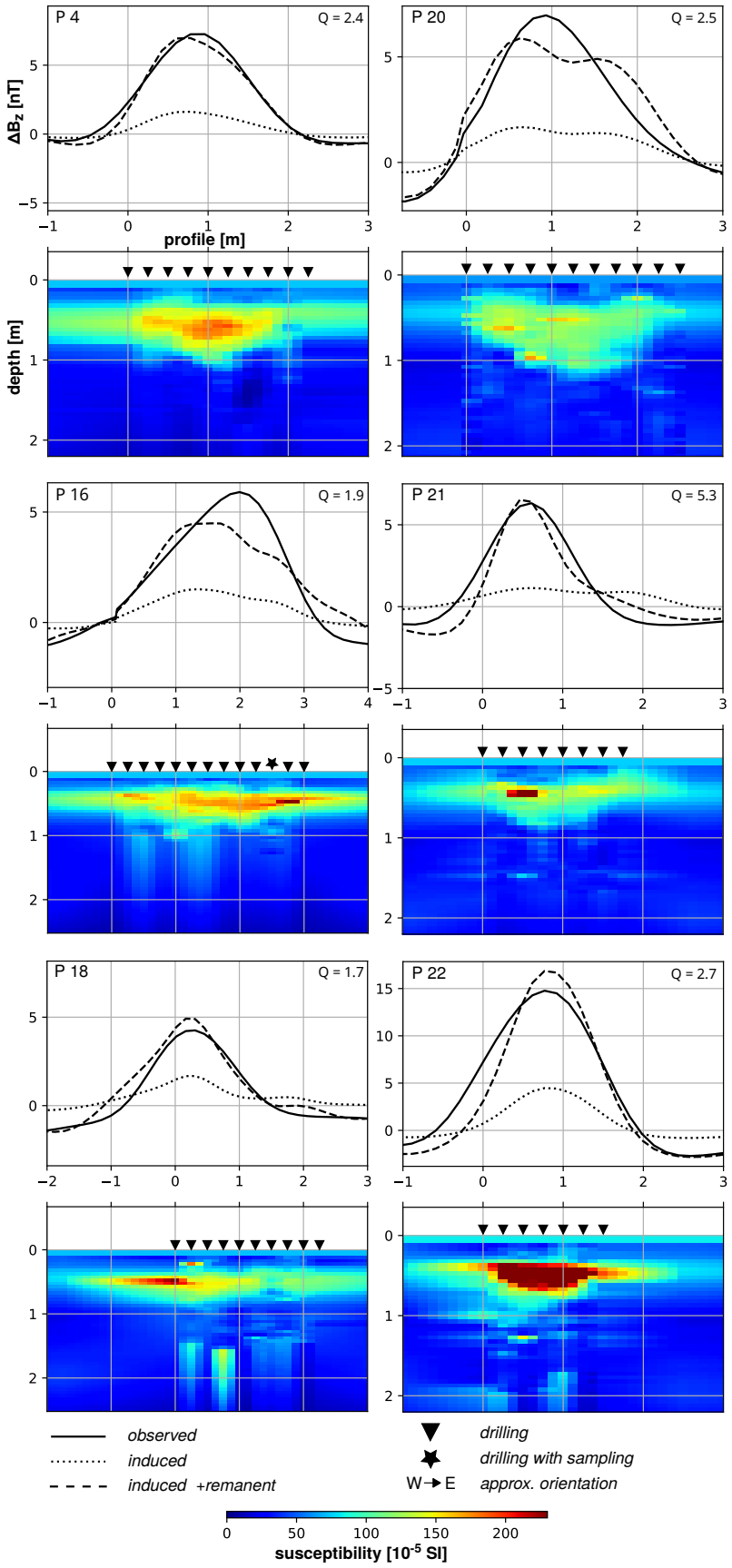

Figure 9: Data of all drilling profiles with the magnetic profiles (observed, induced and induced plus remanent) as line plots (uneven rows). Beneath the magnetic data, the measured susceptibility distributions (even rows) are shown with the drilling locations marked as triangles.

4.2 Sediment Analyses

In this section, we present the laboratory analyses of the samples from core P16_175. This core is part of profile P 16 (cross in Fig. 1) and was sampled to analyse the sediment layer below the loess. The laboratory analyses enable to investigate the causes of susceptibility and remanent magnetization. The samples are mixed samples, which were taken from the Auger corer from 20 to 35 cm long depth intervals.

According to field grain size estimations(Ad-hoc-Arbeitsgruppe Boden der Staatlichen Geologischen Dienste und der Bundesanstalt für Geowissenschaften und Rohstoffe, 2006), the sediment of the upper 164 cm (surface soil, pit fill, loess) could be classified as loamy silt (Ut2). The sediment in a depth of 164- 200 cm is a silty sand (Su2), probably exhibiting a periglacial slope debris layer. The two upper samples were taken from 0.20 - 0.40 m and 0.53 - 0.85 m depth. They are representative for the top soil and the uppermost pit-fill, which consist only of grains $<$ 2 mm. The two deeper samples are from 1.13 - 1.44 m and 1.64 - 2.00 m depth. In addition to the small-grained fraction they also contain a fraction $>$ 2 mm. The fraction $>$ 2 mm of the sample from 1.13 m to 1.4 m depth contains daub and gravel. The sample from 1.64 m to 2.0 m has a small gravel content. The susceptibility was measured on the fraction $<$ 2 mm to be comparable to standard pedological samples as well as on the complete samples to be comparable to the in-situ measurements. All other laboratory analyses were solely conducted on the fraction $<$ 2 mm.

igure 10 shows the results of the different laboratory analyses and, for comparison, the downhole measurements of the susceptibility. Qualitatively the downhole (A) and laboratory (B) measurements show the same trends of susceptibility with depth. This trend shows the highest susceptibility values around 60 cm depth and a decrease below as described already in section 4.1.1. For comparison the downhole measurements are also shown in (B). Some material has been lost during coring and therefore, the sediments might have shifted in the corer. In general, the volume susceptibility measurements in the laboratory show somewhat lower values than the field measurements. This can be explained with the preparation process, in which the samples are decompacted on the way from the drilling to the laboratory measurements. Therefore, laboratory and in-situ densities and related volume susceptibility values of the soil may be somewhat different. The laboratory measurements include also a sample from below 1.5 m depth, which shows again increased susceptibility values.

igure 10 (B) shows the high and low frequency measurements of the complete samples versus the ones of the fraction $<$ 2 mm. For the sample in 1.13 - 1.44 m depth, the complete sample shows higher susceptibility measurements whereas the for the sample in 1.64 m to 2.0 m depth it is vice versa. This is explainable by the detected daub inclusions in sample 1.13 - 1.44 m.

The frequency dependent portion of susceptibility (C) is approximately 9 % for the two uppermost samples and decreases over 6 % down to 0.1 % for the deepest. Even tough the high and low frequency measurements of the fraction $<$ 2 mm and the complete sample for the two deepest samples differ in their absolute values, the resulting frequency dependent susceptibility values are similar.

The trend of the total iron content by weight (D) is similar to the trend of the susceptibility except for the deepest sample. The susceptibility value of the deepest sample is the highest measured one, however the iron content in this sample is the lowest measured one. This ratio points to the presence of iron compounds in the deepest sample with a higher susceptibility than the iron compounds in the other samples.

The xrd mineral assemblage shows small differences between the samples. They consist of quartz, feldspars, mica, with higher amounts of expandable clay minerals in the upper two samples. Spurs of maghemite/ magnetite, gypsum and calcite (lower two samples) are present as well. The Fe_d/Fe_t ratios are the highest in the upper two samples (pit fill) (0.0029 resp. 0.0022), the lowest in the loess sample (0.0018) and increase again in the periglacial debris sample (0.0022). Thus, a clear pedogenic enrichment of iron is present in the topsoil and pit-fill and a dithionite soluble primary iron mineral in the lowest sample is probable to explain the increase of susceptibility within the deepest layer. The content of organic matter is the highest in the topsoil and in the pit fill (ig.10 E). Some carbonates are present in the loess, whereas the deepest sample contains very

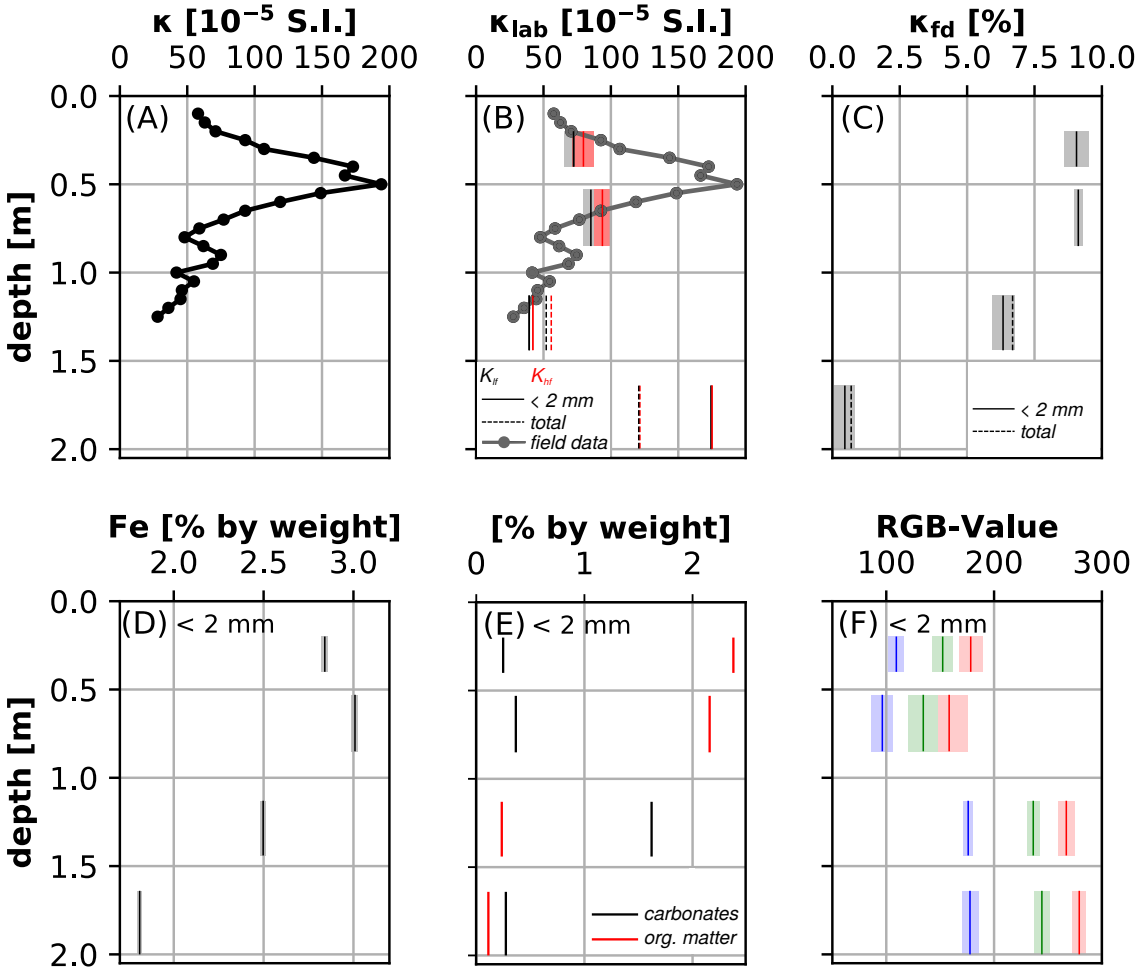

Figure 10: Data of coring P16_175 (location marked with a star in Figures 1 and 9). (A) Susceptibility downhole measurements. Laboratory measurements of (B) low frequency susceptibility and high frequency susceptibility for the fraction < 2 mm and the complete sample (with field measurements for comparison), (C) frequency dependent susceptibility, (D) iron content by weight resulting from XRF, (E) content of organic matter and carbonates, and (F) sample color in red-green-blue (RGB) [scale 0 - 1023]. For the laboratory measurements the vertical line represents the mean value and the faded box the standard deviation for each mixed sample of the respective depth interval.

few organic matter and carbonates. The RGB color values (F) clearly reflect the darker colors of the pit fill and the organic surface horizon, whereas the lower two layers are more reddish brown. The sample from the pit fill (0.53-0.85m) is the darkest layer.

The results of the laboratory analyses can be summarized as follows: The deepest sample (periglacial debris) has the highest susceptibility, however the frequency dependent susceptibility and the iron content by weight are the lowest. Moreover the contents of organic matter and carbonates are very low. The topsoil and pit filling have intermediate susceptibility values with a high frequency dependent susceptibility and a high content of organic matter and iron, whereas the content of carbonates are low. The loess has the lowest susceptibility value with an intermediate frequency dependent portion and an intermediate content of iron. As expected the content of organic matter is very low and the content of carbonates is the highest of all samples.

5 Discussion

In the discussion, we first address the methodical aspects of the inversion approach. Then we turn to the interpretation of the susceptibility distribution in combination with the derived Koenigsberger ratio to analyse the origin of remanence.

5.1 Evaluation of the inversion approach and the results

We presented a novel inversion approach to determine the Koenigsberger ratio from magnetic f ield measurements (gradiometer data) and downhole measurements of the magnetic susceptibility, in which the susceptibility measurements constitute a variable basis function of the inversion. We haven't found other studies, in which this sort of partial parameter coupling has been applied. Even field studies of the Koenigsberger ratio are rare.

For Q the cost function has a single, well-defined minimum and small trade-offs between different model parameters are observed. This shows that our approach yields reasonable values for the Koenigsberger ratio. The trade-off identified between t and l indicates that one of these model parameters should be determined by measurement. For example, the taper length l could be determined implicitly by extending the drilling profile far enough beyond the magnetic anomaly. In this case the complete subsurface section that contributes to the magnetic anomaly would be covered with downhole measurements and taper length l could even be omitted in the equations.

The percentage standard deviation per drilling profile (statistical evaluation B) is larger than the error of the single inversions (statistical evaluation A). Therefore, the influence of different magnetic data sets yields a measure for the overall error.

For profile 16 higher trade-off values and generally higher RMS errors were observed. This probably indicates that the model was not complex enough to explain the observed magnetic anomalies. One possible reason is the approximation of actually three-dimensional susceptibility and remanence distributions with a two-dimensional susceptibility distribution and a parametrization of the remanence with three parameters. Another reason might be a significant contribution of the periglacial debris layer beneath the loess. The laboratory analyses showed that this layer has a high susceptibility. Moreover, the heterogeneity of a debris layer is likely reflected in a heterogeneous susceptibility distribution and possibly also a remanent magnetization. However, we were not able to measure the susceptibility distribution in this layer because it was not feasible to lower the probe. To investigate the magnetic properties of this layer, further studies can comprise test trenches or lined cores to gather undisturbed high resolution samples for laboratory analyses.

For profile 21, especially high values for Q (4.2 - 11.2) were determined in combination with high values for t ($149 - 186 \cdot 10^{-5}$ SI). These locally very restricted areas of high susceptibility values might be related to burned material, i.e. daub or pottery. Both have been documented in the fillings of the pits. Our approach can be extended by an additional parameter for Q, that is only valid for remanent magnetization of heated materials.

5.2 Remanent magnetization in archaeological prospecting

The starting point of our study was a simple check whether or not measured magnetic anomalies fit to calculated anomalies given the downhole-measured susceptibility distributions. This comparison is straightforward, yet not common in archaeological case studies. A similar approach was used by Bruce Bevan to quantify the magnetic anomaly of a potential structure (Dalan, 2008). The geometry of the feature approximated by a wedge and the initial susceptibility contrast for the inversion was derived from downhole susceptibility measurements, too. As in our case, the comparison of the measured and calculated magnetic anomaly showed that the susceptibility contrast was not sufficient to explain the observed anomaly. Instead, it needed to be increased from $45 \cdot 10^{-5}$ SI to $140 \cdot 10^{-5}$ SI. This also indicates a contribution from remanent magnetization (Dalan, 2008). Also Simon et al. (2012) concluded that the measured susceptibility contrast for the modeled simplified source geometry is not high enough to explain the measured magnetic anomaly. With our approach, we offer a solution or an improvement to this mismatch problem in two regards: (1) a direct quantification of the Koenigsberger ratio and (2) the simplified source geometry with susceptibility contrasts is replaced by measured susceptibility distributions so that complex subsurface structures can be accessed.

As suggested by the equivalence principles of potential field theory, simplified magnetic source distributions (e.g. Wilken et al., 2015; Miller et al., 2019) are capable to explain observed anomalies in a satisfying way in many cases. However, our downhole measurements have shown that the assumption of a polygonal zone of constant susceptibility contrast would be an oversimplification of the filling of the neolithic pits. The measured susceptibility distributions are diverse and heterogeneous, hence too complex to be consistently approximated by a simple source geometry.

Furthermore, in general the Koenigsberger ratio and the remanent magnetization are not negligible (cf. Dalan, 2008; Simon et al., 2012). However, the studies using a polygonal zone as source geometry also assume mostly only induced magnetization. However, we have shown that it should be carefully tested if the negligence of remanence is valid. If this is not possible, for example due to missing susceptibility measurements, we recommend to refer to the contrast as an effective susceptibility contrast as resulte from the sum of induced and remanent magnetization so that only a divergent orientation of the remanence is neglected.

However, further tests could examine how dense the drilling locations need to be placed along the anomaly. Also, a variable drilling separation with increased spacing at the edges of the anomaly can improve our approach. On the one hand, this can reduce to number of drillings that need to be conducted to depict the susceptibility distributions. On the other hand, an increased number of drillings outside the pits, makes the tapering parameter l obsolete as this part of the profile gets covered with downholes measurements.

5.3 How do the derived Koenigsberger ratios compare to published values?

The Koenigsberger ratios, that lead to the models with best fits (Tab. 2), range from 1.6 to 10.5 with the majority of the values being smaller than 4. As described above, in archaeological contexts the Koenigsberger ratio is determined in archeomagnetic case studies. These address sites with burned contexts, like e.g. kiln, ovens, fire places. Schnepp et al. (2004) give an overview for archaeological sites in Germany. They divided the samples into three categories of structures heated to different temperatures (low, moderate and high). For all three categories the Koenigsberger ratio ranges from values of approx. 0.1 to values larger than 100. There seems to be a tentative tendency that for higher temperatures the majority of Q values shift to slightly higher values. The variability within the different categories, might indicate how well a specimen was heated. This means that high Koenigsberger ratios are measured for specimens carrying complete thermoremanent magnetization (Schnepp et al., 2004). However, also the parent material with its capability to carry remanent magnetization needs to be considered.

In the present study, we derived representative values of the Koenigsberger ratio assumed to be constant value for a larger volumes of susceptible soil. The actual size and shape of this volume is

determined by the threshold variable determined in the inversion. Therefore, this Koenigsberger ratio must be interpreted as value for a sample 'mixed' from larger soil volumes to be comparable with published measurements. In the present case, the subsurface does not show any traces of burning apart from sporadic daub pieces or pottery fragments. Therefore, the corresponding Koenigsberger ratios represent values of only partly or not heated soils and sediments with loess as parent material. We derived values that are within the range presented by Schnepp et al. (2004). With an approx. range of 0.1 to 10 Kapper et al. (2014b) presented values closer to the here observed one form an archaeological context of burned cave sediments. However, in their study the majority of the values fall into the range of 0.1 to 1, which is considerably lower than the values found for the longpits of the Vráble site.

Without determining the Koenigsberger ratio Batt (1999) measured the NRM of water-lain archaeological sediments of 30 depositional environments within Britain. For the natural remanent magnetization they obtained intensities in the range of burned materials. Therefore, also our determined values of Q of water-logged sediments with an intensity in the range of burned sediments are plausible.

5.4 What is the origin of the remanence?

Both, the observed depth functions of susceptibility and the deduced remanent magnetization within the organic infills of house-accompanying pits of the LBK houses at Vráble could be explained as a result of organic matter decomposition processes in presence of magnetotactic bacteria (e.g. Blakemore, 1975; Bazylinski et al., 2013) and an orientation of particals with a magnetic moment in terms of DRM or postDRM (e.g. Evans and Heller, 2003; Uieda et al., 2013; Batt, 1999).

While magnetotactic bacteria are traditionally studied in freshwater (e.g Blakemore et al., 1979; Spring et al., 1993) or marine environments (Petermann and Bleil, 1993; Stolz et al., 1986), they have been detected in waterlogged soils as well (Fassbinder et al., 1990). There, magnetotactic bacteria were found to thrive close to or below the oxix-anoxid interface Bazylinski et al. (2013). However, considering the habitat conditions of microorganisms in soils, a remarkable microscale variability of water and oxygen access has been documented (e.g. Hartmann and Simmeth, 1990; Hattori, 1973; Sexstone et al., 1985).

The infill of everyday waste containing large amounts of organic matter into the house-accompanying pits of the LBK is probable to have resulted in partly decomposition of the organic detritus under partly anoxic conditions. This seems reasonable considering the regional climate in eastern Slovakia, the form of the house-accompanying pits and the properties of their infill. The climate at Vráble is classified as cold-temperate (Köppen-Geiger Cfb) (Schönwiese, 1994) with an annual mean temperature of 9.9 °C and an annual sum of precipitation of 593 mm for the period 1982 to 2012 (www.climate-data.org, accessed 07.11.2019). Assuming similar conditions throughout the last 7,000 years, results in an average excess of precipitation above evapotranspiration at the site. House-accompanying pits do not have an outlet nor are they sheltered from addition of water by precipitation (e.g. Dreibrodt et al., 2017), required for aerobic decomposition of organic matter according to technical instructions of pit composting (Misra et al., 2003). In fact, the orientation of the pits along the eaves of the LBK houses is even probable to increase the number and duration of waterlogging phases during the lifetime of the prehistoric house. In addition, after the abandonment of the houses, remainders of the pits completely filled or not, were enduring depressions of higher water content compared to the surrounding unbuilt areas. The infill of the pits, studied in numerous excavations, is mainly composed of a dark organic-mineral mixture, often resembling the local topsoil macroscopically (see Fig. 2). Occasionally, thin layers of daub are intercalated, representing usually less than one percent of the total infill volume.

Thus, an organic rich infill as a growing medium for soil bacteria was provided by the prehistoric inhabitants and according to the regional climatic conditions and configuration of the pits probably exposed to phases of anoxic decomposition. Additionally, anaerobic conditions could have been induced by high growing rates of aerobic soil bacteria populations on the organic rich infills consuming large amounts of oxygen. Micro-scale phenomena in infilled soil aggregates provide a third mechanism that could produce locally anaerobic conditions.

We argue that these phases of anaerobic decomposition of the organic trench-infills provided suitable living conditions for magnetotactic bacteria, which in turn resulted in the formation of ferrimagnetic iron compounds. These iron compounds were able to orient in the direction of the earth magnetic field while being mobile due to waterlogging. The outlined scenario is able to explain our record. The typical site-specific downhole trend of susceptibility shows a minimum below the pit fills increased values within the pit fill and a decrease towards the topsoil. This indicates that the process that resulted in the formation of the magnetic anomaly within the pit fill was not in action in the well-aerated topsoil, plowed additionally probably during approx. 2,000 years since site formation (Dreibrodt et al., 2017). Magnetotactic bacteria are known to be restricted to or close to anoxic environments (Bazylinski et al., 2013).

Summarizing, the remanent magnetization deduced by comparison of observed magnetic anomalies and anomalies resulting from induced magnetization in this study is explainable by the outlined scenarios. Although we do not have direct proof, the contribution of magnetotactic bacteria in the decomposition process of the organic rich infill of the investigated prehistoric pits provides the best explanation of the deduced remanent magnetization. Furthermore the degree of remaining remanent magnetization can be weakened by any intensive postdepositional bioturbation. But also reinforced by realignment of the mobile ferrimagnetic iron compounds.

6 Conclusions

Based on our study the conclusions can be derived:

1. Vertical sections of magnetic susceptibility determined from dense drillings and downhole measurements can be used to reliably image cross-sections of house-accompanying pits at the Linearbandkeramik site Vráble 'Farské', and

2. the remanent magnetization of the pit fill and the surrounding loess is not negligible.

3. The representative values of remanent magnetization can be determined through a new inversion approach based on observed magnetic anomalies and two-dimensional in-situ measurements of the susceptibility.

4. The origin of the remanent magnetization can be explained by that magnetotactic bacteria increase the amount of ferrimagnetic iron compounds in the infill of the pits compared to the surrounding and that these align in the waterlogged environment and therefore result in a clearly detectable remanent magnetization.

Incorporating downhole susceptibility measurements in archaeological field campaigns enables an efficient ground truthing of magnetic mapping and determination of cross-sections of key targets. Susceptibility measurements can also be conducted on plana of excavations. Our inversion approach can then be used to determine the Koenigsberger ratio as it is essential for quantitative interpretation of magnetic data to know the ratio between induced and remanent magnetization.

The mean Koeningsberger ratios for six examined pits vary between 1.8 and 7.0, with the majority of values beeing smaller than 3.5. The Koenigsberger ratio acts only on model cells with a susceptibility higher than the mean thresholds between $27 - 160 \cdot 10^{-5}$ SI. The mean length of the horizontal taper, i.e. an area of increased susceptibility values that decrease with increasing distance from the pits center, is between 1.0 and 3.9 m. The gradual decay of the susceptibility might be a consequence of approx. 2,000 years of plowing.

Furthermore, the thorough understanding of the nature of the magnetic anomalies is necessary for the extrapolation of measured susceptibility depth-profiles to the complete magnetic map of the site. Using the measured susceptibility depth-profiles as references and knowing the ratio of induced to remanent magnetization enables inversion of the magnetic map. From the inversion the depth and shape of archaeological features can be derived. This concept makes use of the areal sparse susceptibility data as a base for magnetically guided up-scaling to the complete settlement site.

Acknowledgements

We gratefully acknowledge the help of Erica Corradini, Amelie Klein and especially Raphael Kahn while conducting all the manual drillings and measurements in the heat of summer 2018. Furthermore, we like to thank everybody who was involved in the field works that comprised any form of drilling and sampling as this data advected the image of the site although not presented here.

References

Ad-hoc-Arbeitsgruppe Boden der Staatlichen Geologischen Dienste und der Bundesanstalt für Geowissenschaften und Rohstoffe (2006) *Bodenkundliche Kartieranleitung KA5*. Stuttgart Germany: Schweizerbart Science Publishers.

Allard, P., Hamon, C., Bonnardin, S., Cayol, N., Chartier, M., Coudart, A., Dubouloz, J., Gomart, L., Hachem, L., Ilett, M., Meunier, K., Monchablon, C. and Thevenet, C. (2013) Linear Pottery domestic space: Taphonomy, distribution of finds and economy in the Aisne valley settlements. In *The domestic space in LBK settlements. Nanterre (France), 7-8 October 2010* (eds. C. Hamon, P. Allard and M. Ilett), 9–28. Rahden/Westf.: M. Leidorf.

Batt, C. M. (1999) Preliminary investigations into the acquisition of remanence in archaeological sediments. *Geological Society, London, Special Publications*, **151**, 9–19.

Bazylinski, D. A., Lefèvre, C. T. and Schüler, D. (2013) Magnetotactic bacteria. *The Prokaryotes: Prokaryotic Physiology and Biochemistry*, 453–494.

Blakemore, L., Searle, P. and Daly, B. (1987) Methods for chemical analysis of soils. In *Scientific Report 80. New Zealand Soil Bureau*. Department of Scientific and Industrial Research, New Zealand.

Blakemore, R. (1975) Magnetotactic bacteria. *Science*, **190**, 377–379.

Blakemore, R., Maratea, D. and Wolfe, R. (1979) Isolation and pure culture of a freshwater magnetic spirillum in chemically defined medium. *Journal of bacteriology*, **140**, 720–729.

Branch, M. A., Coleman, T. F. and Li, Y. (1999) A Subspace, Interior and Conjugate Gradient Method for Large-Scale Bound-Constrained Minimization Problems. *SIAM Journal on Scientific Computing*, **21**, 1–23.

Carrancho, Á., Villalaín, J. J., Angelucci, D., Dekkers, M. J., Vallverdú, J. and Vergès, J. M. (2009) Rock-magnetic analyses as a tool to investigate archaeological fired sediments: a case study of mirador cave (Sierra de Atapuerca, Spain). *Geophysical Journal International*, **179**, 79–96.

Catanzariti, G., McIntosh, G., Soares, A. M. M., Díaz-Martínez, E., Kresten, P. and Osetea, M. L. (2008) Archaeomagnetic dating of a vitrified wall at the Late Bronze Age settlement of Misericordia (Serpa, Portugal). *Journal of Archaeological Science*, **35**, 1399–1407.

Dalan, R. A. (2008) A review of the role of magnetic susceptibility in archaeogeophysical studies in the USA: recent developments and prospects. *Archaeological Prospection*, **15**, 1–31.

Dean, W. E. (1974) Determination of carbonate and organic matter in calcareous sediments and sedimentary rocks by loss on ignition; comparison with other methods. *Journal of Sedimentary Research*, **44**, 242–248.

Dreibrodt, S., Furholt, M., Hofmann, R., Hinz, M. and Cheben, I. (2017) P-Ed-XRF-Geochemical Signatures of a 7300 Year Old Linear Band Pottery House Ditch Fill at Vráble-Ve'lké Lehemby, Slovakia - House Inhabitation and Post-Depositional Processes. *Quaternary International*, **438**, 131–143.

Ertepinar, P., Langereis, C. G., Biggin, A. J., de Groot, L. V., Kulakoğlu, F., Omura, S. and Süel, A. (2016) Full vector archaeomagnetic records from Anatolia between 2400 and 1350 BCE: Implications for geomagnetic field models and the dating of fires in antiquity. *Earth and Planetary Science Letters*, **434**, 171–186.

Evans, M. E. and Heller, F. (2003) *Environmental Magnetism: Principles and Applications of Enviromagnetics*. International geophysics series. Academic Press.

Fassbinder, J. W. (2015) Seeing beneath the farmland, steppe and desert soil: magnetic prospecting and soil magnetism. *Journal of Archaeological Science*, **56**, 85–95.

Fassbinder, J. W. E., Stanjekt, H. and Vali, H. (1990) Occurrence of magnetic bacteria in soil. *Nature*, **343**, 161–163.

Furholt, M., Bátora, J., Cheben, I., Kroll, H., Rassmann, K. and Tóth, P. (2014) Vráble-Veľké Lehemby: Eine Siedlungsgruppe der Linearkeramik in der Südwestslowakei. Vorbericht über die Untersuchungen der Jahre 2010 und 2012 und Deutungsansätze. *Slovenská Archeológia*, **62**, 227–266.

Gómez-Paccard, M., Catanzariti, G., Ruiz-Martínez, V. C., McIntosh, G., Núñez, J. I., Osete, M. L., Chauvin, A., Lanos, P., Tarling, D. H., Bernal-Casasola, D. and Thiriot, J. (2006) A catalogue of Spanish archaeomagnetic data. *Geophysical Journal International*, **166**, 1125–1143.

Hartmann, A. and Simmeth, I. (1990) Einfluss des Bodenwasserpotentials auf die Lokalisation mikrobieller Aktivität in Bodenaggregaten eines ariden Sandbodens. *Mitt. Deutsch. Bodenkdl. Ges*, **62**, 39–42.

Hattori, T. (1973) Microbial life in the soil: an introduction. *Tech. rep.*

Herries, A., Kovacheva, M. and Kostadinova, M. (2008) Mineral magnetism and archaeomagnetic dating of a mediaeval oven from Zlatna Livada, Bulgaria. *Physics and Chemistry of the Earth, Parts A/B/C*, **33**, 496–510.

Hunt, C. P., Moskowitz, B. M. and Banerjee, S. K. (2013) *Magnetic Properties of Rocks and Minerals*, 189–204. American Geophysical Union.

Jordanova, N., Kovacheva, M. and Kostadinova, M. (2004) Archaeomagnetic investigation and dating of Neolithic archaeological site (Kovachevo) from Bulgaria. **147**, 89–102.

Jrad, A., Quesnel, Y., Rochette, P., Jallouli, C., Khatib, S., Boukbida, H. and Demory, F. (2014) Magnetic Investigations of Buried Palaeohearths Inside a Palaeolithic Cave (Lazaret, Nice, France): Magnetic Study of Lazaret Palaeohearths. *Archaeological Prospection*, **21**, 87–101.

Kainz, J. and Cotter, J. P. (2018) A broad band magnetic susceptibility test study — the magnetic spectroscopy of a neolithic ditch. *Journal of Archaeological Science: Reports*, **18**, 139–150.

Kapper, K. L., Anesin, D., Donadini, F., Angelucci, D. E., Cavulli, F., Pedrotti, A. and Hirt, A. M. (2014a) Linking site formation processes to magnetic properties. Rock- and archeomagnetic analysis of the combustion levels at Riparo Gaban (Italy). *Journal of Archaeological Science*, **41**, 836–855.

Kapper, K. L., Donadini, F., Mauvilly, M., Panovska, S. and Hirt, A. M. (2014b) New directional archeomagnetic data of burned cave sediments from Switzerland and geomagnetic field variations in Central Europe. *Geophysical Journal International*, **198**, 1208–1221.

Květina, P. and Řídký, J. (2017) Neolithic settlement space waste, deposition and identity. In *Archaeologies of waste: encounters with the unwanted* (eds. D. Sosna and L. Brunclíková), 127–144. Oxford: Oxbow Books.

Linford, N. T. and Canti, M. G. (2001) Geophysical evidence for fires in antiquity: preliminary results from an experimental study. Paper given at the EGS XXIV General Assembly in The Hague, April 1999. *Archaeological Prospection*, **8**, 211–225.

Martińez, M., Lana, X., Olarte, J., Badal, J. and Canas, J. (2000) Inversion of rayleigh wave phase and group velocities by simulated annealing. *Physics of the Earth and Planetary Interiors*, **122**, 3–17.

Meadows, J., Müller-Scheeßel, N., Cheben, I., Rose, H. and Furholt, M. (2019) Temporal dynamics of Linearbandkeramik houses and settlements, and their implications for detecting the environmental impact of early farming. *The Holocene*, **29**, 1653–1670.

Miller, B. K., Miller, B. K., Furholt, M., Bayarsaikhan, J., Tüvshinjargal, T., Brandtstätter, L., Wright, J., Ayush, T. and Wunderlich, T. (2019) Proto-Urban Establishments in Inner Asia: Surveys of an Iron Age Walled Site in Eastern Mongolia. *Journal of Field Archaeology*, **44**, 267–286.

Misra, R., Roy, R. and Hiraoka, H. (2003) On-farm composting methods. *Tech. rep.*, Rome, Italy: UN-FAO.

Müller-Scheeßel, N., Cheben, I., Filipović, D., Hukelová, Z. and Furholt, M. (in press) The LBK site of Vráble in Southwestern Slovakia: Selected results of the excavation season 2016. *Ber. RGK*, **97**.

Müller-Scheeßel, N., Müller, J., Cheben, I., Mainusch, W., Rassmann, K., Rabbel, W., Corradini, E. and Furholt, M. (accepted) A new approach to the temporal significance of house orientations in European Early Neolithic settlements.

Pavón-Carrasco, F. J., Osete, M. L. and Torta, J. M. (2010) Regional modeling of the geomagnetic field in Europe from 6000 to 1000 B.C. *Geochemistry, Geophysics, Geosystems*, **11**.

Petermann, H. and Bleil, U. (1993) Detection of live magnetotactic bacteria in South Atlantic deep-sea sediments. *Earth and Planetary Science Letters*, **117**, 223–228.

Pickartz, N., Corradini, E., Kahn, R., Panning, D., Rassmann, K., Müller-Scheeßel, N., Furholt, M., Wilken, D., Wunderlich, T. and Rabbel, W. (submitted) Extending archaeological documentation from 2D to 3D: The benefits of geophysical on-site measurements in excavations.

Plouff, D. (1976) Gravity and magnetic fields of polygonal prisms and application to magnetic terrain corrections. *Geophysics*, **41**, 727–741.

Rabenhorst, M., Schmehling, A., Thompson, J. A., Hirmas, D. R., Graham, R. C. and Rossi, A. M. (2014) Reliability of soil color standards. *Soil Science Society of America Journal*, **79**, 193–199.

Sanmartín, P., Chorro, E., Vázquez-Nion, Martínez-Verdú, F. M. and Prieto, B. (2014) Conversion of a Digital Camera into a Non-Contact Colorimeter for Use in Stone Cultural Heritage: The Application Case to Spanish Granites. *Measurement*, **56**, 194–202.

Schneider, M., Linzen, S., Schiffler, M., Pohl, E., Ahrens, B., Dunkel, S., Stolz, R., Bemmann, J., Meyer, H.-G. and Baumgarten, D. (2014) Inversion of Geo-Magnetic SQUID Gradiometer Prospection Data Using Polyhedral Model Interpretation of Elongated Anomalies. *IEEE Transactions on Magnetics*, **50**, 1–4.

Schnepp, E. and Pucher, R. (1998) Preliminary Archaeomagnetic Results from a Floor Sequence of a Bread Kiln in Lübeck (Germany). 11.

Schnepp, E., Pucher, R., Reinders, J., Hambach, U., Soffel, H. and Hedley, I. (2004) A german catalogue of archaeomagnetic data. *Geophysical Journal International*, **157**, 64–78.

Schönwiese, C.-D. (1994) *Klimatologie*. Stuttgart: Ulmer Verlag.

Sexstone, A. J., Revsbech, N. P., Parkin, T. B. and Tiedje, J. M. (1985) Direct measurement of oxygen profiles and denitrification rates in soil aggregates 1. *Soil science society of America journal*, **49**, 645–651.

Simon, F.-X., Koziol, A. and Thiesson, J. (2012) Investigating magnetic ghosts on an early middle age settlement: Comparison of data from stripped and non-stripped areas: Magnetic ghosts on an early middle age settlement. *Archaeological Prospection*, **19**, 191–200.

Spring, S., Amann, R., Ludwig, W., Schleifer, K.-H., van Gemerden, H. and Petersen, N. (1993) Dominating role of an unusual magnetotactic bacterium in the microaerobic zone of a freshwater sediment. *Appl. Environ. Microbiol.*, **59**, 2397–2403.

Stolz, J. F., Chang, S.-B. R. and Kirschvink, J. L. (1986) Magnetotactic bacteria and single-domain magnetite in hemipelagic sediments. *Nature*, **321**, 849.

Thébault, E., Finlay, C., Beggan, C., Alken, P., Aubert, J., Barrois, O., Bertrand, F., Bondar, T., Boness, A., Brocco, L., Canet, E., Chambodut, A., Chulliat, A., Coïsson, P., Civet, F., Du, A., Fournier, A., Fratter, I., Gillet, N., Hamilton, B., Hamoudi, M., Hulot, G., Jager, T., Korte, M., Kuang, W., Lalanne, X., Langlais, B., Léger, J.-M., Lesur, V., Lowes, F. J., Macmillan, S., Mandea, M., Manoj, C., Maus, S., Olsen, N., Petrov, V., Ridley, V., Rother, M., Sabaka, T. J., Saturnino, D., Schachtschneider, R., Sirol, O., Tangborn, A., Thomson, A., Tøffner-Clausen, L., Vigneron, P., Wardinski, I. and Zvereva, T. (2015) International Geomagnetic Reference Field: the 12th generation. *Earth, Planets and Space*, **67**, 67–79.

Uieda, L., Jr, V. C. O. and Barbosa, V. C. F. (2013) Modeling the earth with fatiando a terra. In *Proceedings of the 12th Python in Science Conference* (eds. S. van der Walt, J. Millman and K. Huff), 96–103.

Wilken, D. and Rabbel, W. (2012) On the application of particle swarm optimization strategies on scholte-wave inversion: Pso in scholte-wave inversion. *Geophysical Journal International*, **190**, 580–594.

Wilken, D., Wunderlich, T., Majchczack, B., Andersen, J. and Rabbel, W. (2015) Rayleigh-wave resonance analysis: a methodological test on a viking age pit house: Seismic resonance analysis on a pit house. *Archaeological Prospection*, **22**, 187–206.

Wolfram, S. (2013) Two sides of the coin: ceramic taphonomy and domestic space in the Linear Pottery settlements Hanau-Klein-Auheim and Eythra (Germany). In *The domestic space in LBK settlements. Nanterre (France), 7-8 October 2010* (eds. C. Hamon, P. Allard and M. Ilett), 79–90. Rahden/Westf.: M. Leidorf.

A Tables

Table 1: Expected model parameters with standard deviation for every drilling and magnetic profile combination.

profile	magnetics	$\langle Q \rangle$	σ_Q	σ_Q [%]	$\langle t \rangle$ [10^{-5} SI]	σ_t [10^{-5} SI]	σ_t [%]	$\langle l \rangle$ [m]	σ_l [m]	σ_l [%]
P 04	802b_01	1.9	0.1	5.4	107	7	6.4	2.5	0.8	31.1
P 04	802b_02	2.7	0.1	5.0	100	4	3.7	4.5	0.6	14.2
P 04	802b_03	2.4	0.1	2.8	90	3	3.8	3.6	0.1	2.8
P 04	804b_13	2.5	0.1	5.5	97	10	10.7	3.8	0.7	17.6
P 04	804b_14	3.3	0.4	12.3	53	25	47.0	4.5	0.2	3.8
P 04	804b_15	2.7	0.1	2.8	95	12	13.1	4.4	0.5	11.4
P 16	657b_07	1.9	> 0.1	0.9	90	1	1.1	1.9	> 0.1	2.3
P 16	657b_08	2.0	> 0.1	2.4	23	4	15.6	0.7	0.4	54.3
P 16	657b_09	2.7	> 0.1	0.9	22	> 1	2.3	1.5	> 0.1	3.2
P 16	657b_10	2.7	> 0.1	0.9	22	> 1	2.3	1.5	> 0.1	2.8
P 16	657b_11	3.0	> 0.1	0.2	28	> 1	0.1	2.0	> 0.1	0.4
P 18	657b_07	1.5	0.1	5.7	60	2	3.1	1.7	> 0.1	1.0
P 18	657b_08	1.7	> 0.1	2.8	113	3	2.4	1.8	0.1	4.2
P 18	657b_09	1.8	> 0.1	2.5	113	2	1.7	1.9	0.2	10.2
P 18	657b_10	1.9	> 0.1	0.5	114	> 1	0.4	2.3	> 0.1	> 0.1
P 18	657b_11	1.9	> 0.1	2.1	115	4	3.8	2.0	0.2	7.9
P 20	658b_01	3.5	> 0.1	> 0.1	107	> 1	> 0.1	7.6	0.1	1.4
P 20	658b_02	2.7	> 0.1	1.2	74	1	1.0	1.3	0.1	5.9
P 20	658b_03	3.6	> 0.1	0.5	2	1	53.0	0.0	> 0.1	117.8
P 20	658b_04	2.5	0.1	5.7	4	13	348.7	0.2	0.7	470.5
P 20	658b_05	2.5	0.1	2.2	2	2	149.1	0.0	> 0.1	75.8
P 21	661b_06	4.2	3.3	78.2	149	32	21.2	3.9	0.3	8.1
P 21	661b_07	6.8	3.7	54.3	157	32	20.2	0.7	0.6	83.6
P 21	661b_08	10.2	0.9	9.0	181	21	11.5	0.2	0.3	168.0
P 21	661b_09	10.9	1.6	14.6	186	21	11.4	0.2	0.3	226.7
P 21	661b_10	11.2	1.8	16.3	181	20	11.1	0.3	0.4	117.4
P 22	662b_07	2.7	> 0.1	1.4	30	1	2.2	1.1	0.1	7.2
P 22	662b_08	3.7	0.1	2.2	25	1	3.2	1.1	0.1	8.8
P 22	662b_09	3.7	> 0.1	0.3	23	> 1	1.8	1.1	> 0.1	> 0.1
P 22	662b_10	3.9	> 0.1	0.2	27	> 1	0.3	1.4	> 0.1	0.1
P 22	662b_11	3.6	> 0.1	0.2	28	> 1	1.3	1.4	> 0.1	> 0.1

Table 2: Inversion results of the drilling profiles with mean Koenigsberger ratio $\overline{Q}$, mean threshold $\bar{t}$ and mean taper length $\bar{l}$ based on the best fitting inversion results per magnetic profile, that are given in the second half of the Table with the respective root mean square (RMS) error.

drilling profile	$\overline{Q}$	$\bar{t}$ [10^{-5} SI]	$\bar{l}$ [m]	magnetic profile	Q	t [10^{-5} SI]	l [m]	RMS [10^{-1} nT]
				A802b_01	1.9	105	2.9	5.4
				A802b_02	2.7	102	4.9	5.0
P 04	2.3 ± 0.3 (14.8 %)	101 ± 6 (6.3 %)	3.9 ± 0.9 (22.8 %)	A802b_03[1]	2.4	89	3.7	3.8
				A804b_13	2.6	105	4.6	5.0
				A804b_14	2.5	98	4.4	6.5
				A804b_15	1.9	105	2.9	5.4
				A657b_07	1.9	90	1.9	8.6
				A657b_08[1]	1.9	90	1.9	8.6
P 16	2.0 ± 0.1 (4.7 %)	49 ± 37 (75.3 %)	1.1 ± 0.7 (64.5 %)	A657b_09	2.1	23	0.6	8.8
				A657b_10	2.0	22	0.5	8.8
				A657b_11	2.1	23	0.6	8.8
				A657b_07	1.6	60	1.7	6.7
				A657b_08[1]	1.7	112	1.8	6.6
P 18	1.8 ± 0.2 (8.7 %)	92 ± 28 (30.0 %)	2.1 ± 0.5 (24.6 %)	A657b_09	2.0	64	2.9	7.5
				A657b_10	1.8	111	2.1	8.0
				A657b_11	1.8	114	1.7	8.0

[1] Shown in Figure 9 resp. 5.

Table 2: Continuation.

drilling profile	$\bar{Q}$	$\bar{t}$ [10^{-5} SI]	$\bar{l}$ [m]	magnetic profile	Q	t [10^{-5} SI]	l [m]	RMS [10^{-1} nT]
				A658b_01	3.5	107	3.8	9.9
				A658b_02	2.7	74	1.3	9.8
P 20	3.2 ± 0.5 (16.2 %)	37 ± 50 (136.6 %)	1.0 ± 1.7 (162.7 %)	A658b_03	3.6	3	0.0	8.6
				A658b_04[1]	2.5	0	0.0	6.4
				A658b_05	3.6	0	0.0	8.6
				A661b_06	3.3	138	4.0	10.5
				A661b_07[1]	5.3	138	1.0	7.3
P 21	7.0 ± 3.3 (47.6 %)	160 ± 31 (19.4 %)	1.3 ± 1.6 (121.1 %)	A661b_08	5.3	138	1.0	7.3
				A661b_09	10.5	206	0.0	9.8
				A661b_10	10.5	176	0.5	9.9
				A662b_07[1]	2.7	30	1.1	11.0
				A662b_08	3.6	25	1.1	15.3
P 22	3.5 ± 0.5 (14.2 %)	27 ± 3 (9.6 %)	1.2 ± 0.2 (14.2 %)	A662b_09	3.7	24	1.1	16.1
				A662b_10	3.9	27	1.4	18.7
				A662b_11	3.6	28	1.4	16.1

[1] Shown in Figure 9 resp. 5.

B Synthetic case study

With this synthetic case study, we aim to evaluate the importance of the direction of the remanent magnetization. For this we define a schematic house-accompanying pit as a cuboid with a width of 3.0 m and a length of 18.0 m. It is buried 0.6 m under the surface and 0.6 m thick. It is rotated 18° clockwise, which is approximately the rotation of the real features. For the pit, we assume a susceptibility that is $200 \cdot 10^{-5}$ SI higher than the background. In addition, the pit has a remanent magnetization with a Koenigberger ratio $Q = 3$.

We compare the synthetic anomalies for two cases: (1) the remanence is oriented in the same direction as the recent earth's magnetic field and (2) the remanence is oriented so that the largest possible difference to the recent orientation results. The variation of the D, I and B with an error band at 95% of the confidence level during the settlement period of the site is shown in Figure 11 derived from the SCHA.DIF.8K model (Pavón-Carrasco et al., 2010). For the largest difference between recent and ancient magnetic field parameters, we used $D = 55.56°$ and $I = 4.21°$ dating to 5120 BCE. For the synthetic study the variation of the magnetic field strength is neglected since this can equally be represented by a variation of Q. Therefore, a change in B is not distinguishable from a change in Q. The forward calculations are conducted with the formula by Plouff (1976) as implemented in the python-library 'Fatiando a Terra' (Uieda et al., 2013).

igure 12 shows the synthetic anomaly of the model with the remanence oriented in recent (A) and past (B) orientation of the earth's magnetic field. The difference is depicted inFigure 12 (C) and has a maximum of 1.6 nT.

According to the manufacturer, the magnetic sensors have a resolution of 0.2 nT. However, taking field conditions with a motorized system into account, it is doubtful that the difference arising from a different orientation of the remanent compared to the induced magnetization is detectable.

In conclusion this modelling study shows, that the approximation of the orientation of the remanence in direction of the recent earth's magnetic field is permissible.

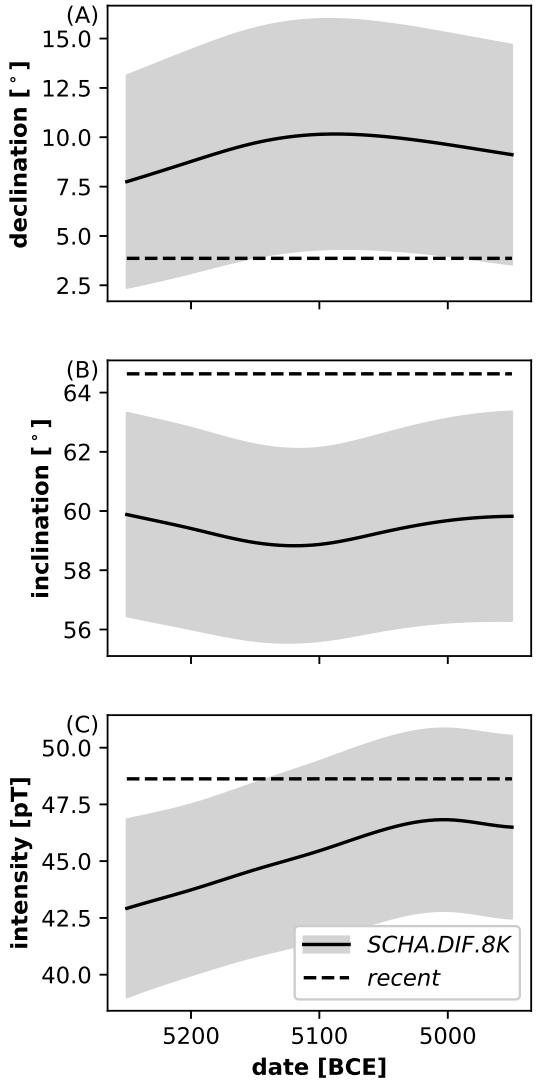

Figure 11: Declination (A), inclination (B) and intensity (C) of the earth's magnetic field during the inhabited time of the settlement (Pavón-Carrasco et al., 2010) in comparison to the recent parameters (Thébault et al., 2015).

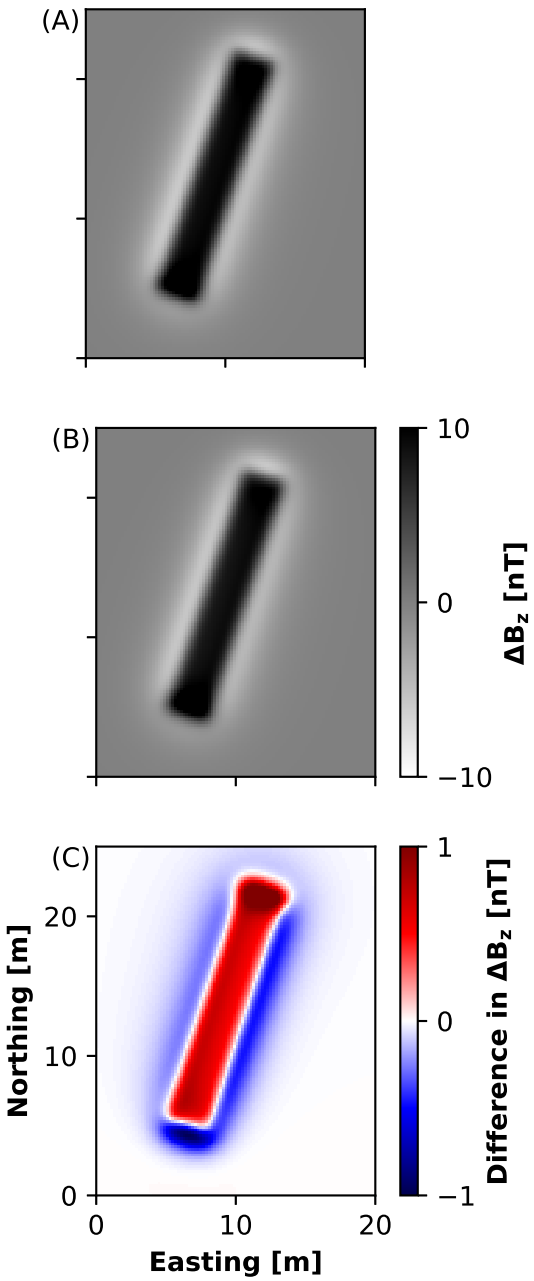

Figure 12: Synthetic anomaly of a schematic pit model for (A) recent orientation and (B) past orientation of the remanent magnetization. (C) Difference between these two cases.

A.3 Paper III

The following article is accepted for publication as Chapter 2.2 in
Furholt, M., Cheben, I., Müller, J., Bistáková, A., Wunderlich, M. and Müller-Scheeßel, N., *Archaeology in the Žitava valley I - The LBK and Želiezovce settlement site of Vráble*. Leiden, Sidestone Press.

Extending archaeological documentation from 2D to 3D: The benefits of geophysical on-site measurements in excavations

Natalie Pickartz[1,2], Erica Corradini[1,2], Raphael Kahn[1], Diana Panning[1,2], Knut Rassmann[3], Nils Müller-Scheeßel[4], Martin Furholt[5], Dennis Wilken[1,2], Tina Wunderlich[1,2], and Wolfgang Rabbel[1,2]

[1]Institute of Geosciences, Kiel University, Kiel, 24118, Germany
[2]Collaborative Research Center 1266, Kiel University, Kiel, 24118, Germany
[3]Romano-Germanic Commission, German Archaeological Institute, Frankfurt a. M., 60325, Germany
[4]Institute of Pre- and Protohistoric Archaeology, Kiel University, Kiel, 24118, Germany
[5]Department of Archaeology, Conservation and History, University of Oslo, Oslo, 0316, Norway

Abstract

Ongoing excavations can be supported by geophysical in-situ measurements to analyse and document the unearthed features with measurements characterising them physically beyond visual inspection. Here, we present results of ground-penetrating radar (GPR), electromagnetic induction (EMI) and magnetic susceptibility (MS) measurements performed on an excavation planum of 'house-accompanying pits' at the Linearbandkeramik (LBK) and Želiezovce settlement site at Vráble (Nitriansky kraj, Slovakia). The measurements enable us to extend the documentation of the excavated area from 2D to full 3D beneath the planum in form of data cubes of GPR reflections and electric conductivity derived from EMI. The shape of house pits at the site of Vráble could be determined in 3D by EMI measurements after local calibration through GPR, excavation trenches and downhole magnetic susceptibility (MS) measurements. It turned out that the pits have an irregular bottom, indicating a discontinuous construction over time. In some cases, it turned out that the pit bottom was about 40 cm deeper than archaeologically documented. Vertical depth sections of the pits could also be generated by sequences of MS downhole measurements, which are a proxy of the iron oxide content of the soil. The uppermost soil layer of the planum showed distinct differences in MS and GPR amplitude strength inside and outside the investigated house. These differences could be seen as evidence of a slight compaction of the sediments originating from the usage of the house floor. Soil structures classified as postholes in the archaeological documentation showed no contrast in susceptibility, GPR, or EMI to the surrounding soils, indicating that only a minimal volume of the posthole fill had remained on the planum.

Keywords: geophysics in excavations, in-situ measurements, geophysical documentation of excavations, ground penetrating radar, electromagnetic induction measurements, magnetic susceptibility

1 Introduction

Knowledge about archaeological sites is usually derived from key targets, which are excavated and, as part of this process, documented. Soil colour, texture, and finds are visually inspected and used to determine the stratigraphy of the excavated structure, and this stratigraphy defines the relative ages of the included layers.

Geophysical prospection methods are used to determine the spatial distribution of physical soil parameters in 2D or 3D, depending on the chosen method. In contrast to soil sampling and geochemical analysis, they can be applied almost continuously, to cover hectare-scale areas. Many archaeological objects can be identified by their physical parameter contrast with respect to the surrounding soil. Conversely, archaeological objects are often not uniquely distinguishable from the surrounding soil by visual inspection alone. Physical soil parameters serve to characterise geological layers and can help to identify recent and ancient anthropogenic site usage (cf. Verdonck et al., 2019). Therefore, we see the determination of geophysical parameters on plana (plan views) and sections and along boreholes as an additional diagnostic tool, one that complements the archaeological documentation.

Against this background, the basic objectives of our study are (1) to investigate to what extent geophysical measurements accompanying excavations can support identifying and characterising underground structures uncovered in plana and trenches beyond optical visibility, and (2) to show how the information gathered on plana can be extended into 3D.

We used the Linearbandkeramik (LBK) and Želiezovce settlement site of Vráble (for location, see inset Fig. 2.2.1) as a case study, whereby we investigated the physical properties of archaeological objects on-site in comparison to the surrounding soil. In this chapter, we demonstrate which geophysical methods can be applied successfully as a complement to excavation, and we evaluate how the geophysical results match the standard excavation documentation and corings.

We conducted measurements in excavation area 22 on planum 1 (approximately 60 cm beneath the modern-day ground surface). Figure 2.2.1 shows the magnetic map (see also chapter 2.1) of the LBK site, which has three settlement nuclei. Excavation area 22 is located in the south-western nucleus (indicated by the solid box). The excavation encircles two long pits that flanked one of the house, one along each side wall. North of these features, a second pair of pits is visible, and these were partly excavated. During the excavation, several postholes were also found. We applied ground penetrating radar (GPR), electromagnetic induction (EMI) and magnetic susceptibility (MS) measurements.

The measurements were conducted directly on the first excavated planum. Additionally, we conducted downhole susceptibility measurements along a transect in the northern area to examine the cross-section of elongated pits located outside of and parallel to the side walls of houses (Fig. 2.2.1, dashed box) (known in German as *hausbegleitende Längsgruben* and in English as house-accompanying pits). To define the spatial context of the excavation area, we also include the magnetic prospection data measured from the surface, which is described and discussed in more detail in chapter 2.1.

This introduction is followed by a brief description of the applied field measurements and data processing. Then, the results of each geophysical method are given and compared with each other and with the archaeological excavation documentation. This comparison forms the basis for the final discussion.

2 Methods

2.1 Magnetic prospection

In magnetic prospection, the strength of Earth's internal magnetic field is measured with an accuracy of up to 1 ppm at Earth's surface. The results are typically presented in the form of maps, in which archaeological features, such as pits, house remains or kilns, can become visible as spatial variation of Earth's magnetic field if they are less or more strongly magnetised than the surrounding soil. Magnetic maps are commonly used directly to identify and categorise archaeo-

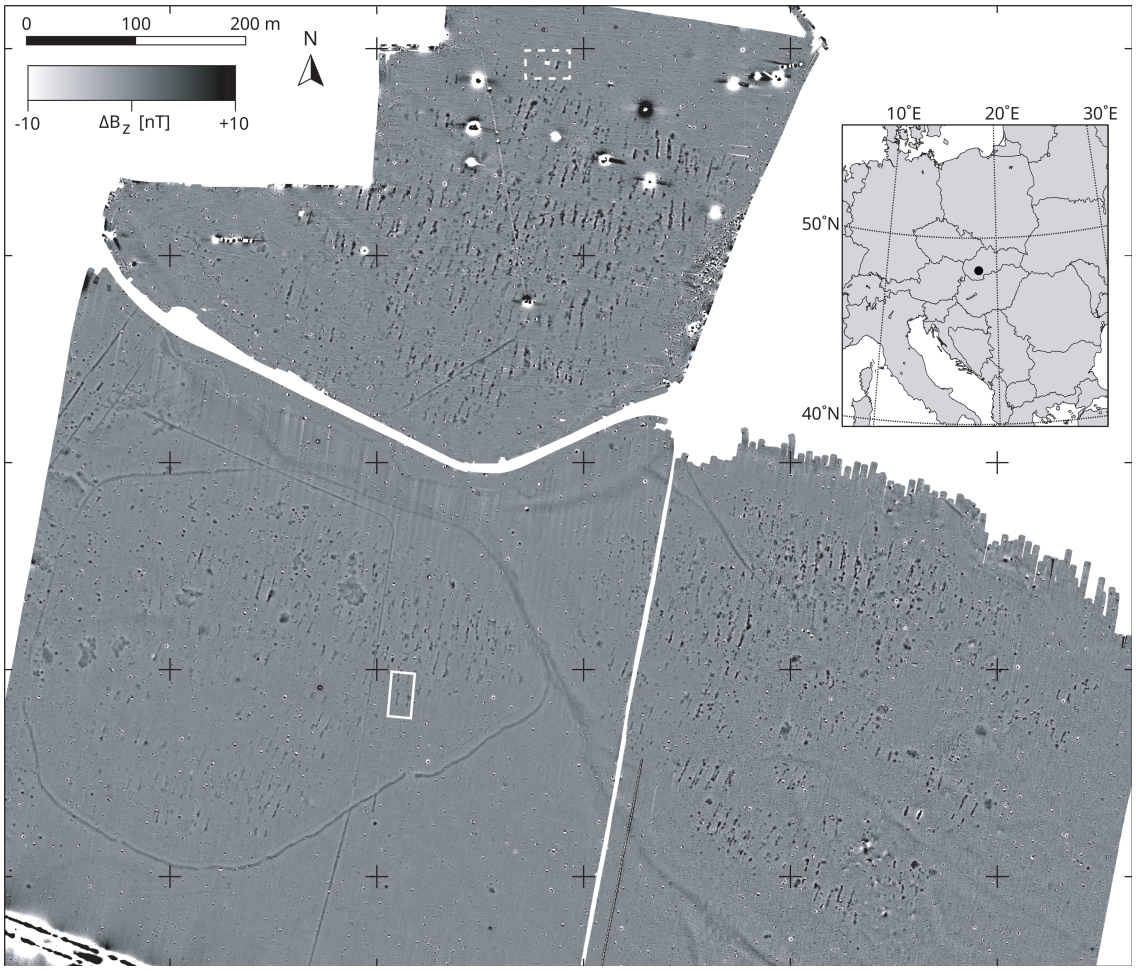

Figure 2.2.1: Magnetic map after Winkelmann et al. (Chapter 2.1), showing the excavation area in the south-western settlement nucleus (solid box) and the area investigated with corings in the northern nucleus (dashed box). Insert: Location (dot) of the site in Slovakia.

logical features, examine features' spatial relations, and plan excavations. Chapter 2.1 discusses the measurement setup for the magnetic mapping.

The magnetisation magnitude of buried material depends mainly on the type and concentration of the contained iron oxides, but also on the grain size distribution of the magnetic minerals. An archaeological structure is detectable by magnetic measurements if its magnetisation differs from that of the surrounding soil matrix. However, the magnetisation can not be mapped directly. So-called inversion computations are required to determine the three-dimensional shape of distinct magnetised bodies or the continuous magnetisation distribution of soils (e.g. Pickartz et al., 2019; Neubauer and Eder-Hinterleitner, 1997). Measured magnetic field anomalies are principally ambiguous with respect to the magnetisation strength and shape of the causative magnetic bodies. Therefore, inversion computations require additional information constraining the mathematically possible solutions. Such constraints may consist of independent measurements of the magnetic soil properties, such as the magnetic susceptibility (see below), or information on the depth and thickness of magnetised layers from excavations or corings.

2.2 Ground-penetrating radar

GPR images the interfaces of subsurface structures in terms of radar reflection amplitudes. A transmitter antenna emits pulses of a few nanoseconds (ns) duration into the ground. These pulses propagate through the subsurface until they are reflected at the interfaces between subsurface layers and objects that differ from each other in terms of electromagnetic soil properties. The reflected signals are measured by a receiver at the surface. GPR is sensitive to the ground's electrical conductivity as well as its dielectric permittivity and contrast therein. Electrical conductivity is responsible for the energy absorption and thus the sounding depth, whereas permittivity and its contrasts affect the propagation velocity of the signal and the strength of the reflection from subsurface interfaces, respectively (e.g. Davis and Annan, 1989). The electrical conductivity and the dielectric permittivity themselves depend mainly on the water content, as well as the clay and silt fractions of the soil. The porosity of the soil, and thereby its water content, depends on the compaction and cementation of the soil. Therefore, compacted or cemented soil volumes may be detected by GPR measurements (e.g. Wunderlich, 2012).

We conducted the GPR survey of the present study with a 200 MHz antenna by GSSI Inc. The underlying loess limits the depth of investigation to approximately 1 m to 2 m. Assuming a velocity of 6 cm/ns, the expected spatial resolution is approximately 0.075 m according to the quarter-wavelength criterion. We measured the excavation area in two different setups: an area of 2 m $\times$ 17 m (northern strip) as well as a larger area of 9 m $\times$ 35 m (western half) (cf. Fig. 2.2.2). We measured the smaller area with 30 cm cross line spacing and the larger area with 60 cm cross line spacing.

We applied the following processing steps to our data: (a) trace repositioning to correct the position of the GPR traces in a profile; (b) time zero correction; (c) a background subtraction filter, which reduces the direct waves and ringing noise; (d) a bandpass filter with cut-off frequencies 10, 50, 350, and 390 MHz; (e) migration with a constant velocity of 6 cm/ns; and (f) an automatic gain control (AGC) amplification with a time window length of 10 ns. To produce time slices, all parallel profiles were combined and cut into 2 ns thick slices in which the squared sum of absolute amplitudes was calculated.

2.3 Electromagnetic induction

EMI instruments consist of a transmitter and a receiver. The transmitter coil emits a 'primary' oscillating magnetic field at a frequency in kHz or 10 kHz range. Dependent on the electrical conductivity distribution of the subsurface, electric eddy currents are induced in the soil, generating a 'secondary' magnetic field recorded at the receiver coil together with the primary field. From these, a direct output is generated consisting of values of the 'apparent electrical conductivity' of the soil and the so called 'in-phase' (IP) component, which is proportional to the magnetic susceptibility. Both these values represent average values of the soil volume encircled by the diameter of a 'footprint', Earth's surface and the sounding depth (Everett and Weiss, 2002). Footprint and sounding depth depend on signal frequency and transmitter to receiver distance. As described above, the electrical conductivity depends on the sediment composition and water content. Like the magnetisation, the magnetic susceptibility depends on the sort and concentration of iron oxides, as described above for the magnetisation.

If the applied EMI instrument enables measurements with different sounding depths, inversion computations can be conducted that convert the corresponding average apparent electrical conductivity values into depth functions of 'true' in-situ electrical conductivity. These depth functions can then be spatially compiled into an approximate 3D distribution of electrical conductivity, from which depth maps of soil layers and interfaces can be derived. The EMI procedure is technically very efficient, but the results need depth calibration by coring or spot excavation because of an inherent physical uncertainty relationship between electric conductivity and layer thickness.

We used a CMD Mini-Explorer by GF Instruments. The device consists of one transmitter and three receiver coils, the axes of which can be oriented horizontally or vertically (HCP or VCP modes). The distance between the transmitter and receivers are 0.32 m, 0.71 m, and 1.18 m, leading to effective sounding depths of 0.25 m, 0.5 m, and 0.9 m in VCP mode and 0.5 m, 1.0 m, and 1.8 m in HCP mode. Further details on the method and the device can be found in e.g. Bonsall et al. (2013).

The area was covered with measurements at 10 Hz sampling frequency along parallel profiles with a cross-line spacing of 50 cm using both coil orientations. The data were then interpolated to a 0.5 m $\times$ 0.1 m grid. Noise resulting from the motion of walking was removed with a low pass filter (third-order Butterworth filter with cut-off wavenumber at 0.7 m^{-1}). The in-phase components that were notably affected by a temporal drift were corrected with the method of Delefortrie et al. (2014).

The filtered conductivity measurements of HCP and VCP coil orientations were used for determining electric conductivity to depth function for each point of the gridded area. These inversion computations were performed with the software IX1D by Interpex. HCP and VCP measurements were jointly inverted using the 'smooth model' mode (Constable et al., 1987). In this mode, the sounded depth range is subdivided into a set of layers with predefined thicknesses, which are kept fixed during the computation, while the conductivity values are altered subjected to smoothness constraints. We defined 10 layers between 0.05 m to 1.5 m depth, with logarithmically equidistant thicknesses. The resulting one-dimensional models were stitched together to form a 'cube' of electric conductivity values. From this 3D model, we cut out a number of 2D vertical sections or horizontal depth slices, which are presented in Figures 2.2.4 and 2.2.5.

The measurements were conducted when the earth moving of the excavations was still in progress. The time interval between the unearthing of the western half of the excavation area and the measurements was longer than for the eastern part. One expected effect of a greater interval is that the subsurface could dry out, and this is, in fact, visible in the measurements and in the inversion result.

2.4 Magnetic susceptibility

The magnetic susceptibility is a specific property of soils and sediments that describes how strongly a material becomes magnetised in the presence of an external magnetic field, in the case of archaeological studies, Earth's magnetic field. Anomalies detected by magnetic prospection originate from variations in the magnetisation of the subsurface. As indicated above, magnetic maps show the location and a 'distorted' contour of the subsurface bodies. To resolve their geometry and magnetic properties, additional information is needed. The magnetic susceptibility is one of these properties. The susceptibility can be seen as a proxy for the iron oxide content and anthropogenic activities – such as fire, deposition of organic materials in pits, and construction of buildings – that enhance the iron oxide content. Therefore, the MS can be used to document archaeological structures. Furthermore, high-resolution measurements with point distances of a few centimetres enable the documentation of gradual variations. This is an important advantage over traditional archaeological documentation, as transitional boundaries are often simplified to discrete boundaries. For the discussion of the measurement technique of induction coil devices, such as the ones we applied, we refer to Evans and Heller (2003).

We measured the susceptibility on planum 1 using the SM-30 by ZH instruments on a 0.2 m $\times$ 0.2 m grid covering an area of 2 $\times$ 9 m. The inline point distance was reduced to 0.1 m in the border area of the pit and at the locations of the postholes. With this device, only point measurements are conducted so that the possible measurement area is limited in size. The values

are displayed as greyscale images.

In addition to mapping, we performed downhole measurements to determine cross-sections of the house-accompanying pits in terms of magnetic susceptibility. Based on the magnetic anomaly, 22 mm diameter auger holes where cored, with a minimum distance of 0.25 m and a maximum depth of 2 m. We measured the susceptibility with the MS3 device and the MS2H sensor by Bartington Instruments Limited for depths deeper than 0.1 m with 0.05 m vertical point distance. Prior to the corings, the susceptibility of the topsoil was measured with the MS2K sensor. For a smooth image, the data is horizontally interpolated to 0.125 m point distance.

3 Results

In Figure 2.2.2, an overview of the results of the different survey methods is given. The red contours mark the pits and possible postholes as they have been identified by visual inspection of the excavated soils and sediments. In the following, we present the results for each method in detail. We close this section with a comparison to the archaeological excavation.

3.1 Magnetic prospection

The magnetic map (Fig. 2.2.1 and Fig. 2.2.2B) was used to plan the excavation. It shows the long pits of the southern house as elongated anomalies. Their shape is irregular, and the eastern long pit is wider in its central part. The amplitude of the anomalies rises up to 6.4 nT and varies throughout the long pits. Apart from the northern pair of long pits, there are no more anomalies visible in the excavation area that can securely be interpreted as archaeologically relevant based on the magnetic prospection data.

3.2 Ground-penetrating radar

The results from the GPR survey show the location of the western long pits of the houses, visible as two elongated features, one in the north and one in the south (Fig. 2.2.2C). The black colour indicates a higher reflection amplitude compared to the surrounding area, which is depicted in white. Between the southern two house-accompanying pits, there is an area of smaller amplitudes compared to those of the long pits, but higher than the surroundings. The archaeologically documented postholes are not visible in the GPR time slice. In addition to the pits, some spot-like or small, elongated anomalies with a higher reflection amplitude are visible in the time slice from 6 to 8 ns. However, these could not be related to any documented archaeological structures.

Figure 2.2.3 shows a GPR profile crossing the western house-accompanying long pit of the southern building. From this profile (Fig. 2.2.3B), the depth of the pit can be estimated to be 1.1 m beneath planum 1. The other profiles of the area show depths between 0.6 and 1.2 m of the pits beneath planum 1. The radargrams also do not reveal any signs of postholes.

3.3 Electromagnetic induction

3.3.1 Magnetic susceptibility mapping through EMI in-phase measurements

The in-phase component of the VCP measurements with the smallest coil separation (Fig. 2.2.2D) shows the western long pits as distinct anomalies, with values lower than the 'background' level, down to 0.57 ppt. The in-phase component seems to be affected by the different time spans between earthworks and measurements. The background level varies between around 1.25 ppt (±0.03 ppt) in the western part and around 1.18 ppt (±0.05 ppt) in the eastern part. The northern quarter of the south-western pit shows values about 1.16 ppt (±0.05 ppt) and such values would be barely

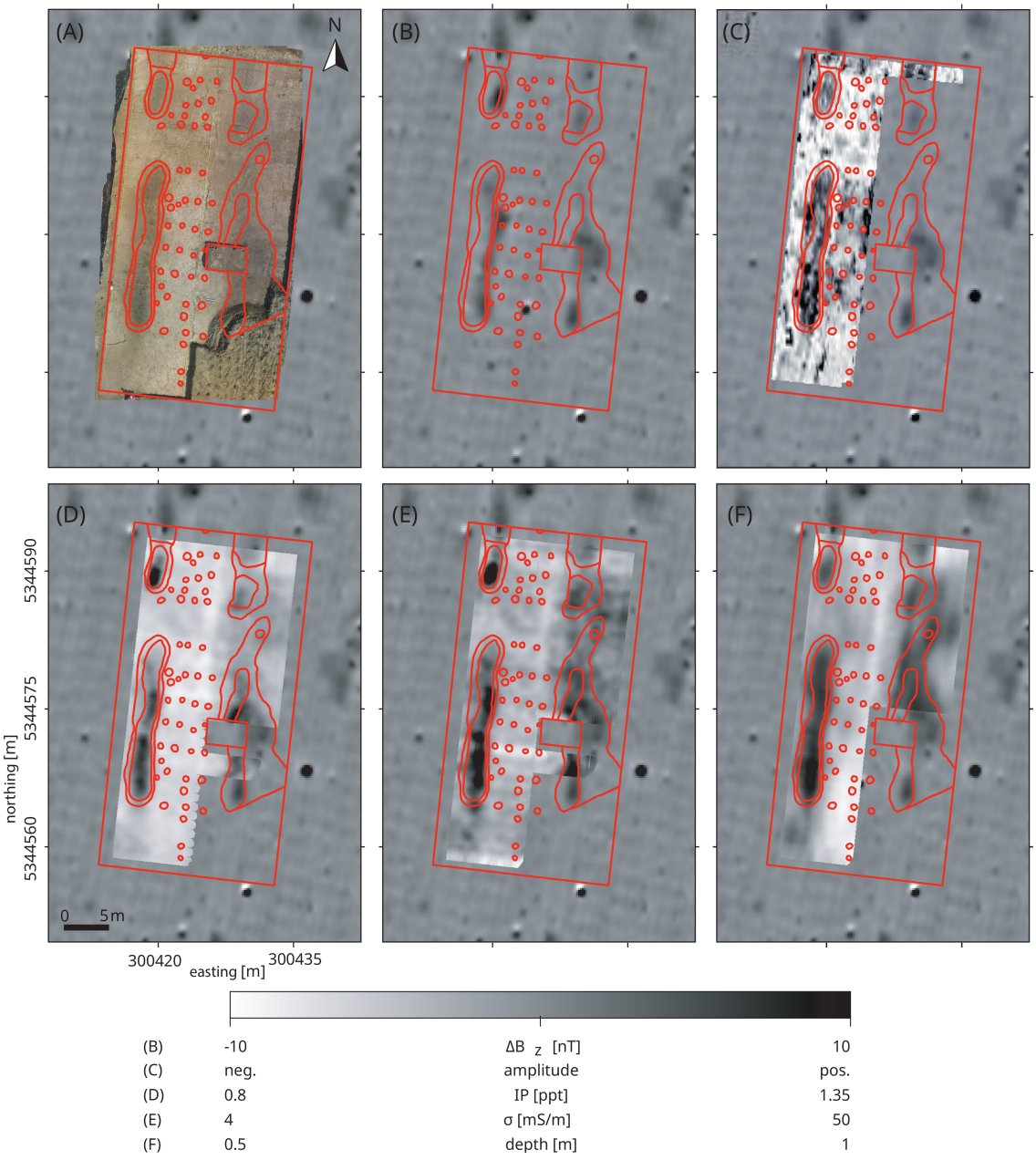

Figure 2.2.2: The excavation area as mapped by the different imaging methods, detailed in the table below the maps. (A) photogrammetry during the opening phase of the excavation; (B) magnetic mapping; (C) GPR time slice from 6-8 ns showing contrasts of permittivity through GPR reflection strength; (D) in-phase component of VCP configuration for the smallest coil separation, visualising the horizontal variation of magnetic susceptibility in a qualitative way; (E) electric conductivity distribution from the inversion of EMI measurements for the first layer (0.05-0.07 m depth); (F) depth of the 18 mS/m iso-surface of the conductivity model beneath planum 1, whereby the iso-surface is interpreted as the bottom of the pits (see below). Each sub-figure shows the magnetic map in the background and the archaeological interpretation (red lines) superimposed.

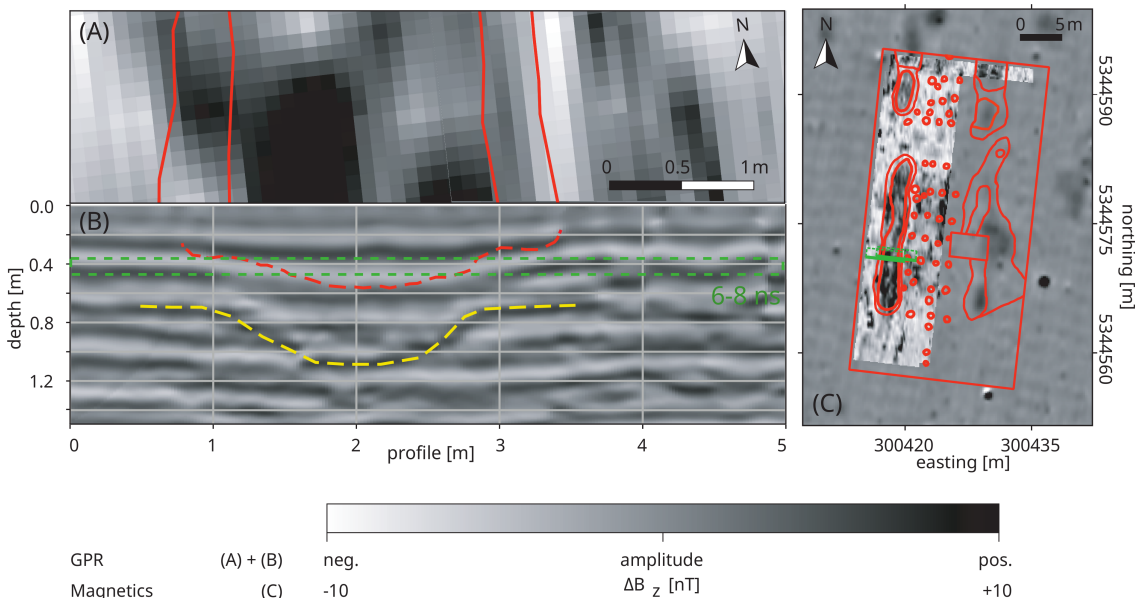

Figure 2.2.3: (A) Time slice at 6-8 ns (corresponding to a depth of about 0.36 m to 0.48 m) of the GPR measurements directly on the planum, with archaeological interpretation (red lines) superimposed; (B) GPR depth profile 38, with the location of the archaeological documentation (red dashed line), the depth determined from the GPR reflection image of the bottom of the pit (yellow line), and the depth of the time slice (green dashed box) superimposed; (C) magnetic map and time slice from 6-8 ns, with the location of profile 38 (solid green line) and the archaeological interpretation (red lines) superimposed.

visible in the eastern part. There are no further anomalies that can be related to an archaeological context.

3.3.2 3D electric conductivity distribution from EMI out-of-phase measurements

The top layer of the determined 3D electric conductivity distribution extends from 0.05 m to 0.07 m depth. It shows the location of the long pits as zones of increased conductivity values up to 79.1 mS/m (Fig. 2.2.2E), whereas the conductivity outside the long pits is only around 19.2 mS/m (±4 mS/m) in the western part of the excavation and around 26.1 mS/m (±5.5 mS/m) in the eastern part. Most probably this difference is caused by the different time spans between the earthworks and the measurements in both parts of the area, during which the soil dried to different extents. Due to the different levels of background conductivities, the western long pits are easier to recognise in the greyscale images than the eastern ones. The north-western long pit is characterised by a distinct region of increased conductivity. The south-western long pit shows variations between 22.9 mS/m and 59.2 mS/m throughout the pit. None of the depth slices show any anomalies that could be interpreted as postholes.

To evaluate the stratigraphic structure suggested by the electric conductivity distribution, we use the depth profiles derived from the 3D distribution in Figures 2.2.4 and 2.2.5. As can be seen in Figure 2.2.4, profiles A and B cut the northern pair of long pits, profile C cuts the northern tip of the south-eastern long pit, and profile D cuts both southern long pits. The cross-sections of the long pits are visible as areas with decreased conductivity down to 1 mS/m. Based on these profiles, different shapes of cross-sections and varying depth extensions can be derived. In profile A, the region of very low conductivity is comparatively small and shallow. Profile B is located 3.5 m southwards and shows a different cross-section for the western long pit. The long pit is wider

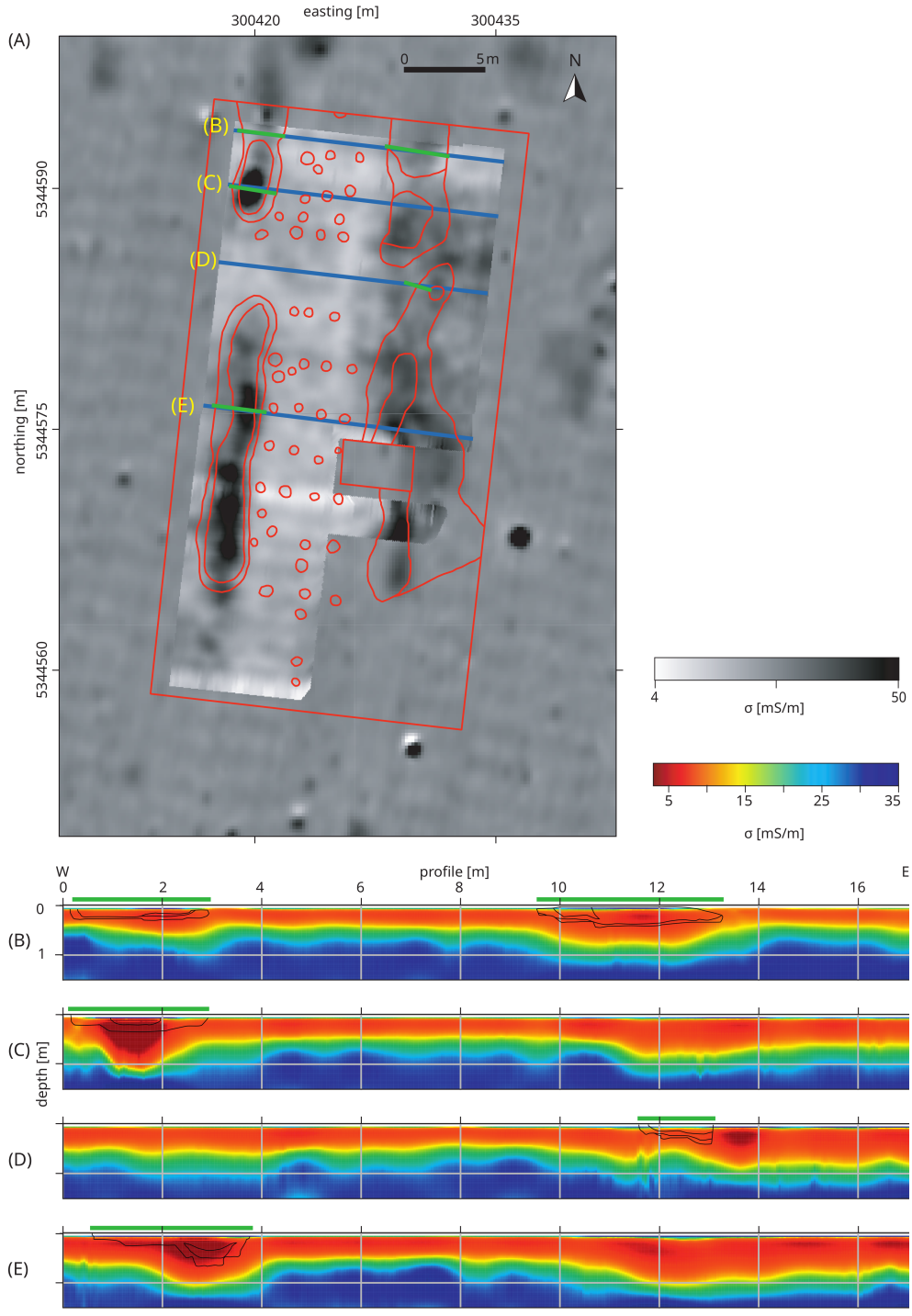

Figure 2.2.4: Electric conductivity depth profiles. (A) Electric conductivity map (first layer of electric conductivity distribution, 0.05-0.07 m depth) with the magnetic map in the background, with the archaeological interpretation (red), the location of the electric conductivity profiles B-E (blue), and the location of the respective archaeological sections (green) superimposed; (B-E) electric conductivity depth sections from EMI measurements, with the drawing of the long pits based on the archaeological interpretation (black) and the location of the respective archaeological sections (green) superimposed.

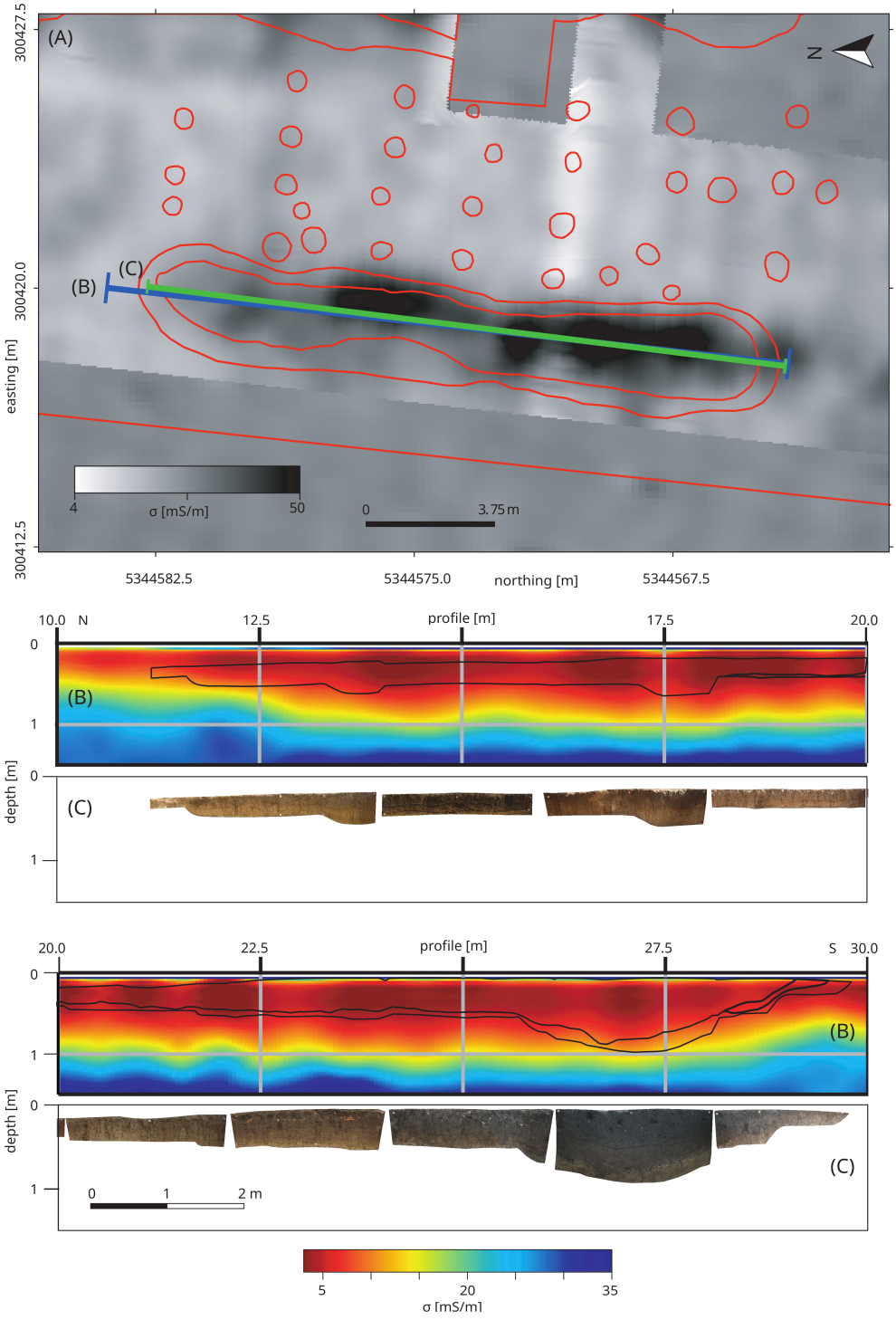

Figure 2.2.5: Electric conductivity longitudinal profile through the south-western long pit. (A) Electric conductivity map (top layer), with the location of the profile and section (blue and green lines, respectively) and the archaeological interpretation (red lines) superimposed; (B) conductivity model through the pit, with the archaeological interpretation of the sections (black lines) superimposed; (C) photogrammetry of the archaeological sections. B and C have been split in two in order to fit the page.

and deeper. In the western part, profile C is not cutting any pit; however, in the eastern part, a pit of small dimension is distinctly visible. As is also visible in the depth slices, regions of decreased conductivity extend over several metres of the profile. Both long pits seem to be 'smeared out' in the direction outside the house. No anomalies are visible that can be related to postholes.

In the GPR depth section, we could identify a reflection from the bottom of the long pit. Using this information, we could define the corresponding conductivity iso-surface as an indicator for the bottom of the linear pit. This enabled us to contour the pit bottom in 3D, as further discussed below.

Figure 2.2.5 shows a profile that cuts the south-western long pit lengthwise. The conductivity model (Fig. 2.2.5B) is stitched from several crossline profiles. The photogrammetry (Fig. 2.2.5C) shows that the fill varies throughout the long pit, which is also reflected in the variation of the conductivity within the long pit. However, there is no obvious correlation between soil colour and conductivity values inside this long pit.

3.4 Magnetic susceptibility

3.4.1 Planum 1

Figure 2.2.6A shows the areal distribution of magnetic susceptibility as derived from point measurements superimposed on the magnetic map (surface measurements) and the excavation results. Figure 2.2.6B is a cut-out of this map. The area of the long pit coincides with increased susceptibility values of up to $214 \cdot 10^{-5}$ SI, with a mean of $(111 \pm 30) \cdot 10^{-5}$ SI. Hereby, some of the higher values correlate with the location of burned clay and some of the lower values correlate with uneven surfaces, leading to bad ground coupling of the susceptibility sensor. The area outside the house (west of the long pit) has a mean susceptibility of $(50 \pm 9) \cdot 10^{-5}$ SI, and the area inside the house (east of the long pit), $(27 \pm 11) \cdot 10^{-5}$ SI.

3.4.2 Cross-section of house-accompanying long pits

In Figure 2.2.7, the downhole susceptibility measurements and the respective magnetic measurements are shown (in the northern area, Fig. 1 dashed box). Generally, the susceptibility increases with depth until a maximum of $192 \cdot 10^{-5}$ SI is reached at approximately 0.4 m to 0.7 m depth. With further depth, the susceptibility decreases again, to values around $30 \cdot 10^{-5}$ SI. This general form of the susceptibility depth curve can be observed in all corings at the site. Consequently, solely the maximum and its location characterise the shape of the cross-section of the long pits. Considering the $150 \cdot 10^{-5}$ SI isoline as boundary of the central part of the long pit, it starts at a depth of 0.4 m and is 1.5 m wide.

The comparison with the magnetic measurements shows that areas of increased susceptibility correlates with the local maximum of the magnetic anomaly.

3.5 Comparison of geophysical results and archaeological documentation

Figure 2.2.2A shows the photogrammetry of the planum at the state of the measurements. The pits are recognisable by the darkest soil colours. The colour contrast to the surrounding material is higher in the western half (light soil colour) than in the eastern half (intermediate soil colour). This difference in contrast may originate from the different air exposure time and the resulting degree of drying or from an actual difference in the composition. Despite this difference in contrast, we observe a correlation between soil colours and geophysical measurement or the respective

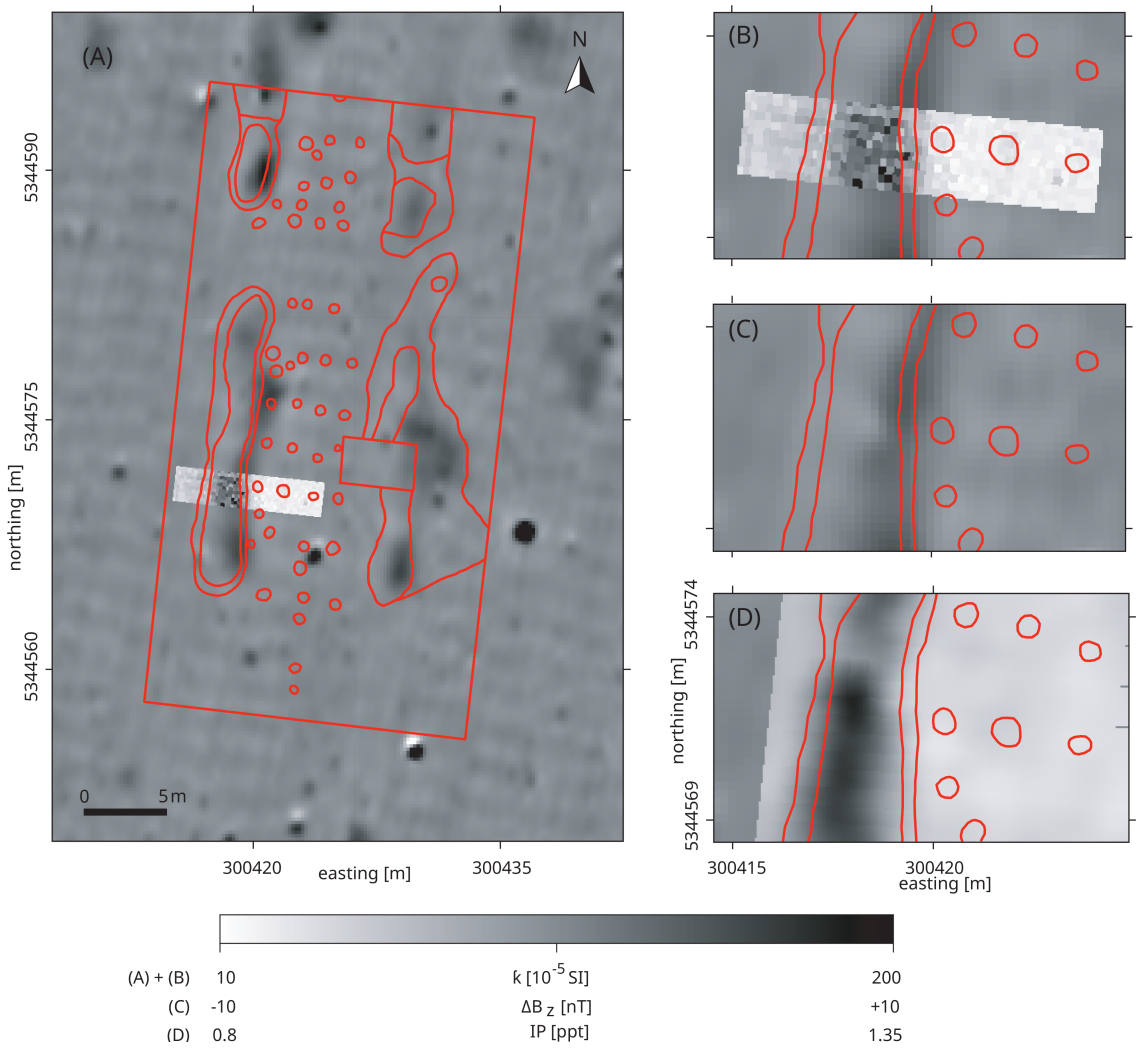

Figure 2.2.6: (A) Areal susceptibility measurements, with the archaeological interpretation (red lines) superimposed and the magnetic map in the background; (B) detail of (A); (C) detail of (A) showing magnetic map only; (D) detail of (A), showing EMI In-phase component of VCP configuration for the smallest coil separation, showing the magnetic susceptibility distribution of the uppermost layer in a spatially smoothed, qualitative way.

deduced specific physical parameter: darker soil colours correlate with higher IP and the respective susceptibility values, higher electric conductivity values, and increased reflection amplitudes in the near-surface time slice from 6-8 ns. For the IP (Fig. 2.2.2D) and conductivity values (Fig. 2.2.2E), this correlation especially applies also the surrounding matrix: dark, intermediate and light soil colours correspond to high, intermediate and low IP or conductivity values. For GPR and MS, no assertion can be made, since measurements were performed only in the western half of the trench. However, the correlation between soil colour and conductivity does not hold for small conductivity variations inside the south-western pit (cf. Fig. 2.2.5).

Having discussed the observed contrast, we can briefly turn to the resultant geometry of the subsurface structures. From Figure 2.2.2, we can see that all methods mapped the long pits horizontally in a similar shape and spatial extent. However, none of the geophysical methods were able to map the documented postholes. This can be seen as an indication that the volume of the

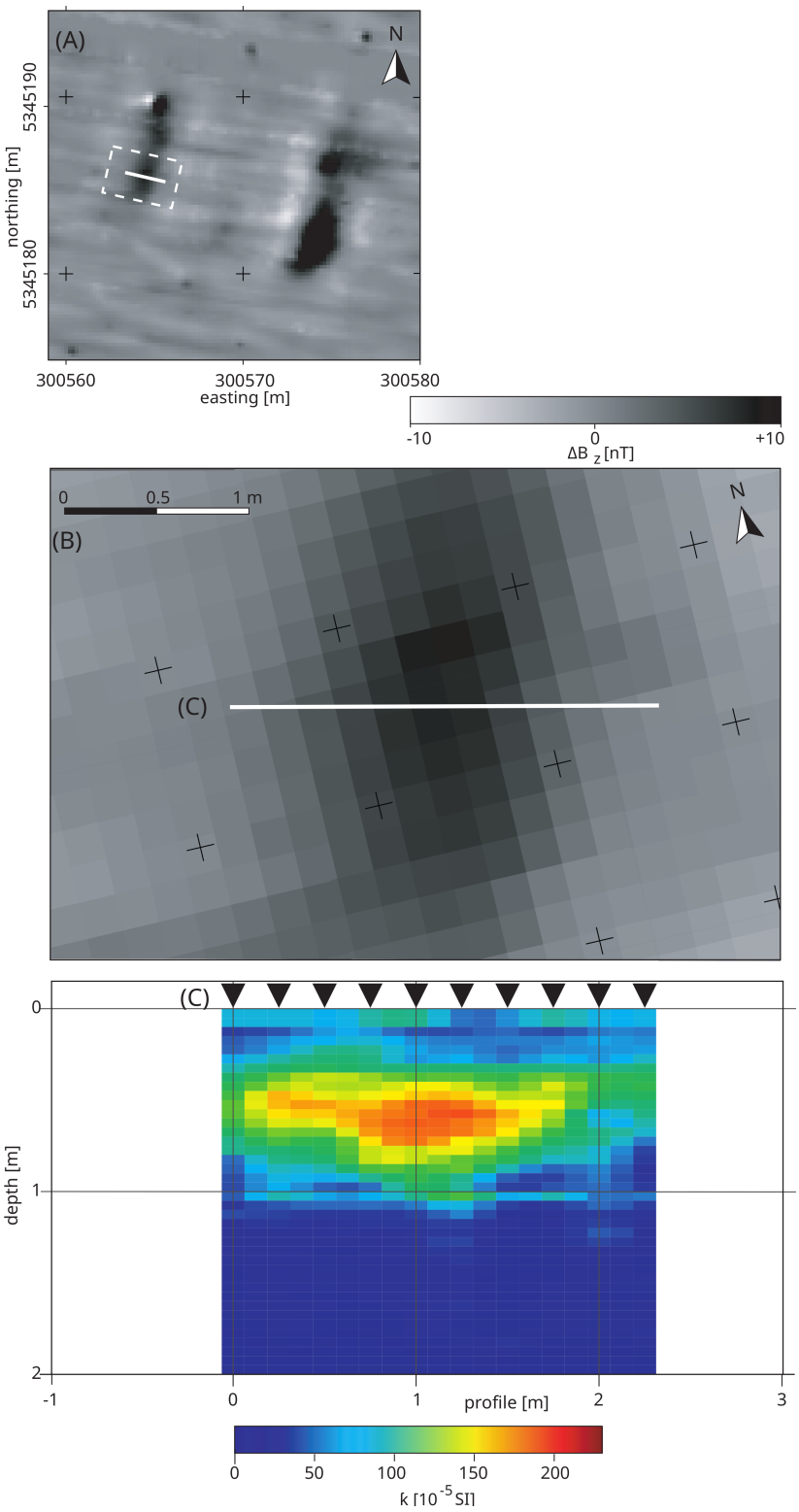

Figure 2.2.7: Susceptibility distribution based on downhole measurements. (A) Magnetic map, with the profile location (white line) and area depicted in (B) (white dashed box) superimposed; (B) magnetic map of the cored long pit, with the profile location (white line) superimposed; (C) susceptibility distribution, with location of corings (black triangles) indicated.

remaining soil fill of the posthole must be vanishingly small. According to the excavation report, the contours of the postholes were visible only for a short time after the removal of the topsoil and 'disappeared' after the planum had dried out.

For the comparison of the depth extension of the pits, we focus on the south-western long pit, as shown in Figure 2.2.8. Figure 2.2.8A shows the magnetic map around the respective profile that is shown in B as a radargram, in C as an EMI inversion result, in D as an overlay of the latter two, and in E as photogrammetry. This comparison shows that the reflections of the GPR as well as the conductivity distribution suggest a deeper bottom of the pit than the archaeological interpretation did. The same interpretation results also from the profiles in Figure 4.

The comparison of the radargram and the conductivity model (Fig. 2.2.8D) suggests that the 18 mS/m iso-surface can be regarded as an estimate for the bottom of the long pits. Figure 2.2.9 shows the depth of this iso-surface under planum 1. This iso-surface has a minimum depth of 0.4 m under planum 1. The south-western long pit is the deepest one, with a depth up to 1.1 m at its southern end. Notably, the bottom of the house-accompanying long pits shows a distinct microtopography, with the deepest part at their southern end. The magnetic map suggests this continuous, elongated pit character of the house-accompanying long pits, whereas the EMI conductivity distribution shows that this applies only to the upper 50 cm of the construction. The microtopography of the bottom revealed by EMI indicates that the long pit structure is composed of a sequence of more or less circular pits.

As shown in Figure 2.2.8, the bottom of the long pit appears to be deeper in the geophysical images than it was supposed to be according to the visual inspection during excavation. In contrast, the deepest part of the south-western long pit (see Figure 2.2.5B and C at approx. 27 m) is documented at approximately the same depth, as indicated by the 18 mS/m iso-surface, in comparison to the archaeological documentation. However, considering also the other parts of this long pit along the profile, the differences in the depths of the pit supposed by the geophysical and archaeological interpretation remain, and they need to be discussed (see next section).

4 Discussion

We begin the discussion with a focus on the investigated targets, outlining the perspectives of geophysical documentation. Then we give an overview of the in-situ measurement approach in general terms. This is followed by a discussion of the details concerning the applied methods.

4.1 Investigated targets: Results and perspectives of geophysical documentation

The presented results show that the archaeological features and the surrounding matrix can be documented in an objective manner based on physical properties. This enables the deduction of conclusions relevant for the archaeological interpretation.

4.1.1 House-accompanying long pits

We derived a map of the bottom of the house-accompanying long pits by combining EMI measurements with depth information from GPR (Fig. 2.2.9). However, we avoided suggesting distinct values of the dimensions of the long pits based on geophysical measurements alone because this necessitates the definition of thresholds between different observed entities (pits and surrounding matrix). In order to obtain the most reliable depth calibration of the geophysical images, we

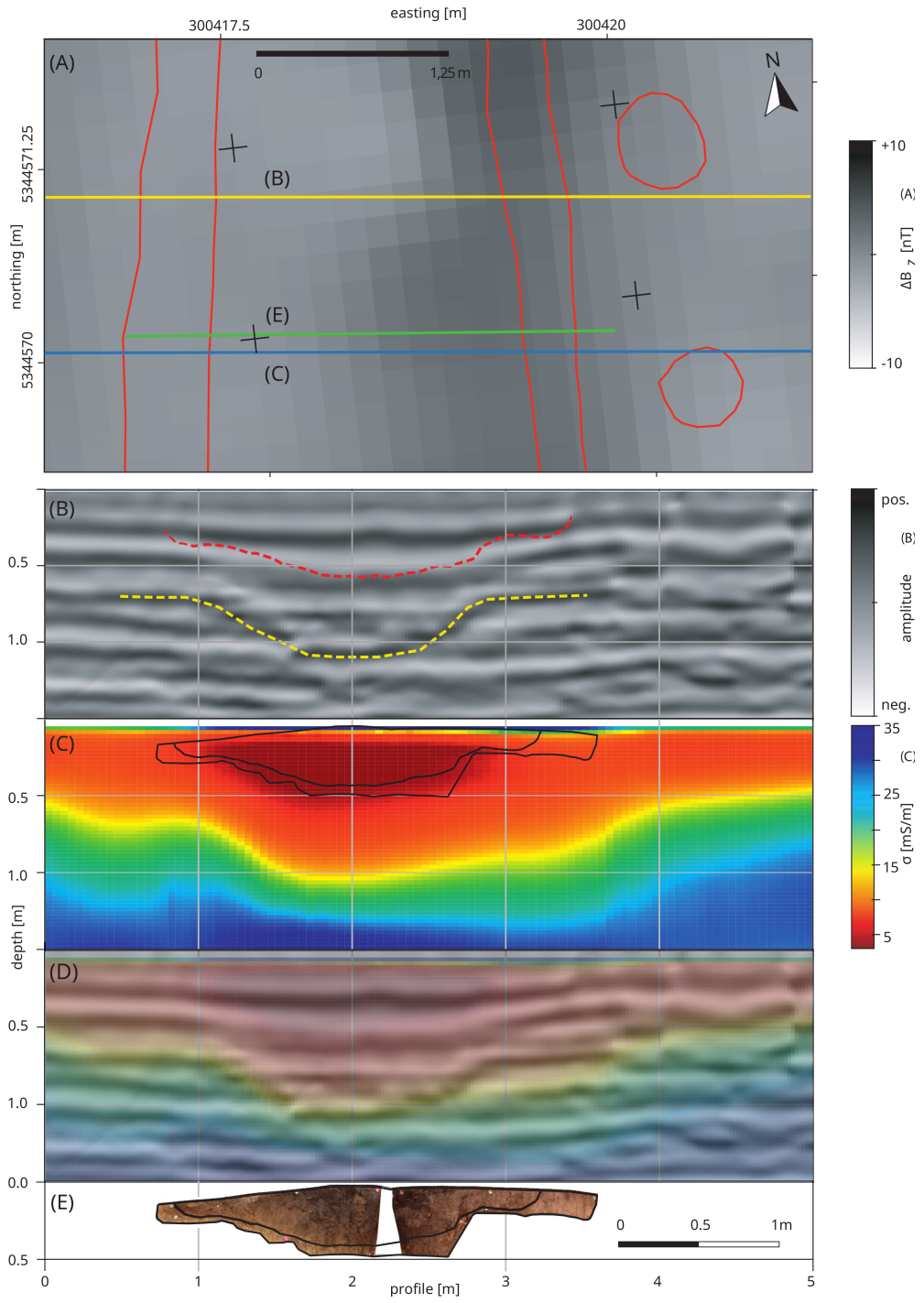

Figure 2.2.8: Profiles of the south-western long pit. (A) Magnetic map, with archaeological interpretation (red lines), the location of the GPR profile (yellow line), the EMI profile (blue line), and the archaeological section (green line) superimposed; (B) GPR depth section of the pit bottom of the long pit, showing the depth as derived from the GPR reflections (yellow), and as determined by visual inspection of soil colour (red); (C) electric conductivity depth section from EMI overlain with the pit bottom (innermost black line) of the archaeological section (outermost black line; same as shown in red in (B)); (D) combined plot of the electric conductivity depth section and the radargram; (E) photogrammetry of the archaeological section from which the pit depth was derived.

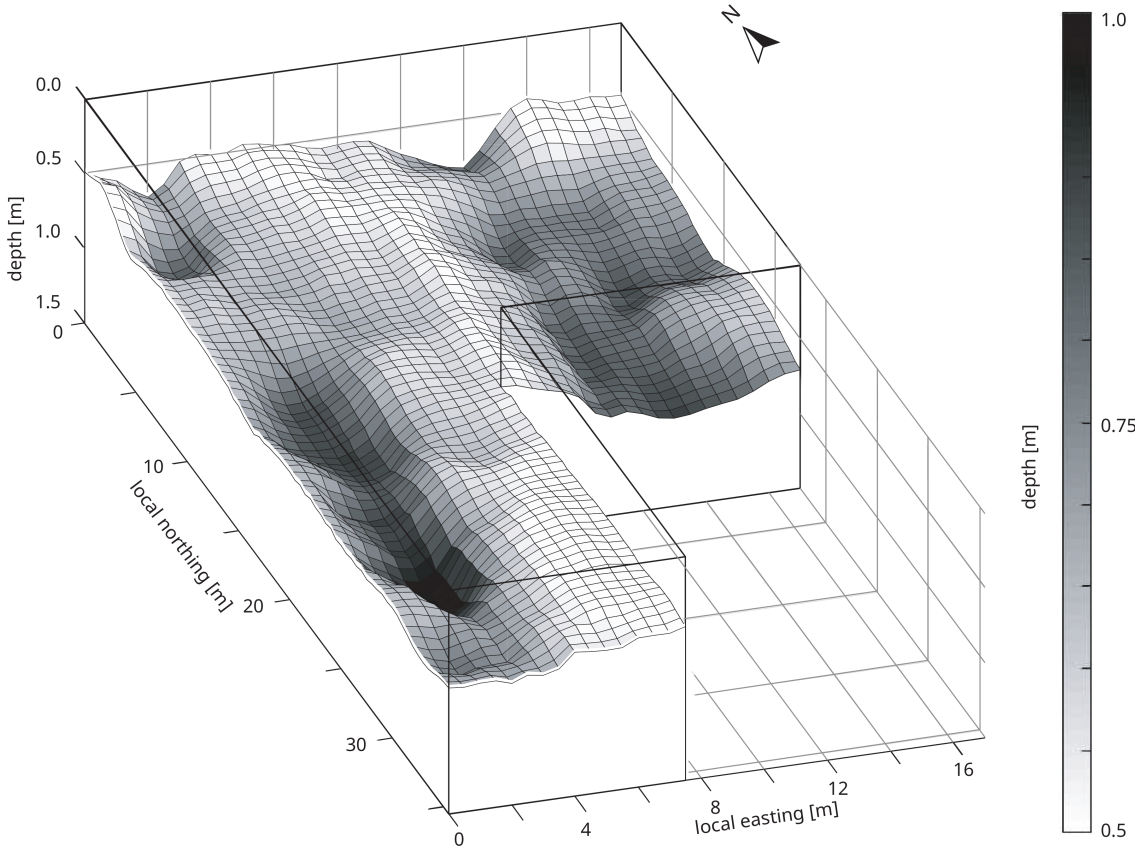

Figure 2.2.9: Map showing the depth of the 18 mS/m iso-surface of the electric conductivity model beneath planum 1 (aspect of depth to horizontal axes 1:5).

recommend complementing the geophysical sounding by shallow corings and geophysical downhole measurements in future. Although the actual depths of the long pits may be somewhat different from the depths of the selected iso-conductivity contour, the lateral depth variations still holds. This means that the segments of the long pits were originally dug to different depths or are preserved only to different degrees. The geometrical shape, i.e. the microtopography, shown in Figure 2.2.9, is irregular and therefore indicates that the long pits were not dug in a single event but, rather, are comprised of an apposition of smaller pits. This was also verified in the excavations. Still, the depth of the pits and the microtopography have to be considered with some care because in many cases conductivity models represent the distribution of soil moisture and clay content rather than stratigraphic interfaces (e.g. Verdonck et al., 2019). Therefore, a change in the composition of the pit fill can, in principal, result in the same geophysical results. To resolve the ambiguity between soil moisture and clay content, coring and geophysical downhole measurements need to be added to the methodology. They would allow us to directly determine soil moisture and clay content at the coring site and to determine geophysical pedo-transfer functions that improve the calibration apart from the coring points.

Pursuing the interpretation with the determined depths of the long pits, we can see that Figures 2.2.4, 2.2.5 and 2.2.8 clearly show that the bottom is indicated as being deeper by the geophysical measurements than by the excavation. A change in the physical properties is not necessarily connected with a change in the soil colour, which is examined with the bare eye in the course of excavation to determine the bottom of the pits. Thus, on the one hand, the observed physical change can be independent from the change in the soil colour and, on the other hand, the definition

of a distinct boundary based on soil colour with the bare eye can be challenging because of the change of water content over time, varying light conditions or gradual changes in the soil matrix.

4.1.2 House interior vs. surrounding soil

The GPR measurements showed increased reflection amplitudes in the area between the long pits. These might indicate an increased compaction of the sediments resulting from the usage of the building. However, a difference in soil composition of the sediments inside and outside the house can result also in differences in reflection amplitude. To test for variation in the clay content by methods other than soil sampling, gamma-ray measurements could be conducted in future investigations.

Also, the horizontal susceptibility distribution shows a distinct image of the long pits. The long pits show up with a significant contrast, of up to 400 per cent, compared with the surrounding soils. The areas of undisturbed soil outside the house, west of the long pit, and inside the house, east of the long pit, also show different average values, of $(56 \pm 12) \cdot 10^{-5}$ SI and $(27 \pm 11) \cdot 10^{-5}$ SI (Fig. 2.2.6). A comparison with results of the extensive coring campaigns shows that the susceptibility values found inside the house are in the same range as those of the underlying loess (cf. Fig. 2.2.7 and Pickartz et al., in review). This indicates that the area between the two house-accompanying long pits at planum level has not been altered over time in terms of the susceptibility, in contrast to the surrounding, where anthropogenic or pedogenic processes have led to an increase in susceptibility compared to the subsoil loess. A slight soil compaction of typically 10 per cent, as may be indicated by GPR, would imply an increase in magnetic susceptibility of the same order, which is not observed. However, we do not see this as a contradiction because the lateral variation of the susceptibility of loess outside the long pits is of the same order of magnitude. Therefore, compacted soil patches are difficult, if at all, to detect by susceptibility measurements. With this approach, other characteristic areas, e.g. workshops, that are not visible to the bare eye could also be detectable (cf. Hulin et al., 2014).

4.1.3 Postholes

None of the applied geophysical methods were able to detect the remains of the archaeologically identified postholes. There are three possible reasons for this: lack of contrast in the physical soil parameters, too small volume of the remaining posthole fill, lack of spatial sampling or horizontal resolution of the sounding methods.

Lack of physical contrast would imply that the posts have been removed and the hole has been filled with the unaltered soil of the surrounding matrix. This is because rotten remains of organic material, such as tree trunks, can be expected to develop anomalies at least in magnetic susceptibility due to the activity of magnetic bacteria (e.g. Fassbinder et al., 1990; Fassbinder, 2015).

To produce a geophysical signal measurable with field instruments, the anomalous soil structure needs to have a certain minimum volume. For GPR, the posthole fill would need to have a thickness of the order of a quarter of the dominant wavelength, that is, ca. 8 cm in the present case. The diameter of the soil volume sounded by in-situ measurements of magnetic susceptibility is of the order of 5 cm. Therefore, it would be unlikely to detect a posthole geophysically if the thickness of the remaining posthole fill were less than these values, even if it were exposed at the planum.

Finally, spatial sampling and horizontal resolution need to be considered as a possible cause. The 13 excavated postholes have widths between 0.35 m and 0.63 m. The horizontal resolution

for GPR is determined by the size of the Fresnel zone, and this depends on the wavelength and the depth. Here, the wavelength is of the order of 0.3 m, resulting in a horizontal resolution of 8 cm at the earth surface and $\sim$ 40 cm at 1 m depth. Therefore, the postholes would have been detected with GPR if the contrasts were large enough. Also, for the horizontal susceptibility measurements with a point distance of 0.1 m, the spatial sampling was high enough because the area sounded by each scan is of 5 cm diameter only. The situation is different for EMI, where the smallest coil distance of the applied instrument was 0.32 m, leading to a sounding volume of about 60 cm diameter. This volume may have been a critical prerequisite to detect the postholes even if a measurable contrast had been present. However, in summary, we can conclude that the lack of visibility of the postholes in the geophysical records is, in this case, not caused by a lack of resolution or coarse sampling, but indeed by a lack of contrast in the respective physical parameters or by a lack of mass of the remaining posthole fill. Comparably, most postholes were hard to locate during the excavation, as the colour of their fill was often almost identical to that of the surrounding soil, due to bleaching or washing out of minerals over time. The postholes are best visible in situations of overall humidity, i.e. directly after excavation, or after a longer period of rain. However, due to the conditions of a summer excavation, such conditions are too seldom encountered.

For the archaeological interpretation, this might indicate that the posts were removed when the house was abandoned and that only anthropogenically undisturbed sediments filled the remaining postholes. Another explanation would be that the remains of the posts eroded completely or were destroyed through ploughing.

To detect putative postholes, it is important to conduct all measurements, including photography, quickly after removing the topsoil. Slight variations in the soil colour indicated the location of the putative postholes; however, the colours faded while exposed to air. This suggests that the contrast in the physical properties can also change due to air exposure. On the one hand, the water content changes and, on the other hand, oxidation processes might take place. In conclusion, the detection of postholes seems to be possible only with very sensitive devices with high spatial resolution and sampling and with prompt measurement after air exposure.

4.2 Methodical discussion: Specific problems and perspectives

4.2.1 General aspects of in-situ measurements

Many authors have stated that integrated surveys using a combination of different geophysical methods (e.g. Linford, 2006; Verdonck et al., 2019; Kvamme et al., 2019) and a high feedback level between geophysicists and archaeologists (e.g. Boucher, 1996; Horsley et al., 2014) are profitable. However, in-situ measurements to aid documentation and characterisation of excavated features still seem to be limited to a few examples compared to the overall number of archaeogeophysical case studies (e.g. von der Osten-Woldenburg et al., 2002; Simon et al., 2012; Hulin et al., 2014; Ard et al., 2015; Kainz, 2016). A technical report (Bevan, 2005) discusses the advantages and disadvantages. As advantages, it lists, inter alia, the accurate imaging of gradual boundaries (vs. the simplification to a discrete boundary), the detection of contrasts that are not visible to the human eye, no influence from surface rubble – or, in this case, the plough zone – and performing the measurements directly on the archaeological features. The latter also enables a better spatial resolution, since the distance between probe and features is smaller. The disadvantages are possible effects of the excavation boundaries (similar to topographical effects) and stronger effects of soil moisture changes, since former deeper layers are now exposed. We also observed most of these advantages and disadvantages, as discussed above and below. Disadvantageous financial and practical aspects are obviously the time and cost of additional survey campaigns. Depending on the method, additional time for processing and interpretation is needed, so that not all measurement results can immediately be incorporated in the ongoing excavation.

In general, the choice of geophysical methods depends on the subsurface and the targets. For the subsurface and targets at the site of Vráble, the combination of GPR and EMI yielded satisfactory results. The application of both methods is also feasible during the course of an excavation, since the instruments are mobile during the measurements. This is in contrast to electrical resistivity measurements, for example, which require the deployment of electrodes to the ground that might hinder the excavation work for a certain amount of time. Both EMI and GPR are electromagnetic methods and accordingly they are both sensitive to the electric conductivity and magnetic soil properties (GPR: magnetic permeability; EMI magnetic susceptibility). This overlapping sensitivity makes the results comparable, as a change of the respective signal is expected at the same depth. Yet, they also complement each other, since the methods work in different frequency ranges. The favourable complementing characteristics are: The lack of spatial resolution of the EMI is complemented with the high resolution of GPR and vice versa, in that the reduced depth of investigation of GPR is complimented by a higher depth of investigation of EMI. Despite the challenging survey conditions (loess as conductive, and therefore damping subsurface and targets as well as surrounding matrix consist of very similar material), the combination of the two methods yields results that clearly show the subsurface structures. The comparison with the excavation documentation shows that these results are plausible.

We have shown that the combination of GPR and EMI measurements after stripping the topsoil allows for the documenting of the archaeological features before being destroyed through excavation. The time for measurements, processing and interpretation obviously depends on the size and complexity of the excavation area. On a prepared area (positioning already done) and with enough labour to partly conduct measurements and processing at the same time, an area like discussed here can be examined to preliminary results within an extended working day. Although the excavation has to stop during the measurements, the advantage is that the gathered data document a piece of cultural heritage which is afterwards destroyed. Moreover, the interpretation of the geophysical measurements can reveal targets as focus for the excavation and, as shown above, can determine the depths of features. This allows the team to adjust the excavation speed and therefore, perform the excavation more efficiently.

4.2.2 EMI measurements

The presented electric conductivity model explains the measured data with a root mean square error predominately between 5 % and 15 %. However, due to the principal of equivalence of EMI sounding, many models exist that explain the measured data equally well. These equivalent models differ in layer thicknesses and electrical conductivity values, but agree in the product of layer thickness and conductivity. The model output by the selected EMI software usually depends on the incorporated inversion algorithm, as well as on the starting parameters of the computation used (i.e. number of layers, minimum and maximum depth, and starting conductivity). Therefore, EMI measurements principally need calibration, for example, with corings, geophysical downhole measurements, excavations or even seismic or GPR surface profiling. Nevertheless, for regular, non-chaotic sedimentation conditions, it can be assumed that the prevailing sediment bedding form and compositional layering of the soil show up in the electric conductivity depth sections with geometrical similarity, even though the absolute layer depths may be different. This may also constitute a geometric similarity between conductivity structures and soil colour contours deduced from photography of trench walls.

Finally, it has to be considered that 3D models of electric conductivity stitched together from 1D conductivity-depth function are only an approximation of the true subsurface conductivity distribution. They need to be considered with care in cases where the archaeological targets show complicated 3D forms at spatial scales that are of the same or smaller size than the diameter of the EMI footprint. However, this is not problematic in the present case because the dimensions of the investigated pits seem to have been accurately mapped by EMI, as shown by comparison with the other methods.

4.2.3 GPR measurements

The GPR measurements directly on the archaeological features introduce difficulties in the interpretation. The direct wave of the 200 MHz antenna has an approximate period of 20 ns, with a respective wavelength of 60 cm. Hence, the reflections of the archaeological features are superimposed by the direct wave. Moreover, the direct wave is also influenced by absorption and coupling effects of the antenna and/or the subsoil's moisture and porosity. The area of the house between the two pits appears as intermediate reflective (Fig. 2.2.2C). The part of the GPR signal causing this anomaly is also part of the direct wave. This change in amplitude may have resulted from a reflection from a denser sediment layer in the area of the house compacted through its usage. This hypothesis could be tested in further excavations with direct analyses of the density and punctual measurements of GPR velocity. To resolve this sort of very shallow structure, an antenna with a much higher frequency than 200 MHz would be needed.

4.2.4 Susceptibility measurements

Our investigations have shown that vertical sections of susceptibility can be generated very efficiently by coring and downhole measurements and that the pit fill can be identified very reliably through its susceptibility value (Fig. 2.2.7). Therefore, we see the susceptibility measurements as a direct method for extending the documentation of pits and similar archaeological features in an objective way to the areas outside excavation trenches and plana (cf. Pickartz et al., in review).

Hand-held susceptibility devices, which are available on the market for mapping excavation plana and trench walls, differ strongly in data acquisition speed. We chose to perform point-mode measurements (single, hand-triggered measurements) instead of continuous-mode measurements (measurements triggered by a fixed sample frequency) to ensure the highest possible measuring accuracy for susceptibility values and positioning. Taking point mode measurements this is a time-consuming procedure. The continuous mode would be faster, but – to our knowledge – none of the available devices was equipment with a suitable positioning system or interface, which complicates mapping areas continuously with centimetre spacing even if they are only a few square metres in area. Hence, an improvement of the practical procedure is necessary to enable fast and accurate measurements in future.

5 Conclusions

We applied ground penetrating radar, electromagnetic induction, and magnetic susceptibility measurements during an ongoing excavation of the Neolithic site of Vráble. The measurements were performed on a planum 60 cm beneath the modern surface to characterize the archaeological structures beyond visual inspection by physical soil parameters and to extend the 2D archaeological documentation of the planum into a 3D model. Incorporating geophysical measurements in the ongoing excavation documents the subsurface structures before being destroyed through excavation. Then the deduced sub-surface models can be used to adjust the excavation process, e.g. in terms of speed of soil removal and small-scale target focussing. Essential for the geophysical documentation is a sound depth calibration of the measurements through coring, geophysical downhole measurements, test excavation and/or comparative measurements with different depth-sensitive geophysical methods at Earth's surface.

Our conclusions relating specifically to the Vráble site are the following:

- The shape of house-accompanying long pits could be determined in 3D by EMI measurements after local calibration through GPR, excavation trenches and downhole susceptibility measurements. It turned out that the long pits have an irregular bottom, indicating a discontinuous construction over time. In some cases, the comparison between archaeological

documentation and EMI and GPR measurements showed that the bottom of the long pits was obviously deeper than excavated.

- The uppermost soil layer of the planum shows distinct differences in MS and GPR amplitude strength inside and outside the investigated house. This difference could be explained by a compaction of the sediments originating from the usage of the house floor. To confirm this hypothesis, more houses need to be investigated, including also soil density analyses.
- At the locations of postholes suggested on the base of visual evidence, no distinct anomalies of geophysical parameters could be detected, even though the spatial resolution of the measurements was sufficient. We therefore conclude that the posthole fill had been basically eroded and dispersed in the removed topsoil, such that only a faint remnant of their very bottom remained by chance on the planum – too little material to be detected by the sensors applied.

To further improve the significance of excavation-accompanying geophysical measurements, we suggest conducting further research to integrate archaeological, geophysical and pedological observations for a thorough understanding of the features and the surrounding subsurface. This can be, inter alia, soil density measurements to test soil compaction and gamma-ray measurements for mapping variations of the clay content of the topsoil. Analyses of the frequency dependence of the magnetic susceptibility, as well as in-situ determination of the content of iron oxides, could be used to examine soil formation processes at the archaeological site. A more detailed characterisation of the magnetic properties could also help to design the site-specific inversion approach for up-scaling interpretations from an excavation area to a complete site established on the basis of areal prospection data.

6 Acknowledgments

We would like to thank Lara and Maximilian Lowe for their assistance with the field measurements.

References

Ard, V., Mathé, V., Lévêque, F. and Camus, A. (2015) A Comprehensive Magnetic Survey of a Neolithic Causewayed Enclosure in West-central France for the Interpretation of Archaeological Features. *Archaeological Prospection*, **22**, 21–32.

Bevan, B. (2005) Geophysics in Excavations. *Tech. Rep. 11*, Geosight, Weems, VA, USA.

Bonsall, J., Fry, R., Gaffney, C., Armit, I., Beck, A. and Gaffney, V. (2013) Assessment of the CMD Mini-Explorer, a New Low-frequency Multi-coil Electromagnetic Device, for Archaeological Investigations. *Archaeological Prospection*, **20**, 219–231.

Boucher, A. R. (1996) Archaeological feedback in geophysics. *Archaeological Prospection*, **3**, 129–140.

Constable, S. C., Parker, R. L. and Constable, C. G. (1987) Occam's inversion: A practical algorithm for generating smooth models from electromagnetic sounding data. *Geophysics*, **52**, 289–300.

Davis, J. L. and Annan, A. P. (1989) Ground-Penetrating Radar for High-Resolution Mapping of Soil and Rock Stratigraphy 1. *Geophysical Prospecting*, **37**, 531–551.

Delefortrie, S., De Smedt, P., Saey, T., Van De Vijver, E. and Van Meirvenne, M. (2014) An efficient calibration procedure for correction of drift in emi survey data. *Journal of Applied Geophysics*, **110**, 115–125.

Evans, M. E. and Heller, F. (2003) *Environmental Magnetism: Principles and Applications of Enviromagnetics*. San Diego: Academic Press.

Everett, M. E. and Weiss, C. J. (2002) Geological noise in near-surface electromagnetic induction data. *Geophysical Research Letters*, **29**, 10–1–10–4.

Fassbinder, J. W. (2015) Seeing beneath the farmland, steppe and desert soil: magnetic prospecting and soil magnetism. *Journal of Archaeological Science*, **56**, 85–95.

Fassbinder, J. W. E., Stanjekt, H. and Vali, H. (1990) Occurrence of magnetic bacteria in soil. *Nature*, **343**, 161–163.

Horsley, T., Wright, A. and Barrier, C. (2014) Prospecting for new questions: Integrating geophysics to define anthropological research objectives and inform excavation strategies at monumental sites. *Archaeological Prospection*, **21**, 75–86.

Hulin, G., Prilaux, G. and Talon, M. (2014) Intégration de la géophysique à un projet archéologique d'envergure. L'exemple du projet canal Seine-Nord-Europe. *Revue archéologique de Picardie*, **1**, 245–260.

Kainz, J. (2016) An Integrated Archaeological Prospection and Excavation Approach at a Middle Neolithic Circular Ditch Enclosure in Austria. In *Digital Methods and Remote Sensing in Archaeology* (eds. M. Forte and S. Campana), 371–403. Cham: Springer International Publishing.

Kvamme, K. L., Ernenwein, E. G. and Menzer, J. G. (2019) Putting it all together: Geophysical data integration. In *Innovation in Near-Surface Geophysics* (eds. R. Persico, S. Piro and N. Linford), 287–339. Amsterdam: Elsevier.

Linford, N. (2006) The application of geophysical methods to archaeological prospection. *Reports on Progress in Physics*, **69**, 2205–2257.

Neubauer, W. and Eder-Hinterleitner, A. (1997) 3D-interpretation of postprocessed archaeological magnetic prospection data. *Archaeological Prospection*, **4**, 191–205.

von der Osten-Woldenburg, H., Chaume, B. and Reinhard, W. (2002) Magnetic imaging of a late Bronze Age tumulus in France before and during excavation. *The Leading Edge*, **21**, 465–466.

Pickartz, N., Hofmann, R., Dreibrodt, S., Rassmann, K., Shatilo, L., Ohlrau, R., Wilken, D. and Rabbel, W. (2019) Deciphering archeological contexts from the magnetic map: Determination of daub distribution and mass of Chalcolithic house remains. *The Holocene*, **29**, 1637–1652.

Pickartz, N., Rabbel, W., Rassmann, K., Müller-Scheeßel, N., Furholt, M., Müller, J., Cheben, I., Wilken, D., Wunderlich, T. and Dreibrodt, S. (in review) What over 100 drillings tell us: A new method for determining the Koenigsberger ratio of soils from magnetic mapping and susceptibility logging. *Archaeological Prospection*.

Simon, F.-X., Koziol, A. and Thiesson, J. (2012) Investigating Magnetic Ghosts on an Early Middle Age Settlement: Comparison of Data from Stripped and Non-stripped Areas: Magnetic Ghosts on an Early Middle Age Settlement. *Archaeological Prospection*, **19**, 191–200.

Verdonck, L., De Smedt, P. and Verhegge, J. (2019) Making sense of anomalies: Practices and challenges in the archaeological interpretation of geophysical data. In *Innovation in Near-Surface Geophysics* (eds. R. Persico, S. Piro and N. Linford), 151–194. Amsterdam: Elsevier.

Winkelmann, K., Bátora, J., Kalmbach, I. H. J., Müller-Scheeßel, N. and Rassmann, K. (forthcoming 2020) Revealing the general picture. Magnetic prospection on the multiperiod site Fidvár/Veľké Lehemby/Farské near Vráble (Slovakia). In *Archaeology in the Žitava valley I - The LBK and Želiezovce settlement site of Vráble* (eds. M. Furholt, I. Cheben, J. Müller, A. Bistáková, M. Wunderlich and N. Müller-Scheeßel). Leiden: Sidestone Press.

Wunderlich, T. (2012) *Geophysical methods for the investigation of soils.* Ph.D. thesis, Kiel University.

Acknowledgments

Zuallererst möchte ich meinem Doktorvater Prof. Dr. Wolfgang Rabbel danken, denn ohne seine Unterstützung in Form der intensiven Betreuung mit ausführlichen Diskussionen wäre diese Arbeit nicht entstanden. Ich danke ihm dabei nicht nur für die konstruktive Kritik, sondern insbesondere auch für die bestätigenden und motivierenden Worte.

Weiterhin danke ich Prof. Dr. Jörg Ebbing für die Übernahme des Zweitgutachtens.

Mein Dank gilt auch allen Kollegen der Arbeitsgruppe 'Angewandte Geophysik', die eine tolle Arbeitsatmosphäre schaffen. Insbesondere meinen Büronachbarn Tina, für alle beantworteten Fragen zu den Themen Geophysik und Nähen, und Raphael, für alle Bohrungen, Abbildungen und lustigen Momente, in denen wir Tränen gelacht haben. Weiterhin gilt mein Dank Dennis, der immer einen fachlichen Rat für mich hatte. Und natürlich Erica für die tollen Tage und Stunden bei der Feldarbeit und dafür, dass sie eine tolle Freundin ist.

Ich danke den Kollegen des Sonderforschungsbereichs 1266, die mir die Möglichkeit gegeben haben, meine Doktorarbeit im Rahmen eines solchen Projektes anzufertigen. Ich bin sehr dankbar für den Einblick in die Forschungswelt im Rahmen eines solch großen und interdisziplinären Projektes. Im Zuge dessen danke ich auch allen Kollegen und Studenten für die tolle gemeinsame Feldarbeit in der Slowakei, Moldawien und der Ukraine.

Ich danke Andreas dafür, dass er ein Fels in der Brandung ist.

Nicht zuletzt möchte ich meiner Mutter von ganzem Herzen dafür danken, dass sie mir meine wissenschaftliche Ausbildung ermöglicht hat und mich über all die Jahre immer wieder auf alle erdenklichen Arten und Weisen unterstützt hat. Danke, Mama.